Optimization and Application of Non-Uniform Sampling for 2D NMR-Based Metabolomics

Dissertation zur Erlangung des Doktorgrades
der Naturwissenschaften (Dr. rer. nat.)
der Fakultät für Biologie und Vorklinische Medizin
der Universität Regensburg

vorgelegt von
Trixi Kristina Freiin von Schlippenbach

aus
Offenbach am Main

im Jahr
2018

Das Promotionsgesuch wurde eingereicht am:

Die Arbeit wurde angeleitet von:

Prof. Dr. Wolfram Gronwald

Unterschrift:

This doctoral thesis was conducted at the Institute of Functional Genomics, University Regensburg, in the time from 01.01.2015 until 31.12.2017. It was financially supported by the Deutsche Forschungsgemeinschaft (DFG KFO 262, grant number GR 1747/8-2).

Contents of this thesis, except for section 3.1.2 on the implementation of enhanced resolution with NUS to urine specimen and section 3.2, were published in parts in a slightly altered version as the following research paper: *Schlippenbach, T. v., Oefner, P. J. & Gronwald, W. Systematic Evaluation of Non-Uniform Sampling Parameters in the Targeted Analysis of Urine Metabolites by ^{1}H,^{1}H 2D NMR Spectroscopy. Sci. Rep.* ***8****, 4249; 10.1038/s41598-018-22541-0 (2018).* More particularly, the referring parts in the research paper on general and urine metabolomics by means of NMR spectroscopy as well as optimizing, validating, and applying time-reduced non-uniform sampling on urine specimens were included in the abstract, objectives and motivation, introduction, materials and methods, results, discussion, and conclusion of this thesis. Furthermore, Figures 5 - 8 and Figures S1 - S17 as well as Tables 1 - 5 and Tables S1 - S14 along with the simulation of NUS spectra were taken from the referring research article at times attributing an adapted numbering. My contributions to this research article included envisaging the project along with Prof. Dr. Wolfram Gronwald and Prof. Dr. Peter J. Oefner, carrying out the laboratory experiments together with Claudia Samol, collecting the NMR spectra, analyzing the data, as well as drafting the manuscript.

TABLE OF CONTENTS

ABBREVIATIONS AND ACRONYMS **6**

ABSTRACT **9**

ZUSAMMENFASSUNG **11**

OBJECTIVES AND MOTIVATION **13**

1. INTRODUCTION **17**

1.1. METABOLOMICS 17

1.1.1. Characteristics *17*

1.1.2. Analytical Platforms *17*

1.2. NUCLEAR MAGNETIC RESONANCE (NMR) SPECTROSCOPY 19

1.2.1. Principals of NMR Spectroscopy *19*

1.2.2. 1D and 2D NMR Spectroscopy *22*

1.2.3. Non-Uniform Sampling (NUS) *23*

2. MATERIALS AND METHODS **25**

2.1. SAMPLES 25

2.2. SAMPLE PREPARATION 27

2.3. NMR SPECTROSCOPY 31

2.4. SPECTRAL ANALYSIS 35

2.5. EVALUATION OF QUANTITATIVE RESULTS 37

3. RESULTS **42**

3.1. NUS ON URINE 42

3.1.1. Spike-in Dataset *42*

3.1.2. Cohort Study Samples *52*

3.2. NUS ON CANCER CELLS 56

3.2.1. Supernatants *56*

3.2.2. Methanol Extracts *58*

4. DISCUSSION **60**

4.1. NUS FOR ACCELERATED QUANTIFICATION 60

4.2. NUS FOR ENHANCED SPECTRAL RESOLUTION 67

5. CONCLUSION 69

6. APPENDIX 70

6.1. SUPPLEMENTAL FIGURES 70

6.2. SUPPLEMENTAL TABLES 89

6.3. SIMULATION OF NUS SPECTRA 103

REFERENCES 105

DANKSAGUNG 111

Abbreviations and Acronyms

ANOVA	analysis of variance
BMS	beat-matched sampling
B_0	external magnetic field
B_1	induced high-frequency field
Cas	CRISPR-associated
CKD	chronic kidney disease
CRISPR	Clustered Regularly Interspaced Short Palindromic Repeats
D	deuterium
DRKS	Deutsches Register Klinischer Studien
e.g.	exempli gratia (for example)
COSY	correlation spectroscopy
CS-IRLS	iterative re-weighted least squares compressed sensing method
CS-IST	iterative soft thresholding compressed sensing method
CV	coefficient of variation
FDA	Food and Drug Administration
FID(s)	free induction decay(s)
FT	Fourier Transform
(k)g	(kilo)gram(s)
GCKD	German Chronic Kidney Disease
GFR	glomerular filtration rate
GNC	German National Cohort
γ	gyromagnetic ratio
h	hour(s)
HSQC	heteronuclear single quantum coherence
(M)Hz	(mega)Hertz
i.d.	inner diameter
I	nuclear spin quantum number
$\vec{I}$	nuclear spin angular moment
IST	iterative soft thresholding
k	thousand
K	Kelvin
kDa	kilodalton
(m)L	(milli)liter(s)
LDHA	lactate dehydrogenase A

LLOQ(s)	lower limit(s) of quantification
LOD	limit of detection
(m)M	(milli)molar
MaxEnt	maximum entropy
(R-)MDD	(recursive) multidimensional decomposition
min	minute(s)
mmol	millimole(s)
$\vec{\mu}$	magnetic moment
µL	microliter
µM	micromolar
$\vec{M}$	bulk magnetization
m^2	square meters
n	number
NMR	nuclear magnetic resonance
NOESY	nuclear Overhauser enhancement spectroscopy
NS	number of scans
NUS	non-uniform sampling
p	probability value
pH	power of hydrogen
pmol	picomole
ppm	parts per million
RF	radiofrequency
s	second(s)
(R)SD	(relative) standard deviation
shRNA	small hairpin ribonucleic acid
S/N	signal-to-noise ratio
sPGS	sinusoidal Poisson-gap sampling
t	time
T	temperature
t_1	interpulse delay
t_2	direct time domain
T_1	spin-lattice relaxation time
T_2	spin-spin relaxation time
TOCSY	total correlation spectroscopy
TSP	3-trimethylsilyl-2,2,3,3-tetradeuteropropionate
US	uniform sampling
w/v	weight per volume

× g	gravitational acceleration
°C	degrees Celsius
1D	one-dimensional
2D	two-dimensional
^{1}H	hydrogen-1
^{13}C	carbon-13

Abstract

INTRODUCTION. Non-uniform sampling (NUS) accelerates the acquisition of otherwise uniformly sampled (US) multidimensional NMR spectra which offer higher resolution than 1D ^{1}H spectra but need considerably longer measurement times. NUS in metabolomics so far has been primarily tested on pure samples or synthetic model mixtures containing predefined metabolites in non-physiological concentrations. Hence, the first aim of this contribution was the systematic quantitative evaluation of the impact of various NUS parameters on the accuracy and precision of 2D NMR measurements of endogenous metabolites in urine specimens. After having optimized and validated various NUS parameters regarding acquisition and processing, NUS was applied to a set of clinically interesting urine specimens to accelerate the acquisition of urine spectra compared to the US equivalent. As NUS can alternatively be implemented to enhance the spectral resolution, its effect on spectral analysis with respect to the time-equivalent US spectra were qualitatively and quantitatively assessed. Afterwards, enhanced resolution NUS spectra were employed with respect to NUS for accelerated quantification for the analysis of cancer cell lines.

METHODS. First, the performance of various NUS parameters was assessed in the context of accelerated quantification in comparison to US. To this end, six endogenous metabolites typically found in urine were spiked into a urine matrix at physiological concentrations. Urine aliquots were spiked with varying concentrations (15.6 - 500.0 µM) of tryptophan, tyrosine, glutamine, glutamic acid, lactic acid, and threonine which can only be resolved fully by 2D NMR. The impact of different reconstruction algorithms, sampling schemes, and seed values on the fraction of indirect points that might be omitted were analyzed. Both ^{1}H,^{1}H-TOCSY (total correlation spectroscopy) and ^{1}H,^{1}H-COSY45 (correlation spectroscopy) NMR experiments were chosen as spectral types. Afterwards, cohort study urine specimens from the German Chronic Kidney Disease (GCKD) and German National Cohort (GNC) studies were taken as a realistic biomedical application to implement the optimized NUS parameters. Employing urine from the GNC study, the applicability of optimized NUS for enhanced spectral resolution was investigated. Finally, supernatants and methanol extracts of two cancer cell lines modified in lactate dehydrogenase A (LDHA) expression were collected to quantitatively assess

optimized NUS for enhanced resolution compared to NUS for accelerated quantification.

RESULTS. It is demonstrated that a reduction to 50% of the US measurement time is feasible for both types of homonuclear 2D NMR spectra when taking sinusoidal Poisson-gap sampling (sPGS) and a compressed sensing approach (CS-IRLS) for spectral reconstruction. Furthermore, the suitability of applying NUS for accelerated quantification of urinary metabolites in the context of cohort studies is shown as there is overall a high concordance in obtained results between the NUS and US spectra. When choosing NUS to enhance the spectral resolution in the selected urine specimen, peak analysis compared to the time-equivalent US spectra benefits from better-resolved peak shapes, newly emerged peaks, and separation of overlapping peaks. Analysis of the cancer cell samples demonstrates for most selected metabolites comparable results between time-reduced and enhanced-resolution NUS spectra but for glutamic acid more reliable quantitative results by means of enhanced-resolution NUS.

DISCUSSION. Given the optimized parameters, applying NUS can obtain comparable quantitative results as with conventional sampling in half the acquisition time. However, as NUS reduces the sensitivity, reliable quantitative results are given only if sensitivity is not limited. In case that NUS is applied for enhanced spectral resolution more and sharper peaks are obtained in comparison to the time-equivalent US spectrum aiding quantitative analysis.

CONCLUSION. The present study demonstrates that optimized NUS provides a suitable alternative to conventionally acquired 2D NMR spectra given complex biological mixtures allowing a considerably reduced measurement time of metabolites given sufficient sensitivity or increased spectral resolution for improved compound analysis. Therefore, NUS allows the application of 2D NMR spectroscopy to large cohort studies comprising up to thousands of samples.

Zusammenfassung

EINLEITUNG. Non-uniform sampling (NUS) beschleunigt die Aufnahme von anderenfalls uniform gesampelten (US) multidimensionalen NMR Spektren, die eine erhöhte Auflösung gegenüber 1D ^{1}H Spektren bieten, aber erheblich längere Messzeiten fordern. NUS in der Metabolomik wurde bisher primär an Reinsubstanzen oder synthetischen Modell-Mischungen mit vordefinierten Metaboliten in nicht-physiologischen Konzentrationen getestet. Daher war die Absicht hier zunächst systematisch den Einfluss von diversen NUS Parametern auf die Genauigkeit und Präzision von 2D NMR Messungen von endogenen Metaboliten in Urinproben quantitativ zu evaluieren. Nachdem verschiedene Aufnahme- und Prozessierungsparameter von NUS optimiert und validiert wurden, wurde zeit-reduziertes NUS im Vergleich zum linear aufgenommenen US Pendant auf ein Set von klinisch interessanten Urinproben angewandt. Außerdem wurde untersucht, wie sich eine Erhöhung der spektralen Auflösung über NUS qualitativ und quantitativ im Vergleich zu zeitäquivalenten US Spektren auswirkt. Anschließend wurden auflösungserhöhte im Vergleich zu zeitreduzierten NUS Spektren herangezogen, um Krebszelllinien zu analysieren.

METHODEN. Zuerst wurde die Verwendung verschiedener NUS Parameter für die beschleunigte Quantifizierung im Vergleich zu US beurteilt. Dabei wurden sechs typischerweise in Urin vorkommende endogene Metabolite in physiologischen Konzentrationen zu einer Urinmatrix hinzugegeben. Hierzu wurden Urinaliquote mit unterschiedlichen Konzentrationen (15.6 - 500.0 µM) von Tryptophan, Tyrosin, Glutamin, Glutaminsäure, Milchsäure und Threonin versetzt, deren Signale in Gänze nur mit 2D NMR aufgelöst werden können. Es wurde der Einfluss verschiedener Rekonstruktionsalgorithmen, verschiedener Schemata der Datenkollektion und der Einfluss von Variationen in den Positionen der ausgewählten Datenpunkte auf den Anteil der indirekten Punkte, die ausgelassen werden können, untersucht. Als Spektrentypen wurden sowohl ^{1}H,^{1}H-TOCSY (total correlation spectroscopy) als auch ^{1}H,^{1}H-COSY45 (correlation spectroscopy) NMR Experimente verwendet. Anschließend wurden Urinproben der German Chronic Kidney Disease (GCKD) und German National Cohort (GNC) Studien herangezogen, um die optimierten NUS Parameter für eine realistische biomedizinische Anwendung zu implementieren. Urin der GNC Studie wurde ausgewählt, um optimiertes NUS zur erhöhten spektralen

Auflösung zu verwenden. Schließlich wurden Überstände und Methanolextrakte zweier Krebszelllinien, deren Laktatdehydrogenase A (LDHA) Expression modifiziert war, gesammelt, um optimiertes NUS zur Erhöhung der spektralen Auflösung im Vergleich zu NUS zur schnelleren Aufnahme quantitativ zu bewerten.

ERGEBNISSE. Es wird gezeigt, dass für beide Typen von homonuklearen 2D NMR Spektren eine Reduzierung auf 50% der US Aufnahmezeit praktikabel ist, wenn ein sinusförmiges Poisson-gap sampling (sPGS) und ein compressed sensing-basierter (CS-IRLS) Ansatz für spektrale Rekonstruktion gewählt wird. Weiterhin wird die Eignung von NUS für die beschleunigte Quantifizierung von Urinmetaboliten im Kontext von Kohortenstudien anhand einer insgesamt hohen Übereinstimmung zwischen NUS und US Spektren gezeigt. Wenn NUS zur Erhöhung der spektralen Auflösung der ausgesuchten Urinprobe gewählt wird, begünstigt dies die Metabolitsignalanalyse im Vergleich zum zeitäquivalenten US Spektrum durch besser aufgelöste Signalformen, neu aufgetauchte Signale und die Auftrennung überlappender Signale. Die Analyse der Krebszellprobe ergibt für die meisten der gewählten Metabolite vergleichbare quantitative Ergebnisse zwischen zeitreduzierten und auflösungserhöhten NUS Spektren, allerdings für Glutaminsäure eine verlässlichere Quantifizierung mittels auflösungserhöhten NUS Spektren.

DISKUSSION. Mit den optimierten NUS Parametern können mit NUS vergleichbare quantitative Ergebnisse zu US in der Hälfte der Aufnahmezeit erzielt werden. Allerdings, da NUS die Sensitivität verringert, können verlässliche quantitative Ergebnisse nur erzielt werden, wenn die Sensitivität nicht beschränkt ist. Wenn NUS zur Erhöhung der spektralen Auflösung genutzt wird, können im Vergleich zum US in der gleichen Messzeit sowohl mehr als auch schärfere Signale erhalten werden, welches die quantitative Analyse begünstigt.

FAZIT. Die vorliegende Studie zeigt, dass NUS eine geeignete Alternative zu konventionell aufgenommenen 2D NMR Spektren von komplexen biologischen Mischungen bietet, was eine maßgebliche Reduzierung der Aufnahmezeit von Metaboliten bei ausreichender Sensitivität oder eine erhöhte spektrale Auflösung für eine verbesserte Komponentenanalyse bietet. Somit ermöglicht NUS die Anwendung von 2D NMR Spektren für große Kohortenstudien mit bis zu mehreren tausend Proben.

Objectives and Motivation

Two-dimensional (2D) nuclear magnetic resonance (NMR) spectra provide increased resolution of complex mixtures such as urine and cell extracts compared to one-dimensional (1D) ^{1}H spectra suffering from considerable spectral overlap. The chemical shift region of 0.7 - 4.7 ppm in ^{1}H NMR spectra of human urine is especially highly populated with signals from low molecular weight compounds giving rise to considerable peak overlap.[1] Therefore, 2D NMR spectroscopy is beneficial for metabolite identification and quantification, albeit at the price of considerably extended acquisition times over 1D NMR spectroscopy. In conventional 2D NMR spectroscopy, indirect data points are sampled at evenly spaced intervals with their spacing dictated by the Nyquist theorem where the last data point determines the achieved spectral resoulution.[2] For good spectral resolution this in turn requires the acquisition of a large amount of data points leading to long measurement times. A possible solution allowing the accelerated acquisition of multidimensional NMR spectra is non-uniform sampling (NUS), which acquires indirect data points in a non-linear fashion. Here, only a subset of the data points acquired in conventional 2D NMR is measured and the remaining data points are reconstructed.[3] As the resulting system is underdetermined, additional assumptions are required for faithful spectra reconstuction.[4] This is one of the main aspects in which the various available reconstruction algorithms differ.[5] With respect to data sampling also a variety of sampling schemes are in common use.[6] NUS has been originally developed for the accelerated acquisition of multidimensional protein NMR spectra as three- and four-dimensional NMR spectra may take several days of measurement time and, therefore, are particularly time consuming to acquire.[7] Numerous other approaches which may be combined exist to reduce the experimental time differing on the underlying strategy, for instance linear prediction or ultrafast.[8] An alternative to NUS which also may be used in combination with NUS is linear prediction. Here, the measured time-domain signal is extended by *in silico* methods assuming the exponential behavior of the time domain signals to increase spectral resolution.[8] In metabolomics, non-uniform sampling (NUS) has been shown to speed up considerably the acquisition of multidimensional nuclear magnetic resonance (NMR) spectra.[9-12] Additionally, the use of relaxation enhancing agents can even further

expedite spectral data acquisition.[13] Furthermore, NUS in metabolomics has in part been applied to enhance the spectral resolution of the indirect dimension.

So far in metabolomics, NUS has been primarily tested on standard mixtures of selected metabolites in often non-physiological concentration ranges.[9,11,14] The aim of this study was to find for realistic biomedical specimens the optimal combination of experimental parameters and reconstruction algorithm that would allow a noteworthy reduction in measurement time while maintaining quantitative accuracy and precision. First, NUS was implemented to reduce the experimental time for accelerated metabolite quantification. Throughout the study, urine was used as a complex biological matrix to systemically compare various parameters affecting the quantitative performance of NUS. Urine is one of the most complex biological fluids in composition typically containing hundreds of different solutes[1] that can only be resolved in part by one-dimensional (1D) ^{1}H NMR. As 2D NMR is beneficial for the quantitative analysis of complex mixtures,[15] the performance of NUS was assessed on urine conducting homonuclear ^{1}H,^{1}H-TOCSY (total correlation spectroscopy) and ^{1}H,^{1}H-COSY45 (correlation spectroscopy) experiments. The parameters tested included the choice of the reconstruction algorithm, sampling scheme, amount of omitted data points, spectra type, and seed value, the latter initiating a pseudo-random number generator to set the sequence of indirect data points to be collected.[16] In total, four reconstruction algorithms, three sampling schemes, two spectra types, three different levels of sparse sampling, and up to six seed values were tested. As an experimental setup, six urinary metabolites were spiked into a urine specimen as a background matrix at six levels spanning a 32-fold change in physiological concentration. The optimized parameters were afterwards validated on a second urinary spike-in dataset.

Next, the best combination of acquisition parameters was applied to the determination of differences in urinary metabolite levels between apparently healthy subjects and patients suffering from chronic kidney disease (CKD). CKD, defined by an abnormal kidney structure or function affecting health lasting for more than three months,[17] stands at the end of several renal and systemic diseases,[18] representing a global health burden with a prevalence of about 10% (2013) of adults.[19] Structural and functional abnormalities of the kidney are associated among others with an

elevated risk of cardiovascular disease, renal failure, and mortality.[19] Physiologically, CKD is present given a reduced glomerular filtration rate (GFR) of below 60 mL/min per 1.73 m^2 and/or increased urinary albumin secretion.[19] As the measurement of the GFR is cumbersome and impractical, its values are usually estimated,[20] either by the use of serum creatinine or cystatine C levels or a combination of both.[21] High-risk factors for CKD are among others diabetes and hypertension,[19] the former being the main reason for worldwide increased occurrence of CKD.[22] Kidney disease resulting from diabetes known as diabetic nephropathy[23] has been shown to be among the three leading causes of CKD.[24] Metabolomic analysis of urine allows to study metabolites closely correlated with kidney function.[25] As for this, urine specimens from patients suffering from chronic kidney disease were analyzed in comparison to urine specimens from apparently healthy subjects for a realistic application of the optimized NUS parameters.

In the last part of this contribution, NUS was applied to enhance the spectral resolution in the indirect dimension. After having assessed metabolite signals in a selected urine specimen in comparison to the time-equivalent US spectrum, enhanced resolution NUS was applied to study the effect of an altered lactate dehydrogenase A (LDHA) expression on metabolite levels in supernatants and methanol extracts of two cancer cell lines. Cancer is responsible for approximately 20% of all deaths in the Western population with about 90% of human deaths from cancer due to distant establishments of tumor cells, so-called metastases.[26,27] Cancer is a malignant tumor, the latter characterized by growth and uncontrolled proliferation of an abnormal cell, having the ability to invade surrounding tissue.[28] Factors influencing the development of cancer include age, lifestyle, environment, and hereditary background.[26] Cancer cells adjust their energy metabolism to meet the demand for continuous cell growth and proliferation, thereby deregulating cellular energetics known as one of the emerging hallmarks of cancer.[29] Proliferating cells show an increased demand for glucose, amino acids, nucleotides, and lipids to generate biomass.[30] Compared to normal cells which rely on oxidative phosphorylation for energy production, cancer cells rely on aerobic glycolysis generating lactate from glucose despite the presence of oxygen, known as “the Warburg effect”.[30] Characteristic for aerobic glycolysis are upregulations of LDHA, being essential for converting pyruvate to lactate, and the plasma membrane glucose

transporter 1 (GLUT1).[31,32] Monocarboxylate transporters (MCTs) export lactate together with associated protons into the tumor microenvironment where lactate accumulates[31] leading to its acidification[32,33] associated with an increased metastatic potential and immune cell suppression.[31,34] Avoiding immune destruction, especially by T and B lymphocytes, macrophages, and natural killer cells, is the second so-called emerging hallmark of cancer.[29] The occurrence of great amounts of extracellular lactate is a general trait of cancer cells[35] and high LDHA expression is associated with a poor prognosis.[31] Targeting LDHA as a key metabolic control point in aerobic glycolysis is therefore promising as a potential cancer therapy[30] to decrease secreted levels of lactic acid to diminish metastasis and reestablish the antitumor immune response.[36] Previous *in vitro* studies have shown that inhibiting LDHA in multicellular tumor spheroids by means of oxamic acid lowered lactic acid concentrations preventing suppression of human cytotoxic T lymphocytes;[37] furthermore, knocking-down LDHA inhibited glioma cell migration.[38] *In vivo* mouse models could show that reducing LDHA expression decreased tumorigenesis in non-small cell lung cancer[39] and tumor growth rate in mammary tumor.[40] Hence, alternating the expression of LDHA is a promising approach in cancer therapy.

1. Introduction

1.1. Metabolomics

1.1.1. Characteristics

Metabolomics belongs to one of the various “-omics” approaches in systems biology.[41] Compared to other “-omics” technologies like genomics, proteomics, and transcriptomics analyzing the respective variabilities upstream of metabolites, metabolomics allowing to contribute an intergrated profile of the biological status.[42] To enable among others to relate metabolic changes to pathophysiological processes,[43] metabolomics aims at the comprehensive analysis of all metabolites in a biological system revealing its metabolome comprising compound identification and quantification.[44] Biological matrices applied in NMR-based metabolomics are for instance biofluids like urine, plasma or serum and cells or tissues.[45] Metabolites are small molecules of typically low molecular-weight (< 1.5 kDa),[22,46] originating either from an endogenous or exogenous source.[47] Metabolites comprise a wide range of compound classes and are largely different in size and polarity[22] with concentrations spanning up to nine orders of magnitude (pmol to mmol).[48] Functions of metabolites include being involved in signaling, energetics, and as parts of biopolymers.[46]

Metabolomics is separated into targeted and untargeted approaches, the latter further divided into metabolic profiling and metabolic fingerprinting.[49] In targeted metabolomics, known metabolites of given pathway(s) are selectively quantified compared to untargeted metabolomics, which is the global analysis of all metabolites.[49] In metabolic profiling, certain classes of compounds are analyzed, while in metabolic fingerprinting metabolic patterns are measured.[49]

1.1.2. Analytical Platforms

Typically, NMR spectroscopy or hyphenated mass-spectrometry (MS) like liquid chromatography-MS (LC-MS) or gas chromatography-MS (GC-MS) are applied in metabolomics.[41,50] Both platforms allow the information-rich simultaneous analysis of a wide range of metabolites different in compound class and chemistry given high

analytical precision.[41] Besides being a unique spectroscopic method allowing structural elucidation at atomic level,[3] NMR spectroscopy enables the simultaneous detection of all compounds in a sample containing the nucleus of interest in a single measurement given sufficient compound concentration. On the contrary, MS techniques often require specific column selection for different substance classes.[41] Compared to MS, NMR spectroscopy is non-destructive to the sample and highly robust.[41] Disadvantages of NMR spectroscopy are that it requires relatively large sample volumes of about 500 µL and that it is limited in sensitivity with a lower limit of detection (LOD) of approximately 1-5 µM.[51] In comparison, MS requires only low µL sample volumes with detection limits in the picomolar range.[41] Given the different strengths and weaknesses of both technologies, the two approaches do not compete but complement each other.[41,52]

1.2. Nuclear Magnetic Resonance (NMR) Spectroscopy

1.2.1. Principals of NMR Spectroscopy

NMR spectroscopy is a spectroscopic technique which uses electromagnetic radiation in the radiofrequency range absorbed and emitted by magnetic nuclei to provide information about the sample of interest.[53] Nuclei with a spin, meaning a spinning motion of electrical charge inducing magnetism,[53] non-equal to zero are NMR-active.[53] The composition of the nucleus determines the nuclear spin.[54] The spin distribution results in a magnetic moment $\vec{\mu}$[54] given by:

$$\vec{\mu} = \gamma \vec{I} \qquad (1)^{54}$$

$\vec{I}$ = nuclear spin angular moment

The gyromagnetic ratio *γ* describes in this context the ratio between the magnetic moment of the nucleus and its spin angular momentum.[55] In presence of a strong external magnetic field B_0, nuclei with a nuclear spin quantum number I = ½ take two different spin states.[7] Positive values of +½ correspond to the lower energy level parallel to the external magnetic field and negative values of -½ denote the higher energy level anti-parallel to B_0.[7] The energy difference between both spin states is given by[54]:

$$\Delta E = \gamma B_0 \qquad (2)^{54}$$

At thermal equilibrium, the macroscopic magnetic moment is aligned along B_0 in *z*-direction (Figure 1, left panel).[54] The population difference between the spin energy levels with the α-state being more occupied than the β-state is described by the Boltzmann distribution[7] as:

$$\frac{n_\alpha}{n_\beta} = e^{\left(\frac{\Delta E}{k_B T}\right)} \qquad (3)^{7}$$

n_α = number of nuclei in parallel orientation

n_β = number of nuclei in anti-parallel orientation

k_B = Boltzmann constant

T = temperature

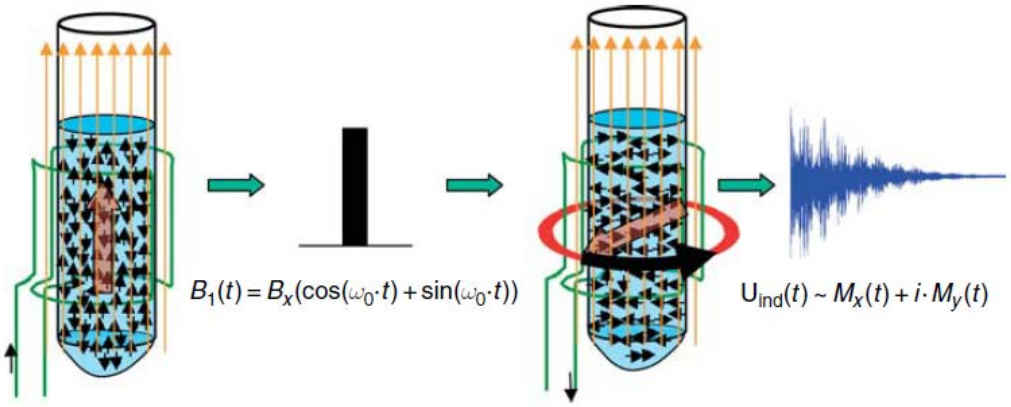

Figure 1. NMR-signal detection. Left panel: When placed into a strong external magnetic field (orange arrows), the spins (black arrows) in the sample align along B_0. Right panel: After applying a high-frequency B_1 field (black bar representing a 90° pulse with the respective equation), the macroscopic magnetization M_0 (transparent red) given at thermal equilibrium aligns along the *x*-axis of the B_1 field, precessing around B_0 (red). This induces a voltage U_{ind} (dark blue) in the detection coil (green) described by the respective equation. Reprinted from Ross *et al.* 2007[54] with permission from Elsevier (http://www.elsevier.com).

As the population difference between the two nuclear energy levels is small at room temperature, NMR is a method of relatively low sensitivity.[49]

During pulsed NMR experiments, a short high-frequency B_1 field (90° pulse) in the orders of several microseconds is applied, transferring the bulk magnetization $\vec{M}$ from the *z*-axis to the *xy*-plane where $\vec{M}$ rotates around B_0 after the radiofrequency (RF) field has been turned off.[54,55] The required frequency of the applied B_1 field is given by the following equation which is equal to the rotation frequency, the so called lamor frequency, of $\vec{M}$ in the *xy*-plane[7]:

$$\Delta E = h\nu \qquad (4)^{7}$$

h = Planck's constant

The rotation of $\vec{M}$ induces a voltage (U_{ind}) in the spectrometer's detection coil (Figure 1, right panel).[7,54] These electrical signals are observed as NMR signals,[7] collected as free induction decays (FIDs)[53] which are time-varying resonances approximated as a superposition of sine-waves.[5] Once the B_1 field is turned off, the nuclei relax back to their equilibrium spin state population.[53] Two different relaxation processes occur, being the T_1 or spin-lattice relaxation time needed to restore the equilibrium and the T_2 or spin-spin relaxation time for the loss of magnetization coherence to take place.[53]

The decay rate of the time domain signal defines the signal envelope.[56] To transfer the FIDs from the time domain into the frequency domain, a Fourier transform (FT) is applied giving rise to a spectral representation of the NMR signals.[53] Here, the signal intensities are distributed according to the nuclear resonant frequencies influenced by their chemical environment.[53]

The peaks in the spectrum give information about the sample, such as the kind of nuclei present and in which concentration, their chemical environment as well as structural knowledge like bondage connectivities.[3] Due to a molecule's surrounding electron clouds, the spin's local magnetic field is altered compared to B_0.[54] Consequently, the resonant frequency or chemical shift of a nuclear spin is influenced by its electronic/chemical environment.[54] The chemical shift is denoted in parts per million (ppm) relative to the internal reference[53] and by division through the spectrometer reference it becomes independent of the B_0 field applied. The spectral width is the ppm range covered by the experiment.[53] Typically, ^{1}H nuclei cover a spectral width of 15 ppm.[54] When two spins interact or couple, they mutually influence the spin's energy level.[53,54] If both spins interact through bonding electrons, this is called scalar (*J*-) coupling.[7] Spin-spin coupling splits the NMR signals up in characteristics multiplet splitting patterns.[53]

Central issues in reliable quantitative NMR are sensitivity and resolution.[7,51] The sensitivity of a measurement, defined by the signal-to-noise ratio (S/N), is dependent among others on the number of spins in the sample, the γ of a given nucleus, the strength of B_0, and the temperature of the wires of the detection coil and the preamplifier.[54] Cryogenic probe heads which reduce the thermal noise from the spectrometer's electronics may improve the S/N by up to a factor of five[41] by substantially cooling down both detection coil and preamplifier. The peak integral is proportional to the number of NMR-active nuclei in a sample.[54] As the natural abundance of ^{1}H denotes 99.98% while it lies at 1.11% for ^{13}C, sensitivity is lower in ^{13}C than in purely ^{1}H-based spectra.[7] By repeating the FID acquisition and consequent summation given by the number of scans (NS), the S/N increases with the signal being proportional to the NS while the noise increases according to $\sqrt{NS}$.[7,54] The spectral resolution needed to separate two lines in the frequency domain determines the sampling time of the FID.[7] Improved resolution ultimately results in sharper signals and increased S/N, this way aiding peak analysis.[14] A fast

decay of the FID resulting for instance from rapid (T_2) relaxation leads to broad line widths and hence poor resolution.[7]

1.2.2. 1D and 2D NMR Spectroscopy

While 1D NMR spectra depict signal intensities in one frequency dimension, 2D NMR techniques separate signals in two frequency dimensions mapping correlations involving two nuclei.[7] Heteronuclear spectra provide knowledge on interactions between two different types of nuclei, like ^{1}H-^{13}C correlations, while homonuclear spectra show interactions between nuclei of the same type, for example ^{1}H-^{1}H correlations.[7] Heteronuclear ^{1}H-^{13}C HSQC (heteronuclear single quantum coherence) spectra, for instance, are based on the scalar coupling between directly bound ^{1}H and ^{13}C nuclei.[54] In 2D homonuclear experiments, peaks along the diagonal of the spectrum, referred to as diagonal peaks, are equivalent to signals observed in a 1D spectrum, while off-diagonal signals, or cross peaks, being the signals of interest arise due to the transfer of coherence between spins.[7] In ^{1}H-^{1}H TOCSY spectra, cross peaks appear for proton correlations within the same spin system given that the *J*-coupled protons reside within a continuous bondage chain.[7] Cross peaks in ^{1}H-^{1}H COSY spectra show that two ^{1}H spins being two or three bonds apart underwent scalar coupling.[7]

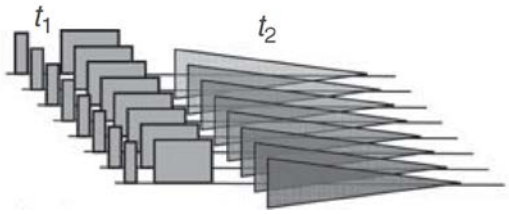

Figure 2. Concept of 2D NMR spectroscopy. During a 2D NMR experiment, a series of 1D spectra is acquired while incrementing the t_1 evolution delay detected in t_2. Reprinted from Ross *et al.* 2007[54] with permission from Elsevier (http://www.elsevier.com).

For a 2D NMR experiment, a set of 1D spectra is measured while systematically incrementing the evolution time t_1 (Figure 2).[54] Considering a coupled two-spin system, the frequency of the first spin is thereby encoded as a modulation of the intensity of the second spin which is detected during the acquisition time t_2.[8]

Following FT with respect to t_1 and t_2, a 2D spectrum comprised of two frequency dimensions is obtained.[54]

1D ^{1}H NMR experiments are among the most commonly applied in NMR based metabolomics.[57] 1D ^{1}H NMR spectra are short in acquisition time but characterized by peak overlap especially in complex mixtures hampering spectral analysis.[46] The acquisition of multidimensional NMR spectra provides increased spectral resolution and, thus, reduced spectral overlap.[46,58] Hence, 2D NMR spectra offer a better separation of resonances because frequencies are spread out into two orthogonal dimensions but take prolonged measurement times.[15] While 1D ^{1}H NMR spectra are typically acquired in minutes, 2D NMR experiments may take several hours.[59] The experimental time needed for 2D NMR experiments to obtain sufficient digital resolution in the indirect dimension is dependent on the number of t_1 increments collected.[11] Long acquisition times may cause spectral artifacts like t_1 noise due to spectrometer instabilities,[9] are impractical for large cohort studies, and are not suited for unstable molecules.[9] Therefore, utilizing 2D NMR for metabolomics is limited in sample size due to time constraints.[52]

1.2.3. Non-Uniform Sampling (NUS)

The acquisition of multidimensional NMR spectra in the conventional way is performed by uniformly collecting all data points in the indirect dimension(s) called uniform sampling (US).[7] US is dictated by the Nyquist Theorem ensuring that the frequencies of NMR signals within a defined frequency range are correctly detected.[2,7] The time interval or sampling rate between the data points acquired in the FID, known as dwell time, is inversely proportional to the spectral width being the difference between the highest and lowest frequency to be detected.[7] In this context the last data point determines the achieved resolution.[7] As data points are sampled at regular intervals, resolution is determined by the amount of sampled data points. The same holds true for the indirect dimension where each data point, known as increment, corresponds to a separate 1D spectrum.[15] As the experimental time needed is proportional to the number of increments collected to obtain high resolution in the indirect dimension, the experimental time increases with the number of increments acquired.[60] Alternative sampling methods have been proposed over the

past years to reduce the acquisition time, such as non-uniform sampling (NUS).[16] NUS, also called non-linear or sparse sampling,[61] picks only a fraction of the indirect data points (Figure 3).[3] A constraint of the FT is, however, that it requires the collection of equidistant time-domain data points.[62] Consequently, the data points missing from NUS have to be reconstructed by non-Fourier methods.[7]

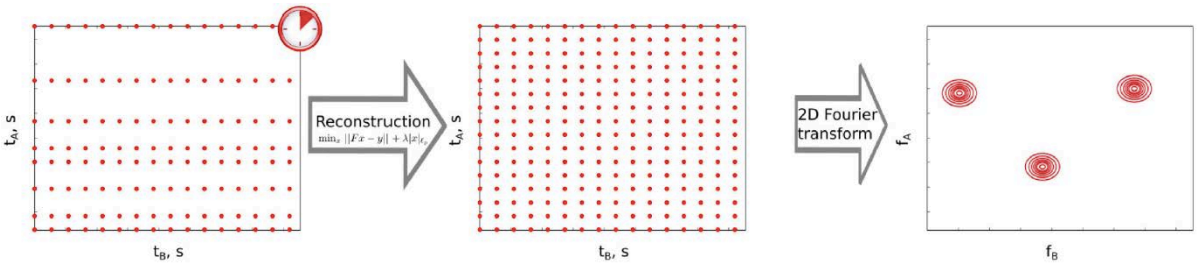

Figure 3. Principal of the time-saving sampling method NUS for a 2D NMR experiment, here exemplarily utilizing a compressed sensing-based reconstruction method of the omitted sampling points followed by Fourier transform. A and B stand for the indirect and direct dimensions, respectively, of the time (t) and frequency (f) domain. Figure reprinted from Dass *et al.* 2017.[3]

The most common implementation of NUS is to accelerate the acquisition time compared to uniform sampling.[63] Compared to time-equivalent US spectra, NUS can furthermore be implemented to enhance the spectral resolution in the indirect dimension or increase the sensitivity or even a mixture of these measures simultaneously.[60] NUS has been initially developed for the NMR analysis of proteins[57] as the widespread acquisition of three-dimensional spectra of these biomolecules may take days with linear sampling.[7] Subsequently, NUS has been successfully applied in this context[64,65] as well as in metabolomics.[11,13]

2. Materials and Methods

2.1. Samples

Urine specimens were used for the generation of spike-in samples to assess NUS for the accelerated quantification of metabolites. Compared with other sample types like serum, plasma, cells or tissue samples, urine generally comprises considerably more metabolites detectable by NMR spectroscopy.[66] Spectral complexity arises from various endogenous and exogenous compound composition influences as well as differences in pH value and salt concentrations that can affect the peak position.[66] The initial urine specimen (urine I) from an apparently healthy female volunteer of the German National Cohort (GNC) had a relatively low[67] creatinine concentration (3.31 ± 0.07 mM) and, thus, an overall relatively low content of solutes. The spike-in dataset based on this specimen was utilized to determine the best combination of parameters for the usage of NUS. To address the effect of differences in matrix composition on the finally chosen NUS conditions, a second, analogous spike-in dataset was generated for another urine specimen (urine II) of the GNC cohort[68] featuring a higher creatinine concentration (20.94 ± 0.27 mM) than urine I. This urine specimen was also used for experiments regarding the enhancement of spectral resolution by NUS. To investigate NUS in context of a biomedical application, 28 urine specimens each were randomly chosen from the GNC study and the German Chronic Kidney Disease (GCKD) study,[24] respectively. In course of the GNC study a random sample of the general population was drawn. The external Ethics Advisory Board of the German National Cohort accompanied all study procedures. The ethics committees of the corresponding study centers provided approvals for all study procedures; written informed consent was obtained from all participants. The GCKD study is a prospective cohort study of patients with CKD treated by nephrologists. It was approved by the local ethics committees and registered in the national registry for clinical studies (DRKS 00003971). Between 2010 and 2012, 5,217 eligible adult patients provided written consent and were enrolled into the study.[24] The study was carried out in accordance with relevant guidelines and regulations. The characteristics of the subjects investigated are provided in Table 1.

Table 1. Characteristics of cohort study participants. Baseline and pre-test characteristics of subsets of individuals with chronic kidney disease enrolled in the German Chronic Kidney Disease (GCKD) study or healthy subjects from the German National Cohort (GNC) study, respectively, whose urine specimens were measured with the optimized NUS parameters. Abbreviations: ACE-I, angiotensin-converting enzyme inhibitor; ACR, albumin/creatinine ratio; ARB, angiotensin receptor blocker; BMI, body mass index; BP, blood pressure; $eGFR_{cr}$, estimated glomerular filtration rate from serum creatinine; mmHG, millimeter of mercury; NA, not available. Published in von Schlippenbach *et al.* 2018.[69]

Characteristic	Chronic Kidney Disease	Healthy
sample size, *n*	28[a]	28
men, %	46.43	53.57
age[b], years	58.71 ± 12.09	52.61 ± 11.77
BMI[b], kg/m²	30.59 ± 6.17	25.51 ± 3.39
systolic BP[b], mmHg	139.21± 19.36	126.93 ± 19.57
diastolic BP[b], mmHg	76.93 ± 8.79	81.96 ± 12.94
serum creatinine[b], mM	0.12 ± 0.03[c]	0.09 ± 0.02 (8 NA)[d]
$eGFR_{cr}$[b,e,f], mL/min per 1.73 m²	54.40 ± 21.77	80.84 ± 18.33 (8 NA)
ACR[g], mg/g	239.18 (37.61-1068.76)	NA
treatment with ACE-I or ARB, %	89.29	10.71

[a] proteinuria classification: < 30 mg/L (*n* = 10), 30-300 mg/L (*n* = 6), > 300 mg/L (*n* = 12)
[b] mean ± SD
[c] *n* = 1 quantified relative to 2.05 mM spiked-in formic acid with Chenomx NMR Suite 8.2 from a 1D ^{1}H-NOESY spectrum of the corresponding plasma sample
[d] determined with MetaboQuant 1.3 from 1D ^{1}H-NOESY spectra of the corresponding serum samples
[e] estimated using the CKD-EPI equation[70] without specifying for the black race
[f] n_{GCKD} = 1 and n_{GNC} = 20 calculated from given or determined serum creatinine concentrations
[g] median (interquartile range)

For the application of NUS to quantify cancer cell metabolites *in vitro*, clones of two metastatic tumor models[71,72] were investigated, modified in their LDHA activity shown to secrete reduced amounts of lactic acid compared to the unaffected clone.[31] Cell culture experiments were carried out by the group of Prof. Dr. Marina Kreutz, Department of Internal Medicine III, University Hospital Regensburg. In the affected murine B16.SIY E12 melanoma cells (B16-LDHA^{low}), LDHA expression was knocked down by stable transfection with an LDHA complementary small hairpin RNA (shRNA) plasmid.[31] Corresponding control cells (B16-Ctrl) were treated with a scrambled shRNA.[31] In the affected murine Panc02-H7 pancreatic adenocarcinoma cells (Panc-LDHA^{null}), LDHA was knocked out by means of CRISPR/Cas9.[31] Respective control cells (Panc-Ctrl) underwent an ineffective transfection with

CRISPR/Cas9.[31] Biological triplicates per clone were cultivated each in T-75 cell culture flasks [Eppendorf AG, Hamburg, Germany] in 20 mL RMPI 1640 medium [Life Technologies GmbH, Darmstadt, Germany] supplemented with 10% fetal calf serum [Merck KGaA, Darmstadt, Germany] and 0.5% (w/v) penicillin-streptomycin solution [Thermo Fisher Scientific, Waltham, MA, USA]. The cell culture flasks and a separate flask containing only the medium were given in a CO_2 incubator for 48 h comprised of a humidified atmosphere at 37°C and 5% CO_2 [Thermo Fisher Scientific]. Cells were passaged in total six times seeding 0.4 - 0.5 × 10^6 cells per flask every three to four days. Afterwards, supernatants and pellets from cultivated cancer cells as well as a control cell culture medium sample were provided for further sample preparation.

2.2. Sample Preparation

Separate stock solutions for each spike-in dataset of six endogenous urine metabolites[67] were prepared in water purified by a PURELAB Plus system [ELGA LabWater, Celle, Germany]. Those metabolites were chosen which give overlapping signals in the aromatic and aliphatic regions of 1D ^{1}H NMR spectra but are resolved in 2D ^{1}H,^{1}H TOCSY and ^{1}H,^{1}H COSY45 spectra (Tables 2 and 3).

Table 2. Presence of overlap in 1D ^{1}H spectra. ^{1}H chemical shifts[73] (for pseudouridine H1 according to AMIX-viewer 3.9.13) in ppm of mutually overlapped spike-in and cohort study metabolite signals. Published in von Schlippenbach *et al.* 2018.[69]

Metabolite	Signal assignment	^{1}H chemical shift [ppm]	Overlap with
Tryptophan	H10	7.19	tyrosine
Tyrosine	H5 H9	7.17	tryptophan
Glutamine	H2	3.77	glutamic acid, D-glucose, pseudouridine
Glutamine	H4A|B	2.45	glutamic acid, citric acid
Glutamine	H3A|B	2.13	glutamic acid
Glutamic acid	H2	3.75	glutamine
Glutamic acid	H4B	2.34	glutamine
Glutamic acid	H3A	2.12	glutamine

Glutamic acid	H3B	2.04	glutamine
Lactic acid	H3A|B|C	1.32	threonine
Lactic acid	H2	4.10	pseudouridine
Threonine	H4A|B|C	1.32	lactic acid
Creatinine	H2A|B	4.05	pseudouridine
Hippuric acid	H8	7.62	pseudouridine
Hippuric acid	H2A|B	3.96	pseudouridine, D-glucose
D-Glucose	H1β	4.63	pseudouridine
D-Glucose	H6Bβ	3.89	hippuric acid, pseudouridine
D-Glucose	H4 H6α	3.82	pseudouridine
D-Glucose	H6Bα H6Aβ H3α	3.73	glutamine, pseudouridine
Citric acid	H2A H4A	2.51	glutamine
Pseudouridine	H12	7.66	hippuric acid
Pseudouridine	H1	4.69	D-glucose
Pseudouridine	H3	4.14	lactic acid
Pseudouridine	H4	4.01	creatinine, hippuric acid
Pseudouridine	H5A	3.84	D-glucose
Pseudouridine	H5B	3.72	D-glucose, glutamine

Spike-in metabolites were comprised of glutamic acid, glutamine, lactic acid, threonine, tryptophan, and tyrosine, all purchased from Sigma-Aldrich, Taufkirchen, Germany.

The stocks, prepared in 5 and 10 mL Erlenmeyer flasks [BRAND GMBH + CO KG and DWK Life Sciences GmbH, Wertheim, Germany, respectively], were each geometrically diluted in six steps so that the added amounts of metabolites represented physiological concentration ranges of 15.6 to 500.0 µM (Table 4).[67]

For the preparation of the six spike-in samples of both datasets, all six metabolites were added at varying concentrations to both urine aliquots equally, thereby ensuring that each concentration level was used only once per compound (Table 4). For each of these samples, in total 200 µL spike-in compounds were mixed with 200 µL of the

corresponding urine. For both datasets, an additional blank sample containing 200 µL purified water and 200 µL of the respective urine was generated.

Table 3. 2D signal assignments. ^{1}H,^{1}H-TOCSY and ^{1}H,^{1}H-COSY45 chemical shifts[73] in ppm of metabolite signals used for quantification. Abbreviations: F1, indirect spectral dimension; F2, direct spectral dimension. Published in von Schlippenbach *et al.* 2018.[69]

Metabolite	**^{1}H,^{1}H-TOCSY**		**^{1}H,^{1}H-COSY45**	
	Signal assignment	^{1}H chemical shift in F1/F2 [ppm]	Signal assignment	^{1}H chemical shift in F1/F2 [ppm]
Tryptophan	H10/H9	7.19/7.72	H3B/H2	3.29/4.03
Tyrosine	H6 H8/H5 H9	6.67/7.04	H6 H8/H5 H9	6.67/7.04
Glutamine	H3A|B/H4A|B	2.13/2.45	H3A|B/H4A|B	2.13/2.45
Glutamic acid	H4A|B/H2	2.34/3.76	H3A|B/H4A|B	2.09/2.34
Lactic acid	H3A|B|C/H2	1.32/4.11	H3A|B|C/H2	1.32/4.11
Threonine	H4A|B|C/H2	1.32/3.57	H4A|B|C/H3	1.32/4.24
Creatinine	-	-	H6A|B|C/H2A|B	3.03/4.05
Hippuric acid	-	-	H7 H9/H6 H10	7.54/7.82
D-Glucose	-	-	H1β/H2β	4.63/3.23
Citric acid	-	-	H2A H4A/H2B H4B	2.53/2.63
Pseudouridine	-	-	H3/H2	4.14/4.29

Table 4. Spike-in sample concentrations equivalent in both spike-in datasets. Metabolite concentrations per spike-in sample given in micromolar. Published in von Schlippenbach *et al.* 2018.[69]

Metabolite	**sample**						
	blank	1	2	3	4	5	6
Tryptophan	-	500	15.6	31.3	62.5	125	250
Tyrosine	-	250	500	125	62.5	31.3	15.6
Glutamine	-	62.5	125	250	500	15.6	31.3
Glutamic acid	-	125	250	500	15.6	31.3	62.5
Lactic acid	-	31.3	62.5	125	250	500	15.6
Threonine	-	15.6	31.3	62.5	125	250	500

To determine the lower limits of quantification (LLOQs) and calibration curves of the metabolites quantified in the cohort study urine specimens, calibration samples were prepared. Fourteen calibration levels were generated containing a 400 µL master mix of geometrically diluted stock solutions comprising the selected metabolites over a concentration range from 6.10×10^{-4} mM to 5.00 mM. Exceptions were creatinine and D-glucose spanning concentrations from 2.44×10^{-3} mM to 20.00 mM. Calibration points below 1 mM were measured in triplicates for the determination of LLOQ values in accordance to FDA guidelines.

Both the cancer cell supernatants and medium control sample were ultrafiltrated according to known protocols[74] by means of a 10 kDa molecular weight cutoff Amicon® Ultra-4 centrifugal filter [Merck Chemicals GmbH, Darmstadt, Germany]. First, the filter was prewashed with 3 mL Millipore grade water, centrifuging at 4000 × g given 22°C for 30 min to remove filter-preserving substances. Then taking new 15-mL centrifuge tubes [Greiner Bio-One GmbH, Frickenhausen, Germany], 1000 µl of supernatant and medium each were ultrafiltrated separately, centrifuging at 4000 × g given 4°C for 60 min to remove unwanted macromolecules.[74] Extracts of the cancer cells pellets were obtained by washing the pellets first with 600 µL 80% methanol [VWR Chemicals, Radnor, PA, USA] and then re-extracting twice with 200 µL 80% methanol [VWR Chemicals]. After each step, vortexing for 60 s and centrifuging at 10.000 × g for 5 min given 4°C was performed, in the last step centrifuging at 12.000 × g. The extracts were collected and combined in 4-mL rolled rim amber glass vials [MACHEREY-NAGEL GmbH & Co. KG, Düren, Germany], spiked with 10 µL of 2 mM nicotinic acid [Sigma-Aldrich] as an evaporation loss control and afterwards concentrated in a CombiDancer vortex evaporator [HETTICH AG, Bäch, Switzerland] for 1 h. Consecutively, the residuals were resuspended in 400 µL purified water. For protein quantification after methanol extraction, the FluoroProfile® Protein Quantification Kit [Sigma-Aldrich] was used to prepare the samples according to the manufacturer's protocol. The protein amount was determined with the fluorometer FLUOstar Omega [BMG LABTECH GmbH, Ortenberg, Germany] and the corresponding microplate reader software OPTIMA [BMG LABTECH GmbH].

Standard sample preparation comprised 400 µL of stock solution, urine matrix, filtrate or resuspended dried extracts if not stated otherwise. To this end, 200 µL of 0.1 M

potassium phosphate buffer (K_2HPO_4, 99%, anhydrous, KH_2PO_4, 99%, anhydrous) [Merck KGaA], pH 7.4, containing 3.9 mM boric acid [Merck KGaA] to prevent bacterial growth and 50 µL of 0.75% (w/v) 3-trimethylsilyl-2,2,3,3-tetradeuteropropionate (TSP) in deuterium oxide (99.9% in D) as internal standard [Sigma-Aldrich] were added to each sample.[74] All mixtures, comprised of a constant volume of 650 µL, were transferred to 5-mm i.d. NMR tubes [Bruker BioSpin GmbH, Rheinstetten, Germany or NORELL, Inc., Morganton, NC, USA] and stored at -20°C until measurement.

2.3. NMR Spectroscopy

1D ^{1}H-nuclear Overhauser enhancement spectroscopy (NOESY), 2D ^{1}H,^{1}H-TOCSY, and ^{1}H,^{1}H-COSY45 NMR spectra were acquired, the latter comprised of a 45° mixing pulse.[54] Experiments were performed at 298 K on an Avance III 600 MHz spectrometer [Bruker BioSpin GmbH] employing a cryogenically cooled triple-resonance (^{1}H, ^{13}C, ^{31}P, ^{2}H lock) probe equipped with *z*-gradients and an automatic cooled sample changer. Before measurement, each sample was allowed to equilibrate for 300 s in the magnet. The probe was automatically locked utilizing the frequency of deuterium to ensure that the magnetic field does not change during experiments.[53] Furthermore, the probe was tuned and matched for the coils to efficiently transmit the RF pulses and receive the NMR signals.[7] Shimming was implemented to re-homogenize the B_0 field after the sample had been introduced into the magnet.[53]

NMR data were collected using the ICON-NMR suite of TopSpin 3.1 [Bruker BioSpin GmbH]. The NUS datasets of the spike-in specimens were either directly measured, being the case for the comparison of R-MDD and CS-IRLS, or generated based on an experimental data set, as done for all consecutive comparisons. Simulations of NUS spectra were achieved by selecting the respective data points from a representative US spectrum, employing in-house scripts (section 6.3) specific for each NUS scheme. 1D ^{1}H-NOESY experiments, comprising one of the most common solvent suppression methods in NMR-based metabolomics particularly for biofluids,[45] were conducted with presaturation of the water resonance during relaxation and mixing time as well as additional spoil gradients for optimal water suppression. Four

dummy scans were applied prior to each measurement followed by the acquisition of 128 scans collected into 64k time data points over a total spectral width of 20.55 ppm with a relaxation delay of 4 s, a mixing time of 0.01 s, and an acquisition time of 2.66 s, resulting in a total experimental time of approximately 15 min. For the 2D experiments, solvent suppression was achieved in the ^{1}H,^{1}H-TOCSY and ^{1}H,^{1}H-COSY45 spectra by a water suppression by gradient-tailored excitation (WATERGATE) scheme and by presaturation, respectively. For the US spectra, 2048 × 512 data points were recorded over a total spectral width of 12.07 ppm in ^{1}H,^{1}H-TOCSY and 13.35 ppm in ^{1}H,^{1}H-COSY45 with 8 transients per increment after initially applying 32 dummy scans. Each 2D spectrum was acquired with a relaxation delay of 3 s, a mixing time of 0.06 s (^{1}H,^{1}H-TOCSY) and an acquisition time of 0.14 s for ^{1}H,^{1}H-TOCSY and 0.12 s for ^{1}H,^{1}H-COSY45 spectra, resulting in a total experimental time of approximately 3 h and 35 min per US 2D experiment.

A chosen sampling schedule defines the distribution of the selected NUS data points.[16] Three sparse sampling densities, namely 25%, 50%, and 75% of the t_1 increments from the corresponding US spectrum, were applied to the spike-in samples employing urine I. The sampling patterns implemented were an unweighted, exponentially weighted, and sine-weighted Poisson-gap sampling. The indirect data points were selected randomly to avoid systematic violation of the Nyquist theorem[75] this way reducing sampling artifacts.[76] In the unweighted sampling, also called uniformly random sampling, the increments are evenly chosen along the evolution time.[16] To obtain higher sensitivity, the amount of collected NUS points can be emphasized by weighted sampling to the highest amplitude at the beginning of the indirect FID where signals are the strongest.[62] For an exponentially weighted sampling, the points are selected in an exponential fashion with more points picked at the beginning of the t_1 time domain.[16] Here, the exponentially weighted sampling was set so that it matched the exponential T_2 signal decay of the spike-in metabolites.[77] The indirect data points selected during sinusoidal Poisson gap sampling followed a sine-weighted Poisson distribution with data dense at the beginning of the sampling scheme.[78] Up to six seed values were set to initialize a random number generator. The equally and exponentially weighted sampling schemes were implemented in TopSpin 3.1, the Poisson-gap sampling distribution

was generated with the web-based Schedule Generator Version 3.0.[79,80] The unweighted sampling distributions were generated either with the Stat Trek Random Number Generator[81] or with TopSpin 3.1.

Before Fourier transform, an exponential window function with 0.3 Hz line broadening and zero filling to 128k points was performed on the FID obtained from the 1D NMR experiments.[58] 1D NMR spectra were then automatically phase and baseline corrected, obtaining a flat baseline by implementing the “baseopt” option in TopSpin 3.1.

The indirect data points of the ^{1}H,^{1}H-TOCSY and ^{1}H,^{1}H-COSY45 US and NUS spectra were quadrupled or doubled, respectively, in data points by forward linear prediction on complex data as well as multiplied with a 90° shifted squared sine-bell and an unshifted sine-bell window function, respectively. Phase sensitive ^{1}H,^{1}H-TOCSY spectra were manually phase corrected, while ^{1}H,^{1}H-COSY45 spectra were acquired in magnitude mode and therefore required no phase correction. Non-uniformly obtained ^{1}H,^{1}H-TOCSY spectra were processed with a Hilbert transformation to generate the missing imaginary part from the real part before phase correction. ^{1}H,^{1}H-TOCSY and ^{1}H,^{1}H-COSY45 spectra were baseline corrected using a polynomial baseline correction of degree 5 or 2, respectively, thereby excluding the solvent area (4.5 - 5 ppm) and for ^{1}H,^{1}H-TOCSY spectra also the reference signal TSP (0.5 - 0 ppm) to prevent influence of baseline distortion.

Non-uniformly sampled spectra were reconstructed either with R-MDD,[82] the iterative re-weighted least squares (IRLS) or iterative soft thresholding (IST) algorithm applied as a compressed sensing (CS) approach[83] or maximum entropy (MaxEnt),[84] the former two implemented in TopSpin 3.1, CS-IST in MestRe Nova v.12.0.1-20560, and MaxEnt in the Rowland NMR Toolkit (Table 5). Spectral processing was achieved with R-MDD and CS-IRLS in TopSpin 3.1, with CS-IST by means of MestRe Nova[85] and with MaxEnt by using the Rowland NMR Toolkit (RNMRTK)[86] shared on the NMRbox platform.[87] In context of reconstruction by MaxEnt, NmrPipe and NmrDraw were used to convert the raw data format as well as to display and analyze the reconstructed data.[88]

Table 5. Reconstruction algorithm usages. Overview of the reconstruction algorithm usages on measured or simulated NUS ^{1}H,^{1}H-TOCSY and ^{1}H,^{1}H-COSY45 spectra according to the sampling scheme applied. Abbreviations: UwSa, unweighted sampling; ExSa, exponentially weighted sampling; sPGS, sine-weighted Poisson-gap sampling; R-MDD, recursive multidimensional decomposition; CS-IRLS, compressed sensing approach employing the iterative re-weighted least squares method; MaxEnt, maximum entropy; CS-IST, compressed sensing approach employing the iterative soft thresholding method. Published in von Schlippenbach *et al.* 2018.[69]

Sampling scheme	**^{1}H,^{1}H-TOCSY NUS**		**^{1}H,^{1}H-COSY45 NUS**	
	measured	simulated	measured	simulated
UwSa	-	CS-IRLS	-	-
ExSa	R-MDD, CS-IRLS	CS-IRLS	-	-
sPGS	-	CS-IRLS, MaxEnt	CS-IRLS	CS-IRLS, CS-IST

MDD assumes that a multidimensional spectrum can be modeled by the sum of tensor products of one-dimensional vectors.[61] In R-MDD, the FID's autoregressive behavior is exploited to incorporate it into processing with MDD.[82] CS states that if the frequency signals are sparse, only as many data points as signals present in the spectrum are needed to be sampled to resolve the multidimensional spectrum.[89] Two variants of CS-based reconstruction algorithms were implemented: CS-IRLS and CS-IST. During the CS-IRLS approach, the l_p norm penalty function is reformulated into a regulized least-squares minimization problem.[83,90] Basis for IST is that peaks above an iteratively set threshold are selected followed by the inverse FT of the updated sought vector.[83,90] Afterwards, the non-experimental points are either set to zero or added to the initial FID input.[90] In contrast to CS, MaxEnt reconstruction utilizes maximizing entropy as a regularizer instead of maximum sparsity to yield spectra consistent with the measured data.[8,84]

The optimized NUS parameters, being a 50% sampling density, a sine-weighted Poisson-gap sampling (sPGS) scheme, and a CS-IRLS reconstruction approach, were applied to the calibration samples, cohort study urine specimens including the urine specimen utilizing NUS for enhanced resolution, and cancer cell samples using the default seed value of the random number generator implemented within TopSpin 3.1. The calibration sample set was measured with a ^{1}H,^{1}H-COSY45 pulse sequence in a uniformly sampled and a 50% non-uniformly sampled manner. Exceptions were NUS spectra of tryptophan, tyrosine, and threonine, which were

simulated from the corresponding US spectra. The 2D spectra of the urine specimen used to analyze enhanced spectral resolution by NUS were measured with a ^{1}H,^{1}H-COSY45 pulse sequence collecting 512 increments in a non-uniform or uniform fashion to obtain time-equivalent US and NUS data. Spectral processing of the NUS data with CS-IRLS resulted in twice as many data points (1024) in total as the time-equivalent US spectrum. Additionally, an enhanced-resolution US ^{1}H,^{1}H-COSY45 spectrum with 1024 data points was acquired. The cancer cell samples were measured with a ^{1}H,^{1}H-COSY45 pulse sequence collecting 256 increments for the time-reduced 50% NUS spectra and 512 indirect data points for the enhanced resolution 50% NUS spectra. After reconstruction with CS-IRLS, 512 and 1024, respectively, indirect data points were given.

2.4. Spectral Analysis

Chemical shifts were referenced relative to the TSP resonance at 0 ppm. Signal assignment was performed with the help of overlaying the spectrum with pure compound reference spectra acquired under comparable experimental conditions present in the Bruker Biofluid Reference Compound Database BBIOREFCODE (2-0-3) in AMIX-Viewer 3.9.13 [BrukerBioSpin GmbH].[74] Quantification of signals was done relative to TSP with AMIX 3.9.13 [Bruker BioSpin GmbH]. The cross peaks in the 2D spectra were picked in the upper spectral triangle, except for D-glucose in the cohort study samples quantified in the lower triangle because of its selected signal in the upper triangle being otherwise too close to the water signal for reliable quantification. For automated peak identification the peak picking threshold was set to a signal to noise ratio of 3.5. For relative and absolute quantification of metabolites from the 2D NMR spectra, a single, intense, unambiguous, and well-dispersed cross signal per compound was chosen (Table 3). Following peak-picking, signals were automatically integrated. Employing test samples, the best integration method being either peak-shape analysis or peak area integration was selected for each signal. By default, scaling the peak integral to the integral of the TSP peak in the spectrum was performed to correct for spectrometer instabilities. While in 1D spectra peak areas on a given NMR machine and at given measurement conditions given full relaxation relate merely to the number of spins contributing to a signal and the compound concentration,[15] cross peak volumes in multidimensional NMR spectra depend on

various factors like pulse sequence parameters such as evolution times as well as on compound-structural properties like *J*-coupling constants.[15,58] Taking individual peak intensities into account, absolute concentrations in multidimensional NMR can be achieved by setting up calibration curves for each separate compound signal[58] based on a dilution series of the pure compound. The average of three technical replicates is taken and then a regression line is fitted. Data from calibration curves were also used for the determination of LLOQs.[58,91] According to FDA guidelines, the LLOQ was defined as the lowest concentration where quantifying the calibration sample triplicates yielded a relative standard deviation (RSD) of at maximum 20%. Absolute concentrations obtained from 2D spectra were calculated manually following the work-flow of MetaboQuant 1.3.[91] Absolute quantification of 1D ^{1}H spectra was carried out with MetaboQuant 1.3 or Chenomx NMR Suite 8.2 [Chenomx Inc., Edmonton, Canada], the latter allows signal deconvolution of overlapping signals. Here, to match the reference compound clusters to the individual resonance peaks of a metabolite, a subtraction line was utilized to adjust the clusters for an optimal fit. Absolute concentrations of creatinine in the spike-in urines were determined from 1D ^{1}H spectra (n = 5 for urine I, n = 3 for urine II) of the blank control sample by MetaboQuant 1.3, taking into account a dilution factor of two. Levels of selected metabolites in the cohort study samples, namely hippuric acid, pseudouridine, lactic acid, D-glucose, citric acid, and glutamine, were normalized to the corresponding creatinine level in each sample to account for variations due to differences in fluid intake.[92] For statistical power analysis in context of the GKCD and GNC study ^{1}H,^{13}C-HSQC spectra have been acquired according to standard protocols.[74] Metabolite quantification from these spectra was automatically performed with MetaboQuant 1.3.

Those metabolites assigned in the enhanced resolution spectra of the cancer cells with AMIX-Viewer 3.9.13 were absolutely quantified by integrating the peak areas. Only metabolites were considered which showed values above the LLOQ in all samples. Here, the quantified metabolites in the cell pellets were corrected by the individual extraction loss determined from the deviation of nicotinic acid in the sample from the spiked-in level of 2 mM. The deviation of the nicotinic acid concentration quantified in the individual methanol extraction sample relative to the expected concentration was considered to relate to the amount of the other metabolites lost

during extraction. Consequently, metabolite concentrations determined were corrected for this proportional loss. The quantified metabolite values in the cell pellet were normalized to the corresponding total protein amount after 48 h incubation time to account for unwanted differences in protein content between samples. The absolute metabolite concentrations in the medium control sample were subtracted from the corresponding averaged metabolite levels in the supernatant. In *n = 5* supernatant samples as well as in the medium control when having measured ^{1}H,^{1}H-COSY45 spectra with time-reduced 50% NUS spectra did not yield quantifiable glutamate signals. Consequently, the glutamic acid level in the medium control was not subtracted from the respective level in the supernatant of cancer cell samples of both time-reduced and enhanced-resolution NUS spectra for reasons of comparison.

2.5. Evaluation of Quantitative Results

Accuracy and Precision

First, the quantitative performance of NUS compared to US was evaluated on the spike-in sample set employing urine I. Here, the recovery of a metabolite signal intensity with NUS relative to US was analyzed, taking into account only signals present in all spectra. Initially, US and NUS spectra were measured to evaluate the influence of CS and R-MDD on reconstructed NUS data. Here, five US and three NUS spectra, the latter varying in seed value, were acquired as technical replicates. Afterwards, six NUS spectra differing in seed value were simulated from one measured US spectrum. According to the Food and Drug Administration (FDA) guidelines, the mean relative intensity of a given metabolite derived from spectra obtained with NUS had to be within 15% of the value of the corresponding US spectrum for accurate quantification.[93] Furthermore, the deviation of the total peak volume in the US and NUS spectra was not to exceed 15% of the coefficient of variance (CV) for precise results.[93] For the spike-in dataset, the number of recoveries observed per parameter was taken into account. Theoretically, this number amounts to 40 per NUS level and 120 over all NUS levels for ^{1}H,^{1}H-TOCSY spectra. Note that the two missing signals in the blank and lowest spike-in concentration of glutamic acid of the theoretically observable 42 in these spectra were not considered.

Consequently, these 40 recoveries were also accounted for in ^{1}H,^{1}H-COSY45 spectra when compared to ^{1}H,^{1}H-TOCSY spectra. When regarding ^{1}H,^{1}H-COSY45 spectra solely, 42 recoveries per NUS level and 126 over all NUS levels were looked at.

Fold Changes

To address effects of the individual urine matrix on the performance of the selected NUS parameters, the derived fold changes from both spike-in datasets were compared to the expected fold changes. For determining fold changes in the spike-ins, first the relative signal intensity of a quantified metabolite in the corresponding blank sample was subtracted from that in the associated spike-in sample. Exceptions in the urine I dataset were glutamic acid showing no peaks in three of the six NUS spectra of the blank sample and lactic acid yielding a negative fold change with one of the six seed value when subtracting the blank. For the NUS data, always six different seed values were employed. Next, the compound intensities corresponding to a fold change of two or of two to thirty two were compared pairwise, resulting in a set of up to fifteen fold changes for each dataset. Because spike-in concentration ranges spanned a 32-fold difference between the lowest and highest spike-in concentration, minor deviations in relative intensities derived from the lowest spike-in led to large differences in fold-changes. To address this observation, the derived fifteen fold changes between all possible spike-in level comparisons were divided by the respective factor to yield a fold change of two. This way, the effects on quantitation were compared to the results obtained from merely relating each spike-in level with the next highest one. Then, the fold changes were averaged and the difference as well as the linear dependency between expected and observed fold changes, for the latter comparing both spike-in datasets, was depicted in bar charts or as a regression analysis, respectively.

Analysis of Cohort Study Specimens

Visualization of 50% NUS compared to US of the cohort study samples was conducted via boxplots and Bland-Altman plots, for the latter also comparing 50% NUS to 1D ^{1}H spectra. Boxplots give a graphical representation of the symmetry of the data distribution with the box representing the interquartile range between the first and third quartile, a horizontal line locating the median, straight lines depicting

the most extreme values, and circles the outliers.[94] Bland Altman plots are well suited to assess how well two experimental methods agree.[58]

Statistical Analysis

Statistical analysis was performed and graphical plots were generated with Excel 2013 [Microsoft Corporation, Redmond, WA, USA] and *R* version 3.2.3 in RStudio version 0.99.491 [RStudio, Inc., Boston, MA, USA]. Figures were assembled in PowerPoint 2013 [Microsoft Corporation]. Tests considering the spike-in dataset employing urine I were performed over all concentrations, either over all spike-in metabolites or per metabolite, either over all NUS levels or per NUS level considering accuracy and precision separately as derived from the recovery plots. Statistical significance of a given comparison was considered given a *p*-value of less than or equal to 0.05. To test for significant differences in the quantitative performance between implemented variants of given NUS parameters (Figure 4), those signal intensities missing in the NUS spectra were imputed with zero. The respective mean ratios and CVs were calculated from non-imputed data.

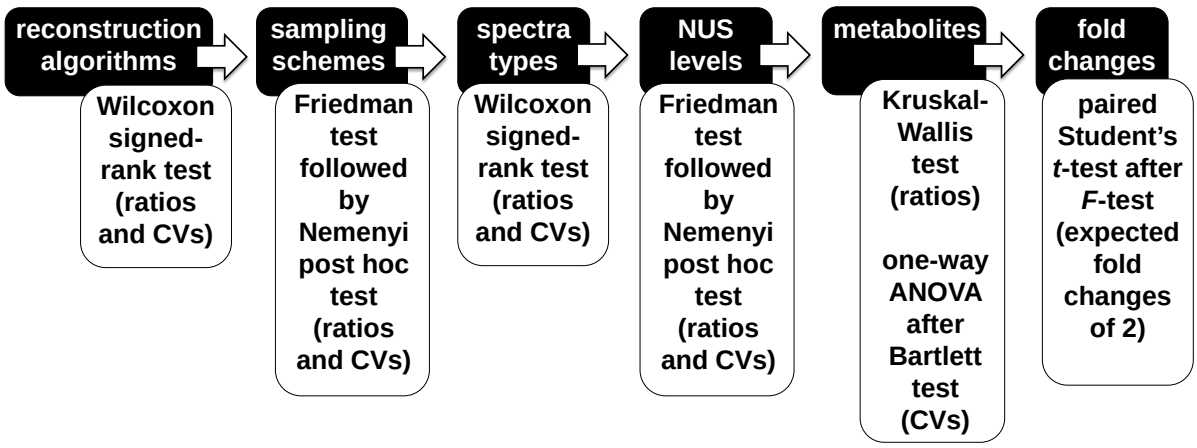

Figure 4. Overview of consecutively applied statistical tests on ratios and CVs derived from recovery plots obtained from the spike-in dataset according to analyzed influences on the performance of NUS.

Normal distribution was tested for with the Shapiro-Wilk test which tests for the hypothesis that the investigated samples come from a normally distributed population.[95] The Student's *t*-test hypothesizes that the means of two normally distributed populations having equal variances following a Student's *t*-distribution are equal.[94] A paired Student's *t*-test, applied on expected fold changes

of two (Figure 4), takes into account that two samples are dependent on each other.[94] The Wilcoxon signed-rank test is a non-parametric alternative to the paired Student's *t*-test, hypothesizing that the two population distribution differences are symmetrical around the median.[94] A Wilcoxon signed-rank test was considered when two groups were compared, being the case for analyzing the influence of reconstruction algorithms and spectra types on NUS data (Figure 4). A Friedman test (paired data) was applied in the case of data derived from taking different sampling schemes and NUS levels (Figure 4). The Friedman test is appropriate when comparing more than two dependent, non-parametric groups.[96] A post-hoc test is performed for pairwise multiple comparisons given that a test taking into account more than two groups shows significance.[97] As post hoc tests, either the Nemenyi test or a paired Student's *t*-test was implemented, the latter after testing for equal variances with an *F*-test. The Nemenyi test applies as a post-hoc test after a Friedman test has shown significance.[97] An *F*-test applies to estimate equal variances for two populations for performing a Student's *t*-test.[94] To test for quantitative differences between metabolites, a Kruskal-Wallis test and one-way analysis of variance (ANOVA) were implemented, for the latter furthermore applying a Bartlett test to test for homogeneity of variances (Figure 4). Performing an ANOVA is suitable when testing for the equality of means from more than two normally distributed independent populations showing equal variance.[94] The Bartlett's test, applicable as a test for homogeneity of variance checked for before applying an ANOVA, tests the hypothesis that the standard deviation is equal in the groups.[98] The Kruskal-Wallis test is a non-parametric alternative to ANOVA hypothesizing equal distributions of the more than two independent populations.[94]

Statistical Power Analysis

For the cohort study samples, an a priori statistical power analysis was performed to control for the statistical power before conducting the study.[99] In order to calculate the minimum number of samples required from each cohort study to spot trends between them,[59,74] an a priori statistical power analysis was performed with G*Power version 3.1.9.2.[100] As the sample variability within the groups was not known before recruiting the total number of samples, a set of ten specimens was randomly selected from each group for a pilot study to estimate the effect size, from there calculating the minimum amount of samples needed for each group given a significance level and

minimal statistical power of interest.[49,74] To detect the population effect size, power analysis was performed with quantified metabolite concentrations derived from ^{1}H,^{13}C-HSQC spectra normalized to the sample's urinary creatinine concentration. For statistical power analysis D-glucose and glycine values were considered, both associated with diabetic nephropathy.[101] Power analysis employing a conventional significance level α = 0.05 and a statistical power 1 – β = 0.8[99] led to a necessary amount of 28 specimens per group considering equal sample sizes to detect significant metabolic differences between them.

Statistical Analysis of Selected Biological Groups

P-values derived from statistical comparisons of metabolite total peak volumes between the cohort study samples are based on a Mann-Whitney *U*-test. The Mann-Whitney *U*-test is a non-parametric test applied when comparing two independent groups.[96] To test for significant differences between metabolite levels derived from time-reduced and enhanced-resolution ^{1}H,^{1}H-COSY45 spectra for each of the control and affected clones of B16.SIY E12 and Panc02-H7 cells, a Mann-Whitney *U*-test was applied imputing those signal intensities missing in the NUS spectra with zero.

3. Results

3.1. NUS on Urine

3.1.1. Spike-in Dataset

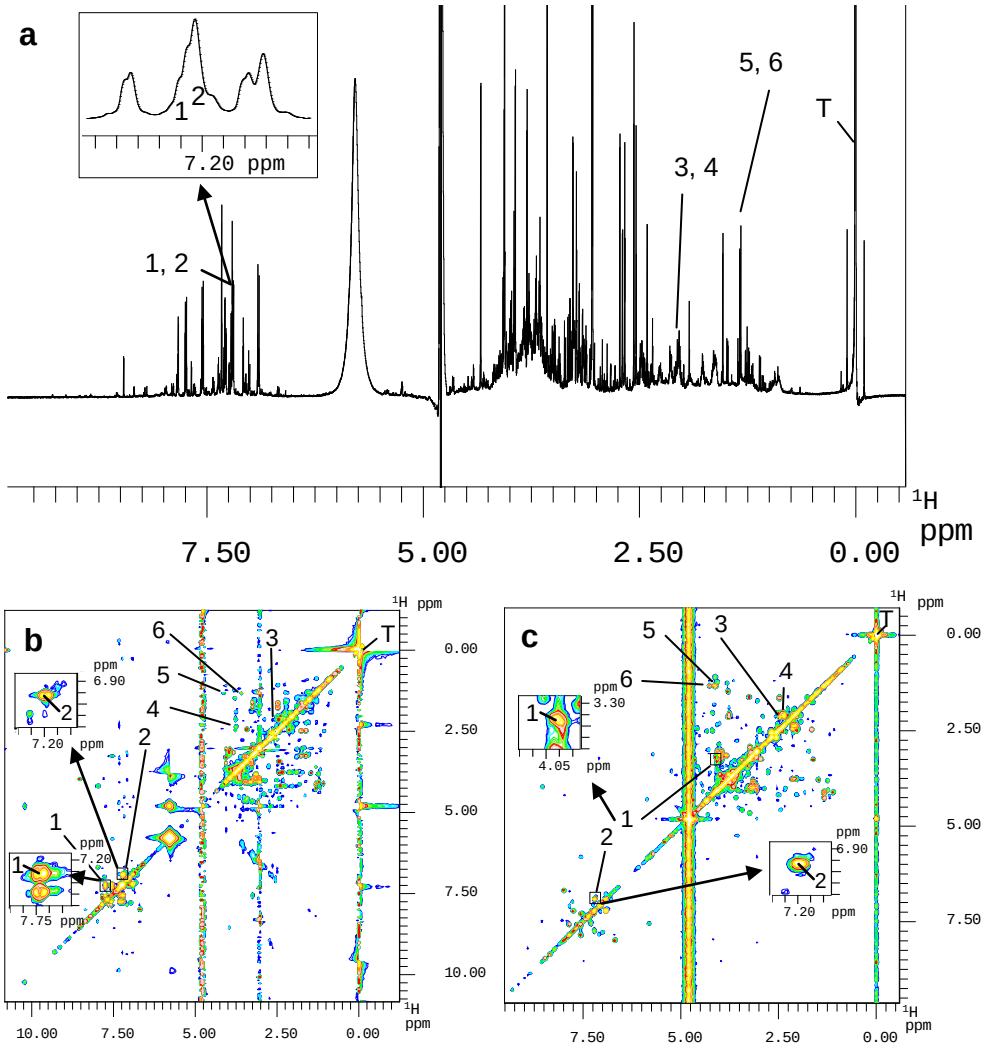

Figure 5. Exemplary NMR spectra of the human urine I specimen. Selected signals in the aromatic and aliphatic regions of the spectra were assigned to the six endogenous metabolites tryptophan (1), tyrosine (2), glutamine (3), glutamic acid (4), lactic acid (5), and threonine (6), which had been spiked-in at concentrations between 15.6 and 500.0 µM. While 1D ^{1}H NMR spectroscopy failed to resolve the selected signals (**a**), both 2D ^{1}H,^{1}H-TOCSY (**b**) and ^{1}H,^{1}H-COSY45 (**c**) experiments yielded sufficient resolution as exemplarily shown for tryptophan and tyrosine via inserts. The contour levels of both 2D spectra are zoomed in close to the noise level. Key: T, 3-trimethylsilyl-2,2,3,3-tetradeuteropropionate. Published in von Schlippenbach *et al.* 2018.[69]

Accelerated Quantification. To test the impact of the choice of sampling scheme, reconstruction algorithm, and seed value, a urine specimen (urine I) from an apparently healthy donor was spiked with varying concentrations of three pairs of

urinary metabolites, namely tryptophan/tyrosine, glutamine/glutamic acid, and lactic acid/threonine. These metabolites had been chosen because of the inability of 1D ^{1}H NMR spectroscopy to resolve them sufficiently for quantitation (Figure 5 **a**). Figures 5 **b** and 5 **c** show their successful spectral resolution by 2D ^{1}H,^{1}H-TOCSY and ^{1}H,^{1}H-COSY45 NMR spectroscopy, respectively.

RECONSTRUCTION ALGORITHMS. The two reconstruction algorithms initially tested were recursive multidimensional decomposition (R-MDD) and the compressed sensing approach employing the iterative re-weighted least squares method (CS-IRLS), which both are implemented in TopSpin 3.1. ^{1}H,^{1}H-TOCSY spectra were chosen as this type of spectrum yields a larger number of signals than ^{1}H,^{1}H-COSY45 spectra, thus rendering reconstruction of NUS more challenging. Figures 6, S1, and S2 depict the recovery of metabolite signal intensities relative to uniform sampling (US) as a function of the level of sparse sampling (75%, 50%, and 25% of data points). The ratios between NUS and US serve as a measure of accuracy whereas the coefficients of variation (CVs) of these ratios reflect precision as exemplarily shown for glutamine (Figure 6 **a**, **c**) and glutamic acid (Figure 6 **b**, **d**). For the chosen levels of sparse sampling, separate bars are displayed for each spike-in level and the blank control. For the US ^{1}H,^{1}H-TOCSY spectra and for each level of sparse sampling, five and three spectra were acquired, respectively. The replicate spectra employing NUS were measured with an exponentially weighted sampling scheme and a different seed value for each replicate. To illustrate correlation trends between US and NUS, additional scatter plots with peak volumes normalized to TSP were generated (Figure S3).

For a NUS level of 25%, in particular, it is obvious that R-MDD failed more often than CS-IRLS to reconstruct signals for example for glutamine (Figure 6 **a**, **c**) and tryptophan (Figure S1 **a** and S2 **a**) at the lower spike-in concentrations. Regarding the number of reconstructed signals per and across NUS levels (Table S1, first two columns), CS-IRLS always outperformed R-MDD, yielding e.g. 112 compared to 103 recoveries over all NUS levels, respectively. Note that one signal was selected per metabolite, each present at 6 different concentrations in the different spike-ins and the blank sample. For glutamic acid, only five signals were considered as its signal intensities in the blank sample and at the lowest spike-in concentration were not

present or too low for reliable integration even in the US ^{1}H-^{1}H TOCSY spectra. Therefore, a total of 40 signals were considered per NUS level.

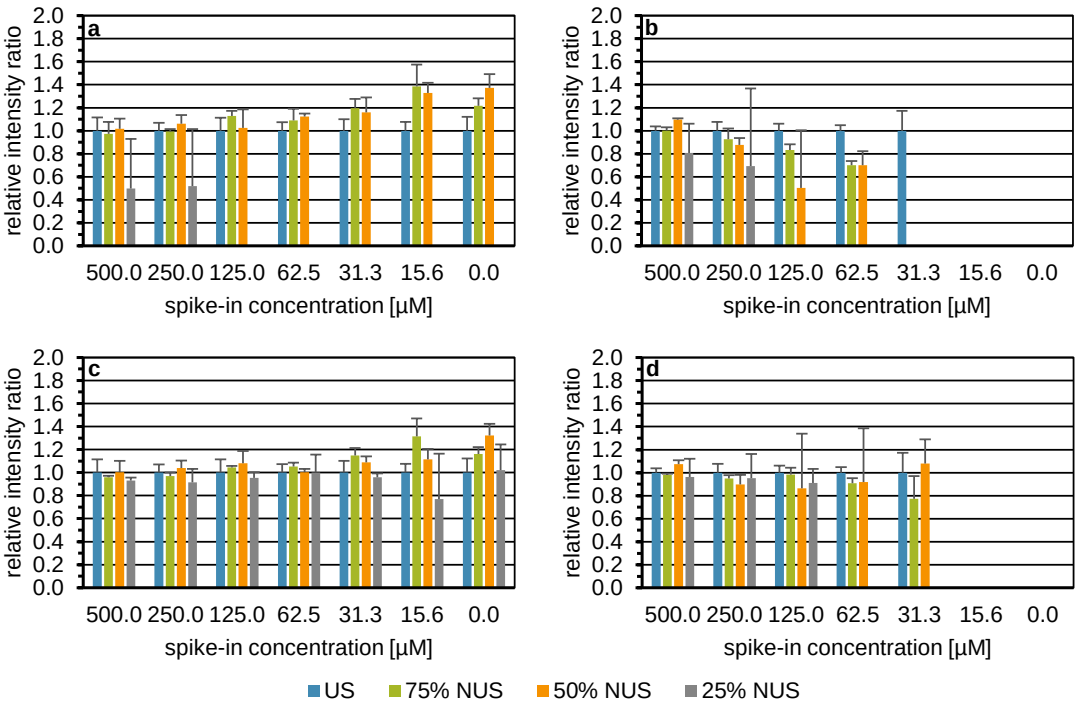

Figure 6. Impact of signal reconstruction with recursive multidimensional decomposition (**a**, **b**) and compressed sensing employing the iterative re-weighted least squares method (**c**, **d**), respectively, on the recovery of the relative intensity of a selected cross signal in the spike-in samples and the blank control employing urine I, exemplarily shown for glutamine (**a**, **c**) and glutamic acid (**b**, **d**). US ^{1}H,^{1}H-TOCSY spectra (n = 5) indicated by blue bars. NUS ^{1}H,^{1}H-TOCSY spectra (n = 3 each) measured with 75%, 50%, and 25% of the uniformly sampled data points depicted by green, orange, and gray bars, respectively. Each NUS spectrum was acquired with an exponentially weighted sampling scheme and three seed values per NUS level. The x-axis depicts the spike-in concentration in micromolar. The intensity ratio of the total cross peak integrals scaled to the internal standard 3-trimethylsilyl-2,2,3,3-tetradeuteropropionate (TSP) of the metabolite signal (mean + SD) obtained with US or NUS to US is plotted on the y-axis. Published in von Schlippenbach *et al.* 2018.[69]

A Wilcoxon signed-rank test on the ratios and the coefficients of variation (CVs) across all spike-ins showed significant differences between CS-IRLS and R-MDD across all NUS levels (Table S2, first two columns) for both the ratios (p = 4.109*10^{-6}) and CVs (p = 0.037). When comparing the mean ratios and CVs between CS-IRLS and R-MDD for each and across all NUS levels (first four columns of Table S3), CS-IRLS yielded more accurate and precise results than R-MDD. Taking all NUS levels into account, the mean ratio obtained by CS-IRLS was 0.96 with an average CV of 12.30%, whereas the corresponding values for R-MDD were 0.89 and 17.16%, respectively.

However, it is also obvious that the performance of both reconstruction algorithms declined with decreasing numbers of acquired indirect data points. In the case of the reconstruction of the 75% and 50% NUS spectra by CS-IRLS, though, almost identical ratios of 0.98 and 0.99, respectively, were obtained. Overall with regard to both the signals reconstructed and the accuracy and precision obtained, CS-IRLS proved superior to R-MDD. Therefore, CS-IRLS was used for further parameter optimization.

SAMPLING SCHEMES. Next, the influence of the three different sampling schemes and the choice of the seed value was investigated on the quantitative performance of ^{1}H,^{1}H-TOCSY experiments as a function of the fraction of indirect data points acquired. To assess the influence of the seed value regardless of the measurement error, simulated NUS spectra were generated by extracting data points of the indirect dimension from a single US spectrum in a fashion corresponding to an intended percentage of sparse sampling, seed value, and sampling scheme. Figure 7 shows exemplarily for lactic acid (**a**, **b**, **c**) and tyrosine (**d**, **e**, **f**) the influence of an unweighted (**a**, **d**), exponentially weighted (**b**, **e**), and sinusoidal Poisson-gap (**c**, **f**) sampling scheme on the recovery of signal intensities relative to US. For each NUS level (75%, 50%, and 25%), six different seed values were employed for data extraction from the US spectrum. All NUS spectra were reconstructed by CS-IRLS. Data from Figure 7, S4, S5, and S6 on the effect of the sampling scheme on the other four metabolites are also depicted as scatter plots (Figure S7).

Of the three sampling schemes, sinusoidal Poisson-gap sampling performed best especially with regard to the number of reconstructed weak signals like lactic acid (Figure 7 **c**). While the tyrosine signal could be reconstructed with good accuracy by each of the sampling schemes, unweighted sampling failed to reconstruct the lactic acid signal at spike-in concentrations below 250 µM. Further, only sinusoidal Poisson-gap sampling allowed quantification of lactic acid in the blank employing 50% NUS.

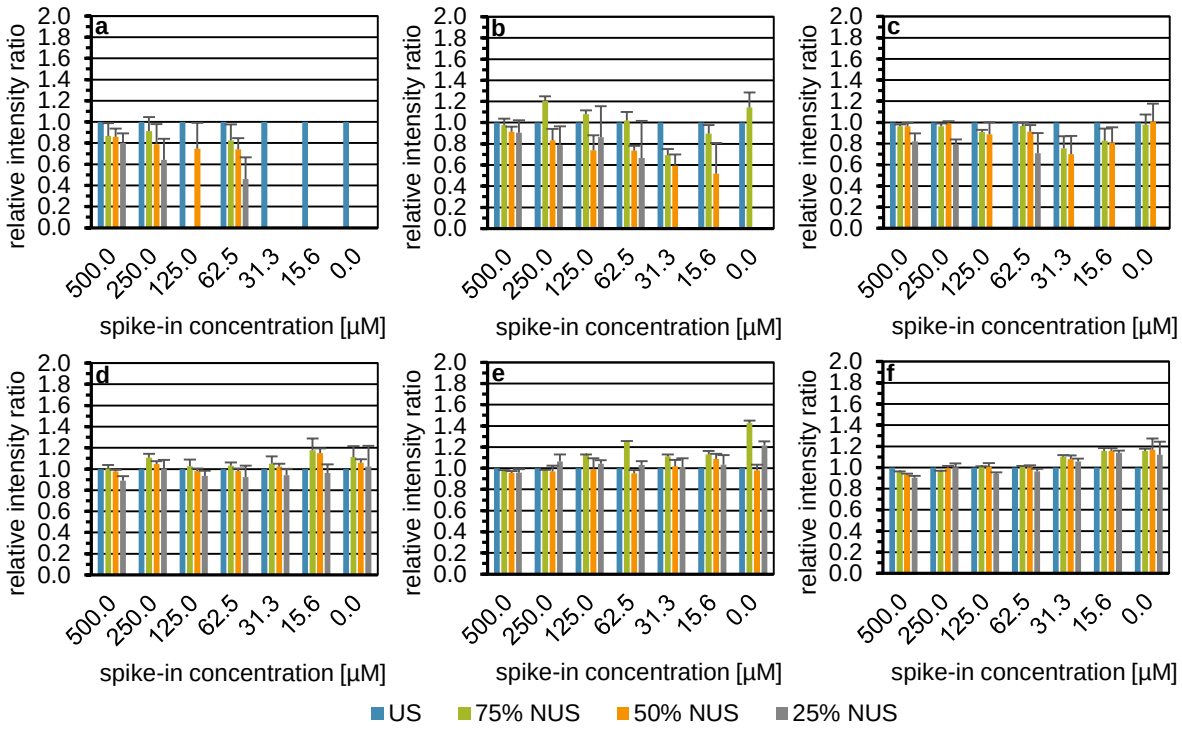

Figure 7. Influence of unweighted (**a**, **d**), exponentially weighted (**b**, **e**), and sinusoidal Poisson-gap (**c**, **f**) sampling on the recovery of the relative intensity of a selected cross signal in each spike-in and the blank employing urine I, exemplarily shown for lactic acid (**a**, **b**, **c**) and tyrosine (**d**, **e**, **f**). US ^{1}H,^{1}H-TOCSY spectrum (n = 1) indicated by blue bars. NUS ^{1}H,^{1}H-TOCSY spectra simulated from the US spectrum displayed with 75%, 50%, and 25% of the US data points depicted by green, orange, and gray bars, respectively. Each NUS spectrum was constructed with six seed values per NUS level and reconstructed with the compressed sensing approach employing the iterative re-weighted least squares method. On the x-axis, the spike-in concentration is given in micromolar. The intensity ratio of the total cross peak integral scaled to the internal standard TSP of the metabolite signal (mean + SD) obtained with US or NUS to US is plotted on the y-axis. Published in von Schlippenbach *et al.* 2018.[69]

Considering the number of recoveries observed over all NUS levels with either sampling scheme (Table S1), it is evident that the sine-weighted Poisson-gap sampling scheme recovered the most signals, in total 113 recoveries compared to 112 with exponentially weighted sampling and 98 with unweighted sampling. The same was true for 50% NUS, while for 75% and 25% NUS sine-weighted Poisson-gap and exponentially weighted sampling performed equally well. Looking at the ratios (accuracies) over all spike-in metabolites and concentrations, the Friedman test (Table S2) showed significant differences across NUS levels (p = 2.536*10^{-8}). Subsequent application of the Nemenyi post hoc test (Table S4) showed that both exponential weighted and sinusoidal Poisson-gap sampling differed significantly from unweighted sampling (p = 3.9*10^{-5} and p = 1.8*10^{-7}, respectively) while the former two did not differ significantly (p = 0.54).

Regarding ratios across all NUS levels (Table S3), the three sampling schemes differed little in accuracy. Unweighted, exponentially weighted, and sinusoidal Poisson-gap sampling yielded average ratios of 0.97, 1.02, and 1.03, respectively. Regarding precision, the Friedman test (Table S2) showed a significant difference between the three sampling schemes over all NUS levels ($p < 2.2*10^{-16}$). The Nemenyi post hoc test (Table S4) revealed no significant difference between unweighted and exponentially weighted sampling. In terms of precision, significant differences, however, were observed between sinusoidal Poisson-gap and the other two sampling schemes (last two columns of Table S4). Results given in Table S3 demonstrate, that precision (CV) depends on the chosen sampling scheme, with the sinusoidal Poisson-gap sampling scheme depending the least on the seed value chosen showing a CV of 5.39% over all NUS levels compared to unweighted and exponentially weighted sampling with a CV of 12.06% and 9.59%, respectively. In light of the greater number of signals recovered and the lowest seed value dependency, sine-weighted Poisson-gap sampling was used for all further evaluations and applications of NUS.

SPECTRA TYPES. To investigate a potential differential impact of NUS on the type of homonuclear 2D experiment used, ^{1}H,^{1}H-TOCSY spectra were compared to ^{1}H,^{1}H-COSY45 spectra. Figure 8 shows exemplarily the recovery of the tyrosine (**a**), glutamine (**b**), and lactic acid (**c**) signals in ^{1}H,^{1}H-COSY45 spectra, which share the same cross signal positions in ^{1}H,^{1}H-TOCSY spectra. Results for the other three spike-in metabolites are depicted in Figure S8. Note that sine-weighted Poisson-gap sampling in combination with CS-IRLS was used here. Data from Figure 8 and Figure S8 depicting the influence of the spectra type on the other three compounds are also displayed as scatter plots (Figure S9).

When comparing columns five and six in Table S1 and Figures 8, S6, and S8, the number of signals reconstructed successfully over all NUS levels was higher for ^{1}H,^{1}H-COSY45 than ^{1}H,^{1}H TOCSY. For both 75% and 50% NUS both spectra types showed a recovery of all 40 considered signals, whereas for 25% NUS 33 and 38 signals were recovered for ^{1}H,^{1}H TOCSY and ^{1}H,^{1}H-COSY45, respectively. When considering accuracy and precision, Table S2 shows that over all NUS levels significant differences were obtained between the two spectra types using the

Wilcoxon signed-rank test (p = 1.075*10^{-4} regarding accuracies and p = 4.585*10^{-8} concerning precisions). Next, for each NUS level, mean ratios and CVs were compared separately (the last two columns of Table S3 for ^{1}H,^{1}H-TOCSY and Table S5 for ^{1}H,^{1}H-COSY45).

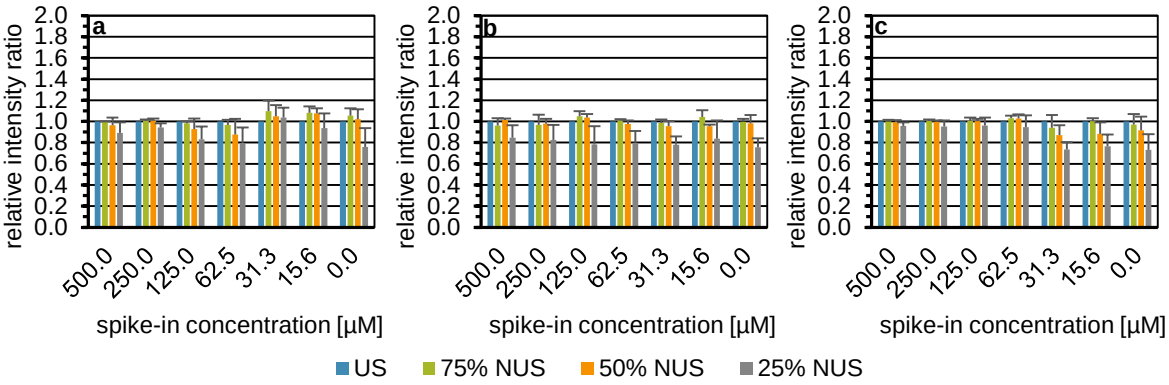

Figure 8. Influence of the spectral type on the recovery of the relative intensity of a selected cross signal in each spike-in sample and the blank employing urine I, exemplarily shown for tyrosine (**a**), glutamine (**b**), and lactic acid (**c**). US ^{1}H,^{1}H-COSY45 spectrum (n = 1) indicated by blue bars. NUS ^{1}H,^{1}H-COSY45 spectra simulated from the US spectrum displayed with 75%, 50%, and 25% of the US data points depicted by green, orange, and gray bars, respectively. Each NUS spectrum was constructed with a sinusoidal Poisson-gap sampling scheme taking six seed values per NUS level and reconstructed with the compressed sensing approach employing the iterative re-weighted least squares method. On the x-axis, the spike-in concentration given in micromolar is shown. The intensity ratio of the total cross peak integral scaled to the internal standard TSP of the metabolite signal (mean + SD) obtained with US or NUS relative to US is plotted on the y-axis. Published in von Schlippenbach *et al.* 2018.[69]

Results indicate that at NUS levels of 75% and 50%, ^{1}H,^{1}H-TOCSY and ^{1}H,^{1}H-COSY45 yielded similar accuracies with ratios of 1.06 and 1.02 at 75% NUS and of 1.05 and 0.96 at 50% NUS, respectively. At 25% NUS, in contrast, a considerable drop in accuracy was observed for ^{1}H,^{1}H-COSY45 spectra with the ratio to US decreasing to 0.80. In terms of precision, ^{1}H,^{1}H-TOCSY was more precise than ^{1}H,^{1}H-COSY45 with CVs of 5.39% and 8.89%, respectively, across the three NUS levels. However, the differences in accuracy and precision between ^{1}H,^{1}H-TOCSY and ^{1}H,^{1}H-COSY45 were mostly observed at the 25% NUS level. Having applied the Friedman test, significant differences in accuracy and precision were observed across the different NUS levels in ^{1}H,^{1}H-COSY45 spectra (p <2.2*10^{-16} and p = 4.0*10^{-6}, respectively) (Table S6). In terms of accuracy, the Nemenyi post hoc test showed significant differences in Table S6 for each NUS level comparison with p = 4.9*10^{-4} for 75% vs. 50% NUS, p = 2.5*10^{-14} when comparing 75% against 25% NUS and p = 2.7*10^{-6} when testing 50% against 25% NUS. The same was true

in terms of precision except for the comparison of 75% against 50% NUS resulting in $p = 0.065$ (Table S6).

In conclusion, ^{1}H,^{1}H-TOCSY or ^{1}H,^{1}H-COSY45 appear to have performed equally well with regard to the number of signals reconstructed, accuracy, and precision as long as the fraction of data points acquired did not drop below 50%. However, ^{1}H,^{1}H-COSY45 is the more simple pulse sequence and, therefore, may be better suited for large metabolomic studies. The number of expected signals per metabolite was generally lower in ^{1}H,^{1}H-COSY45 than in ^{1}H,^{1}H-TOCSY spectra, which reduces signal overlap in highly complex biofluids such as human urine. Therefore, ^{1}H,^{1}H-COSY45 spectra have in this context a slight advantage over ^{1}H,^{1}H-TOCSY spectra.

Having shown that a sine-weighted Poisson-gap sampling scheme in combination with 50% NUS performed best on the experimental setup, two other commonly applied reconstruction algorithms were chosen to be evaluated, namely the Iterative Soft Thresholding Compressed Sensing method (CS-IST) implemented in the MestRe Nova software suite and the maximum entropy (MaxEnt) approach implemented in the Rowland NMR toolkit. CS-IST was evaluated on ^{1}H,^{1}HCOSY45 spectra acquired in magnitude mode as these spectra provide a slight advantage over phase sensitive ^{1}H,^{1}H-TOCSY spectra. As reconstruction by the applied MaxEnt approach is restricted to phase-sensitive data, MaxEnt reconstruction was investigated on ^{1}H,^{1}H-TOCSY spectra. When comparing the number of signals reconstructed with the so far best performing method CS-IRLS, with CS-IST, and MaxEnt in Figure 8 and Figures S8, S10 and S11, respectively, as well as in Table S7, CS-IRLS outperforms the other two reconstruction algorithms. This is particularly true for MaxEnt which is able to recover merely 31 out of all possible 42 signals compared to CS-IRLS yielding nearly all observable recoveries (Table S7). Recoveries obtained from data having applied MaxEnt show heavy underestimation for tryptophan, glutamic acid, lactic acid, and threonine and on the other hand strong overestimation of tyrosine signal volumes (Figure S11). Results show that CS-IRLS allows a more accurate and precise quantitation with a mean ratio of 0.96 and a CV of 8.01% in comparison to CS-IST with a mean ratio of 0.93 and a CV of 8.47% (Table S8). The difference is even more striking when comparing to MaxEnt

showing a mean ratio of 0.61 and a CV of 13.70% (Table S8). Table S9 shows that significant differences in ratios but non-significant differences in CV were obtained between the three reconstruction algorithms having applied the Friedman test. Results from the Nemenyi post-hoc test show that significant differences in ratio are derived from results obtained from data reconstructed with MaxEnt (Table S10).

METABOLITES. Next, applying 50% NUS on ^{1}H,^{1}H-COSY45 spectra with a sinusoidal Poisson-gap sampling scheme and spectral reconstruction by CS-IRLS, metabolite-dependent differences in accuracy and precision were investigated. Table S11 lists the median ratios and mean CVs of a given spike-in metabolite over all concentrations and per spike-in concentration, respectively.

All metabolites yielded acceptable accuracies and precisions according to FDA guidelines for the upper four spike-in concentrations, with tyrosine, glutamine, and lactic acid even yielded adequate accuracy and precision for the lower spike-in levels. Having applied a Kruskal-Wallis test on ratios (p = 0.0533) and a one-way ANOVA on the CVs (p = 0.1359), for the latter showing homogeneity of variances with the Bartlett test (p = 0.1502), no significant differences could be seen between the metabolites.

FOLD CHANGES. Next, employing urine I, the determination of fold changes was investigated. For each metabolite, the difference between expected and observed fold changes was analyzed. Note that before calculation of fold changes the corresponding signal intensities of the blank were subtracted from the spike-in data. Figure S12a summarizes the results for the n = 5 fold changes of two.

For Figure S12b, all fold changes between 2 and 32 were considered to compute 15 fold changes of two. For reasons of comparison, also fold changes obtained from the corresponding US spectrum were included.

For expected fold changes of two (Figure S12a), the mean observed fold change over all metabolites was 2.08 for US, while it was 2.15 for 50% NUS showing an average error for both US and 50% NUS of less than 10%. Over all metabolites and six spectral replicates, 50% NUS had an acceptable precision according to FDA guidelines with a mean precision of 9.26%. Further, with the exception of lactic acid

which yielded a CV of 22.52% in the 50% NUS data, the expected fold changes of two could be determined with an error in accuracy and precision of less than 15%. A paired Student's *t*-test applied over all metabolites showed no significant differences in the observed fold changes between US and 50% NUS (p = 0.0666). Consideration of all fold changes of 2 to 32 (Figure S12b) resulted in stronger deviations in accuracy and precision for all metabolites. For example, lactic acid showed a difference between expected and observed fold changes in 50% NUS spectra of -0.23 with an SD of ± 0.05 when taking five fold changes of two while it yielded a difference between expected and observed fold changes in 50% NUS spectra of -0.79 with an SD of ± 0.38 when taking fifteen fold changes of two. For expected fold changes of 2 to 32, Figure S12c depicts the linear dependency between expected and observed fold changes over all spike-in metabolites in urine I as a further measure to assess the reproducibility of determining fold changes.

The regression lines of both the US and 50% NUS dataset nearly overlap, each with a slope of about one, an offset near zero, and coefficients of determination of 0.999 (Figure S12c). Stronger variations of the observed fold changes from the expected fold changes determined with 50% NUS compared to US can be seen in the wider standard deviation ranges for 50% NUS.

PARAMETER VALIDATION. So far parameters were optimized based on one spike-in dataset. For validation purposes, a second spike-in dataset (urine II) was generated in the same manner as the first one except that this time a more concentrated urine matrix was used. As described above, for each sample a US ^{1}H,^{1}H-COSY45 spectrum was acquired and data points were drawn from this experimental data for the *in silico* generation of 50% NUS spectra employing sinusoidal Poisson-gap sampling. Spectra were reconstructed employing CS-IRLS. Table S12 lists the median ratios and mean CVs of a given spike-in metabolite over all concentrations and per spike-in concentration, respectively.

With the exception of tryptophan, all metabolites yielded acceptable accuracies and precisions for all spike-in concentrations. For the lower spike-in concentrations of tryptophan, deviations in both accuracy and precision that exceeded FDA recommendations were observed. This is explained by the comparatively weak

endogenous tryptophan signals of urine II. Overall, results from the two spike-in datasets agreed well. Thus, it is concluded that the set of optimized parameters is applicable to different urinary matrices.

3.1.2. Cohort Study Samples

Application of Accelerated Quantification with NUS to Urine Specimens. Next, 1D ^{1}H NOESY and 2D ^{1}H,^{1}H-COSY45 spectra with and without 50% NUS were acquired for 28 urine specimens each selected at random from the GCKD study and the GNC study. A short description of both studies is given in section 2.1. To compare the performance of the three types of NMR experiments, Bland-Altman plots were generated for a small selected set of metabolites of medical relevance in chronic kidney disease, namely creatinine, hippurate, lactate, D-glucose, citrate, glutamine and pseudouridine (Figures S13, S14, and S15). In Figure S14, the spike-in metabolites were considered in addition, being lactic acid, threonine, tryptophan, and tyrosine, except for glutamine shown in Figure S15 **a** and glutamic acid, which could not be detected in any of the GCKD and GNC urine specimens. The Bland-Altman plots depicted in Figure S13 revealed no bias in the concentrations of creatinine (**a**), hippuric acid (**b**), and D-glucose (**d**) determined by 1D ^{1}H NOESY and 50% NUS 2D ^{1}H,^{1}H-COSY45. In case of lactic acid (**c**), 1D ^{1}H NOESY yielded increasingly higher concentrations compared to 50% NUS 2D ^{1}H,^{1}H-COSY45 with elevated urinary levels of lactic acid, while for both citric acid (**e**) and glutamine (**f**) deviations between the two methods considerably enlarged with higher concentrations. For the comparison of 2D ^{1}H,^{1}H-COSY45 data acquired by US and 50% NUS, respectively, no systematic bias was obvious and with the exception of tryptophan only minimal variations were observed for any of the ten metabolites investigated (Figures S14, and S15 **a**). The agreement in urinary cohort sample metabolite levels determined by 50% NUS and US ^{1}H,^{1}H-COSY45 NMR spectroscopy, respectively, is furthermore demonstrated in the boxplots depicted in Figures S15 **b** and **c**, S16 and S17. The boxplots show the levels of glutamine, hippuric acid, lactic acid, D-glucose, citric acid, and pseudouridine, respectively, normalized against the respective creatinine level in each specimen for the two cohorts.

Using a Mann-Whitney *U*-test, significant differences in the urinary levels of pseudouridine, citric acid, and glutamine between the two cohorts were observed (Table S13). The *p*-values derived from US and 50% NUS spectra were in each case comparable. The average amount of pseudouridine was higher in the CKD specimens, while the opposite applied to glutamine and citric acid.

Further, while the lower limits of quantification (LLOQs) for lactic acid, D-glucose, and glutamine did not differ between 50% NUS and US, the latter yielded two-fold lower LLOQs for hippuric acid, citric acid, and pseudouridine, and in case of creatinine the LLOQs differed even by a factor of 4 (Table S14). However, this did not affect the number of quantifiable signals of these four metabolites in the urine spectra due to the presence of endogenous concentrations above the LLOQ derived from 50% NUS spectra. In comparison, the corresponding LLOQs for 1D ^{1}H spectra are around 3 µM with the exception of glutamine, which yielded an LLOQ of 39 µM.

Implementation of Enhanced Resolution with NUS to Urine Specimen. Additionally, the applicability of NUS to enhance the spectral resolution in the indirect dimension without increasing measurement time compared to the US equivalent was analyzed. For this, urine II selected in the spike-in dataset having an above average creatinine concentration was selected and ^{1}H,^{1}H-COSY45 spectra were acquired. In the 50% NUS spectrum implementing the optimized NUS parameters and the time-equivalent US spectrum, the number of experimentally sampled data points in the indirect dimension was kept constant, therefore yielding after reconstruction twice the amount of indirect data points in the NUS spectrum. Additionally, a US spectrum with twice as many indirect data points was measured to yield the spectral resolution comparable with NUS. Figure 9 exemplarily depicts three spectral areas (**a**, **b**, **c**) derived from the time-equivalent US (**1**), 50% NUS (**2**), and enhanced resolution US (**3**) ^{1}H,^{1}H-COSY45 spectrum.

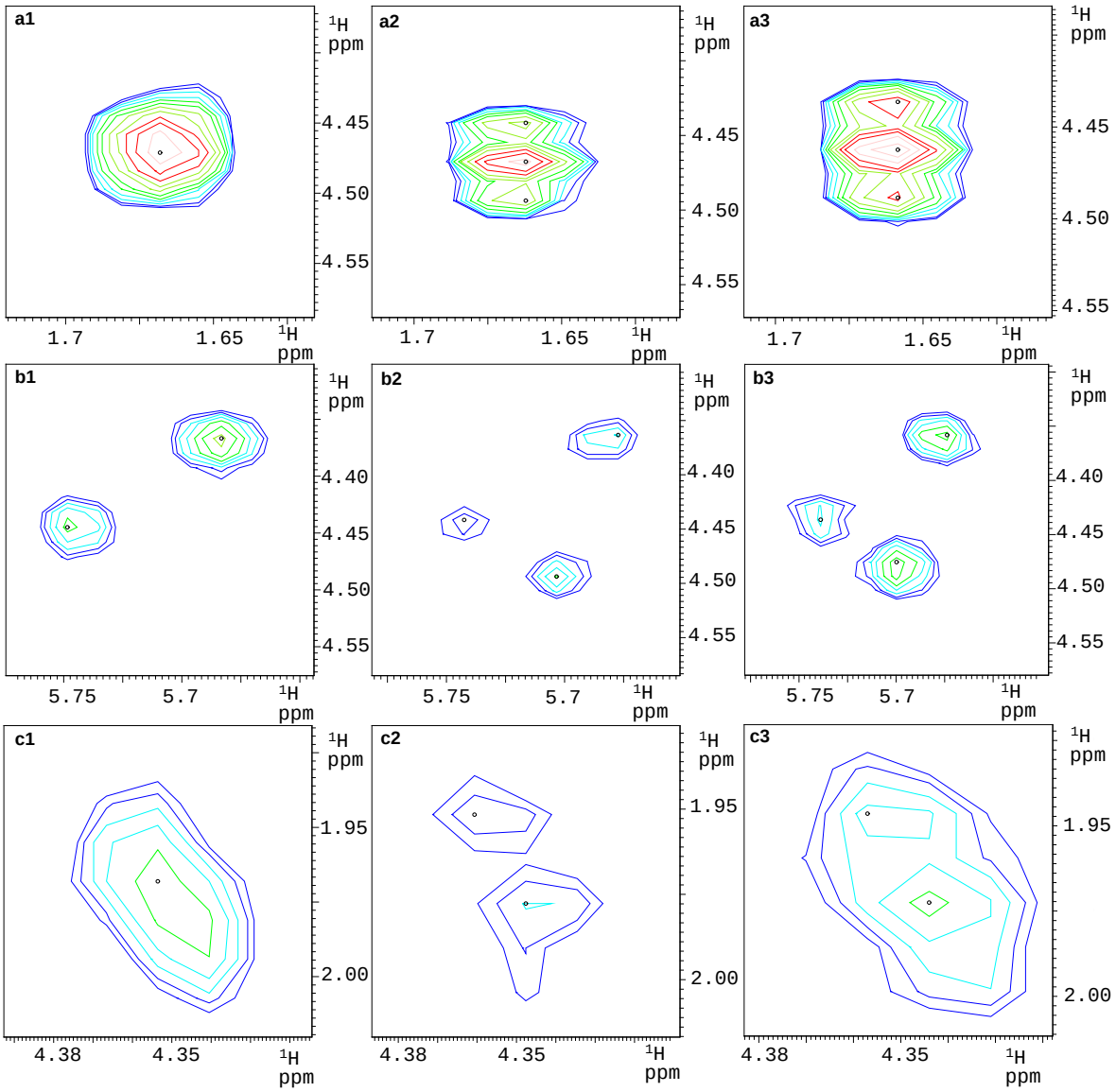

Figure 9. Three selected spectral areas (**a**, **b**, **c**) derived from a time-equivalent US (**1**), enhanced resolution 50% NUS (**2**), and enhanced resolution US (**3**) ^{1}H,^{1}H-COSY45 spectrum, respectively. The NUS spectrum was acquired by means of sine-weighted Poisson-gap sampling with a single seed value and reconstructed using CS-IRLS. The contour levels are zoomed in close to the noise level.

When comparing the number of automatically picked peaks after manual removal of those belonging to the diagonal, noise, artifacts, and the lower triangle in the time-equivalent US and NUS spectrum, a surplus of 107 peaks between the spectral area of 0 to 10 ppm were picked in the NUS spectrum (2111 peaks with US and 2218 peaks with NUS), being an increase in peak number of about 5%. With respect to quantitatively assessing the effect of enhanced resolution with NUS, Figure 9 shows its influence on three spectral areas. Panel **a** shows an example for peaks of the same compound more resolved in NUS and enhanced resolution US spectra due to the increased resolution in the indirect dimension. In the spectral region depicted in

panel **b**, the enhanced resolution spectra reveal a newly emerged peak not visible in the time-equivalent US spectrum. Merged peaks of different signals present in the US spectra are separated in the NUS spectrum, seen in panel **c**. Here, the enhanced resolution US spectrum is able to resolve two peaks while in the time-equivalent US spectrum merely one peak is picked. When looking at the contour plots of all three spectral areas, there is a slight decrease in peak intensity in the enhanced resolution NUS spectrum compared to the enhanced resolution US spectrum. Note that increased F_1 ridges in the enhanced resolution spectra, predominantly between 3.20 and 4.10 ppm, compared to the time-equivalent US spectrum were observed.

3.2. NUS on Cancer Cells

Comparison of NUS for Accelerated Quantification and Enhanced Resolution. After having compared the quantitative difference between US and time-reduced NUS spectra on urine specimens, the quantitative performance of NUS was evaluated when applied to accelerate the acquisition or enhance the spectral resolution. Here, the enhanced resolution NUS spectra were comprised of twice as many indirect data points. The higher the intended resolution in the indirect dimension, the more increments have to be collected. As shown for the selected urine sample in section 3.1.2, enhancing the digital resolution in the indirect dimension aids peak analysis.

After having addressed the difference between both NUS applications qualitatively in the second part of section 3.1.2, the affects were analyzed quantitatively taking cancer cells. To investigate the difference in quantitative performance between time-reduced and enhanced resolution 50% NUS of cancer cell samples, all metabolites assignable with AMIX-Viewer 3.9.13 showing concentrations above the LLOQ in all samples were absolutely quantified, resulting in seven metabolites in the supernatants and three in the cell pellets. Afterwards, quantitative differences in metabolite levels in the supernatants and methanol extracts of the cell pellets were tested for statistical significance. As an application, B16.SIY E12 melanoma and Panc02-H7 pancreatic adenocarcinoma cells in which LDHA was knocked down, respectively knocked out, were compared to their corresponding controls unaffected in LDHA expression. For each clone, three biological replicates of both cell lines were available.

3.2.1. Supernatants

Figure 10 shows the average quantified levels derived from time-reduced (**a**, **c**) or enhanced resolution (**b**, **d**) 50% NUS ^{1}H,^{1}H-COSY45 spectra of seven identified compounds having subtracted the corresponding metabolite level in the cell culture medium from the mean level. The level of glutamic acid in the medium, however, was not subtracted from the corresponding level in the supernatant because glutamic acid could not be quantified in the medium (section 2.4). Each metabolite level was normalized to the amount of protein per pellet after 48 h of cultivation. For reasons of

depiction due to large differences in compound levels between metabolites, glucose together with lactic acid (**a**, **b**) as well as citric acid, glutamine, glutamic acid together with tyrosine (**c**, **d**) are shown separately.

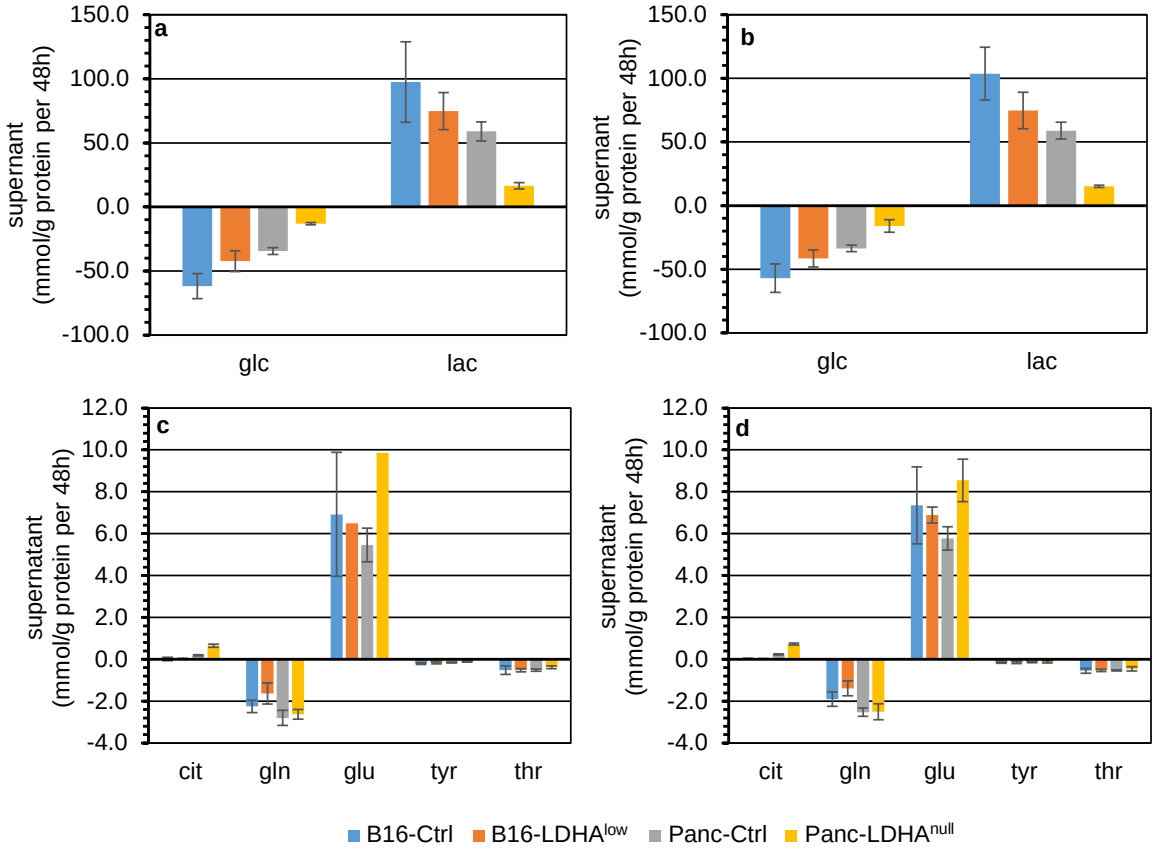

Figure 10. Amount of glucose (glc) and lactic acid (lac) (**a**, **b**) as well as citric acid (cit), glutamine (gln), glutamic acid (glu), and tyrosine (tyr) (**c**, **d**) given in the supernatants of B16.SIY E12 (B16) melanoma and Panc02-H7 (Panc) pancreatic adenocarcinoma cells having subtracted the corresponding metabolite level in the medium from the mean level with the exception of glutamic acid which was excluded, normalized to the amount of protein per pellet given in g after 48 h. The metabolite levels present in millimol derived from time-reduced (**a**, **c**) or enhanced resolution (**b**, **d**) 50% NUS ^{1}H,^{1}H-COSY45 spectra (n = 3 biological replicates per clone with the exception of glutamic acid in the B16-Ctrl samples given n = 2 as well as the B16-LDHA^{low} and Panc-LDHA^{null} each given n = 1 in time-reduced NUS spectra due to excluded signals) are given in mean ± SD. A Mann-Whitney *U*-test was applied to test for significant differences in normalized compound levels between the control (Ctrl) and affected clones (LDHA^{low} and LDHA^{null}) of the corresponding cancer cell line.

Overall, the quantitative results derived from both NUS spectra were similar. However, the standard deviation (SD) in time-reduced NUS spectra is overall higher than in the enhanced-resolution NUS spectra seen for instance for glutamic acid, showing in B16-Ctrl clones a SD of ± 2.96 (taking n = 2) in time-reduced

while ± 1.84 (taking *n* = 3) in enhanced resolution NUS spectra. A Mann-Whitney *U*-test revealed no significant differences between metabolite levels of a given compound in the supernatants derived from time-reduced and enhanced-resolution ^{1}H,^{1}H-COSY45 spectra for any of the four clones. Note that six of the time-reduced 50% NUS spectra including the medium control did not yield quantifiable glutamic acid signals.

3.2.2. Methanol Extracts

Next methanol extracts of the cancer cell pellets were analyzed. Figure 11 shows the average quantified metabolite levels derived from time-reduced (**a**) or enhanced resolution (**b**) 50% NUS ^{1}H,^{1}H-COSY45 spectra in the methanol extracts of the cell pellets of both cell lines, normalized to the amount of protein per pellet given after 48 h of cultivation. Note that one out of three biological replicates of the Panc02-H7 LDHA^{null} clones did not show quantifiable tyrosine signals.

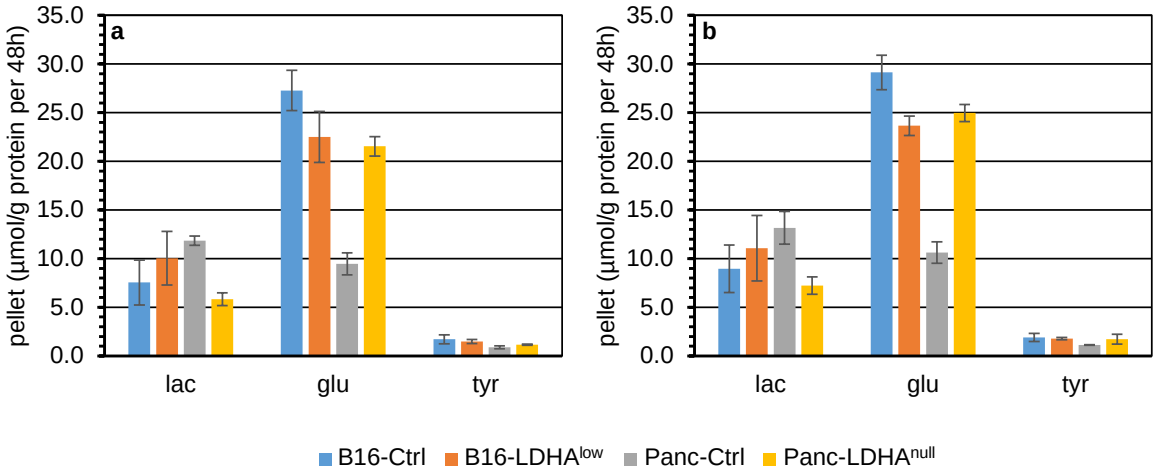

Figure 11. Amount of lactic acid (lac), glutamic acid (glu), and tyrosine (tyr) given in the methanol extractions of B16.SIY E12 (B16) melanoma and Panc02-H7 (Panc) pancreatic adenocarcinoma cell pellets, normalized to the amount of protein per pellet given in g after 48 h. The metabolite levels present in micromole derived from time-reduced (**a**) or enhanced resolution (**b**) ^{1}H,^{1}H-COSY45 spectra (*n* = 3 biological replicates per clone with the exception of tyrosine in the Panc-LDHA^{null} samples acquired with both NUS settings given *n* = 2 due to one missing value) are given in mean ± SD. A Mann-Whitney *U*-test was applied to test for significant differences in normalized compound levels between the control (Ctrl) and affected clones (LDHA^{low} and LDHA^{null}) of the corresponding cancer cell line.

The Mann-Whitney *U*-test revealed no significant differences between metabolite levels in the methanol extracts derived from time-reduced and enhanced-resolution ^{1}H,^{1}H-COSY45 spectra for any of the four clones. The metabolite levels in both NUS

spectra showed high concordance, for instance lactic acid in the B16-Ctrl clones revealed a metabolite level of 7.55 µmol/g protein in time-reduced while 8.96 µmol/g protein in enhanced resolution NUS spectra. The SD was overall comparable, showing exemplarily a value of ± 2.31 in time-reduced and 2.45 in enhanced resolution NUS spectra.

4. Discussion

4.1. NUS for Accelerated Quantification

SPIKE-IN DATASET

So far, there has been a lack in a comprehensive evaluation of different NUS parameters given a common reference dataset[84,102] and their validation in context of metabolomic data analyses.[103] Although various NUS settings exist e.g. in terms of sampling scheme and spectral reconstruction, there is still a lack of agreement on best practices.[104] Designing an optimal NUS sampling scheme is further limited by a lack of predicting the performance of a NUS schedule a priori and a consent performance metric.[102] To date, different NUS parameters in 2D NMR-based metabolomics have mostly only been preliminarily evaluated against each other.[9,12-14,16,78] In this contribution, a number of combinations of sampling scheme, reconstruction algorithm, NUS level, and spectra type have been tested. It is clear that the combinations tested are by no means exhaustive and, therefore, it is possible that other combinations will give similar or even better results.

RECONSTRUCTION ALGORITHMS

The strategies applied to date to the reconstruction of NUS spectra are versatile[5] and differ in their assumptions about the properties of the time domain signal or reconstructed spectrum.[3,4] Assumptions applicable to NUS processing include the introduction of a certain model of a spectrum as exploited in MDD,[4] a spectrum containing the least amount of information consistent with the measured data as assumed in maximum entropy[60,84] and in forward maximum entropy reconstruction,[12] knowledge on empty regions in a spectrum[105] and maximum sparsity underlying compressed sensing (CS) approaches. Typical methods applied in the context of CS include iterative re-weighted least squares (IRLS),[90] iterative soft thresholding (IST),[90] orthogonal matching pursuit (OMP),[90] its predecessor CLEAN,[90] and SCRUB.[106] Reconstruction algorithms appropriate for NUS are commonly non-parametric signal processing methods. However, parametric approaches such as maximum likelihood

and Bayesian methods, where the time-domain signal is described as a sum of exponentially decaying sinusoids, have also been used.[6] Another suitable parametric method is the sparse multidimensional iterative lineshape enhanced (SMILE) algorithm, which integrates a priori information about NMR signals for robust signal reconstruction.[107] In general, sufficient S/N is critical in the performance of reconstruction algorithms.[7,108]

For this contribution we included the two reconstruction methods implemented in TopSpin 3.1, R-MDD and CS-IRLS and additionally implemented MaxEnt and CS-IST. The latter two algorithms were chosen because MaxEnt is known to be a well established, very robust and versatile non-Fourier method which efficiently reduces artifacts[5,60,84,104,109] and CS-IST is a popular CS-based approach next to CS-IRLS.[90] For the purpose of this contribution, the number of reconstruction approaches was restricted to R-MDD, CS-IRLS, CS-IST and MaxEnt. In literature, CS has been shown to be the preferred reconstruction approach over R-MDD for 2D NMR in metabolomics, the latter resulting in increased noise artifacts.[9] As stated by others, heavy artifacts derived from strong peaks can mask weak signals,[90] making quantitative NMR analysis cumbersome.[75] With regard to the evaluation of NUS on the first spike-in dataset, there is a clear difference in signal recovery fidelity between R-MDD and CS-IRLS. Especially for the reconstruction of weak signals, CS-IRLS is clearly superior to both R-MDD and MaxEnt, whereas it performed slightly better than CS-IST. Findings from literature that MaxEnt enhances strong peaks and reduces weak peaks[64] match the results here that the strong signal of tyrosine is overestimated while the other four weak signals are severely underestimated. In particular, reconstruction of weak peaks in spectra with large dynamic range are more feasible with CS than with MaxEnt as the latter tends to diminish their peak intensities.[109] Although quantitative accuracy is not significantly different between CS-IRLS and CS-IST, CS-IRLS does reconstruct slightly more signals and overall is more accurate and precise. Kazimierczuk *et al.* explained their observed limited performance of IST compared to IRLS in that IST is well suited for spectra with a modest dynamic range while CS-IRLS is more suited for cases with a high dynamic range as is the case here.[83]

SAMPLING SCHEMES

Clearly, spectral quality does not only depend on the reconstruction technique to compute the NUS spectrum but also on the sampling scheme chosen.[76,102,110] The possible selection of NUS sampling schemes addressing issues of sensitivity, resolution, and randomness is manifold.[6] NUS schemes can be divided into on-grid and off-grid sampling. The former is characterized by sampling along the analogous US evolution times, while the latter does not fall on this Cartesian grid.[6,102] Off-grid sampling is applied mostly to spectra of more than two dimensions or requiring particularly narrow peak widths.[111] Examples of sampling schemes with point coordinates not falling on the Cartesian grid are radial sampling, spiral sampling, and concentric ring sampling (CRS).[6,111] As in this contribution solely 2D spectra were dealt with, on-grid sampling schemes such as unweighted, exponentially weighted, and sine-weighted Poisson gap sampling were concentrated on. Others have also investigated these sampling schemes for example with regard to the introduction of t_1 noise. It was noticed that unweighted sampling introduced F_1 ridges at high NUS densities while Poisson gap sampling clearly performed better in that regard.[14] Recently, Le Guennec *et al.* reported to have overcome t_1 noise arising from unweighted sampling below 25% NUS by using Poisson gap sampling.[14] Improved sensitivity, achievable for instance by choosing a scheme that samples more points where signal intensity of the FID is high,[16] is especially relevant to distinguish weak signals[110] from noise or artifacts.[102] It was shown that a substantial time reduction is achievable with an optimized sampling scheme.[11,14] Other sampling schemes known from the literature include for example burst sampling.[6] Similar to the on-grid sampling schemes applied in this contribution, it addresses the aspect of gaps in its sampling schedule.[6] In contrast to sPGS, which minimizes the length of gaps, burst-mode sampling minimizes the number of gaps.[6] Furthermore, beat-matched sampling (BMS) matches the sampling density to the signal envelope analogous to exponentially weighted sampling, but considers in addition the finer details of the predicted time-domain data.[6,56,102] Employing a set of known frequencies the expected time-domain signal is modeled as a sum of exponentially decaying sinusoids and the BMS pattern is adapted to collect data only at the greatest intensities of the modeled signal.[56] However, to date BMS has only been tested with moderate success on synthetic data.[56] As far as the data here are concerned,

sinusoidal Poisson-gap sampling outperformed unweighted and exponentially weighted sampling particularly in the reconstruction of weak signals.

VARIATIONS IN SEED NUMBER

The variation introduced by the seed number used for initializing the random number generator, which has been reported to influence the reliability of spectral reconstruction,[12] is particularly evident where data points are sparsely sampled.[63] The observation that sinusoidal Poisson-gap sampling is less affected by the seed value chosen than the unweighted and exponentially weighted sampling is in line with literature findings.[16] In fact, Hyberts *et al.* already showed in 2010 by means of an L^2 norm analysis on a synthetic FID of a single resonance given 25% NUS that sPSG is almost insensitive to the seed value chosen.[78] It was shown that even with sPSG, the chosen seed value exerts some influence on the results obtained. One has to keep this additional source of variation in mind when interpreting results obtained from NUS spectra because the results may not be reproducible without knowledge of the actual data points picked.[63] Employing 10.000 different seed values it has been demonstrated that the average sPGS scheme in combination with 12.5% NUS does not yield optimal results with regard to chemical shifts.[11] Optimizing the seed value chosen for the sPGS scheme may yield improved results with a spectral quality comparable to the US spectrum.[11]

SPECTRA TYPES

With regard to the performance of NUS considering the pulse sequence implemented,[9] NUS was expected to be more successful on the sparser ^{1}H,^{1}H-COSY45 than ^{1}H,^{1}H-TOCSY spectra. Surprisingly, for 75% and 50% NUS ^{1}H,^{1}H-COSY45 and ^{1}H,^{1}H-TOCSY are fairly comparable given the chosen dataset with 75% and 50% NUS. At 25% NUS, neither ^{1}H,^{1}H-TOCSY nor ^{1}H,^{1}H-COSY45 can be recommended for quantification, albeit ^{1}H,^{1}H-TOCSY is here slightly more accurate and precise.

OMITTED DATA POINTS

The spectral quality obtained from NUS depends critically on the amount of experimentally measured data points in the indirect dimension. The minimum amount of data points required to reliably reconstruct a spectrum is influenced by the signal density[112] and spectral type.[12] It is advised to choose a more conservative approach when dealing with many signals,[12] crowded spectra[113] or complex mixtures.[57] Generally, non-uniform sampling of only a subset of the full uniformly sampled dataset results in decreased sensitivity, however, if constructed properly, the sensitivity per unit measurement time can be increased.[102] As a consequence, a drastic reduction in experimental time by means of NUS is only possible if sensitivity is not limited.[114] Sensitivity depends on the cross signal intensity determined by the compound concentration, structure of the compound, and experimental factors.[13,58] Intrinsically strong peaks as in the spike-in datasets, for instance the selected tyrosine signal (H6 H8/H5 H9), are comparably insensitive to the sampling scheme and reconstruction technique applied.[110] Previously, often either pure compounds,[11] synthetic samples containing selected metabolites,[9,14] or samples comprising metabolite concentrations in the millimolar[9,11] range were analyzed, thereby drastically reducing the importance of sensitivity issues. When the sensitivity or number of collected indirect data points is too low, NUS spectra are prone to artifacts.[7] While dependent on the sample and processing procedure, a rule of thumb for biological samples is that the sampling density per indirect dimension needs to be roughly one-third relative to the US amount to reduce sampling artifacts and maintain sufficient sensitivity.[62] A considerable, approximately 22-fold reduction in acquisition time compared to the conventional linear sampling of lyophilized human urine specimens was accomplished acquiring one third of the linearly sampled data points with the use of a relaxation enhancing agent applying forward maximum (FM) entropy reconstruction on *J*-compensated $^{1}H,^{13}C$-HSQC spectra given added metabolite concentrations of 300 µM and higher.[13] Other observations taking 12.5% NUS of multiplicity edited $^{1}H,^{13}C$-HSQC spectra were derived from highly concentrated pure samples of 20 and 80 mM.[11] As the author of the cited study states himself, such a low NUS percentage is not expected to deliver adequate results for complex samples or spectra containing large numbers of signals. Le Guennec *et al.* observed a substantial increase in t_1-noise ridges at a threshold of

below 30% NUS and for thresholds of below 25% a drop in peak intensities.[9] Applying NUS for accelerated quantification in 2D NMR while maintaining spectral quality is typically performed with NUS levels of 20-30%.[14] Furthermore, low amounts of sparse sampling yield a higher reconstruction fidelity when the amount of indirect data points to sample from is high, concluding that the results obtained with NUS rely rather on the relation of the amount of collected data points to the number of expected signals than the NUS percentage taken.[11] This explains why in the study by Hyberts *et al.* in 2007,[12] the amount of in total 8k t_1 increments for the conventionally sampled ultrahigh-resolution ^{1}H-^{13}C HSQC spectrum of leukocyte extracts is high enough to yield a reliable reconstruction even when the amount of data points sampled is reduced to one-seventh, which is still impractically long for routine applications. As the authors of this study state themselves, the information content recorded is high compared to the information needed for spectrum reconstruction, this way explaining the feasibility of NUS given the reduced dataset. In comparison to the above cited literature, data here show that reliable quantitative results can be obtained with slightly higher levels of experimentally sampled data points (50%), whereas at a NUS level of 25%, a substantial drop in accuracy, precision and number of recovered signals is observed. This can be explained by the fact that urine as a real, highly complex biological matrix was taken in which metabolites were added in relative low physiologically relevant concentrations. Also, ^{1}H,^{1}H TOCSY and ^{1}H,^{1}H-COSY45 spectra were employed that contain a large number of metabolite signals, choosing a total number of data points (including measured and reconstructed data points) in the indirect dimension in the range typically applied in 2D metabolomics.[9,14] Here, the use of 50% NUS did not affect the determination of the urinary levels of metabolites of interest. In some cases, however, relative intensity ratios larger than one between NUS and US spectra were observed. This is explained by the fact that if a very weak signal is reconstructed by means of the applied reconstruction algorithm, reconstruction is more challenging which may lead to an over- or underestimation.

PARAMETER VALIDATION

Concerning compound concentrations, the performance of NUS with 50% omitted data points and the optimized parameters with regard to US is comparable given different urine matrices as could be shown by comparing the median ratios and mean CVs of a given spike-in metabolite using either a low (urine I) or highly (urine II) concentrated urine.

COHORT STUDY SAMPLES

To demonstrate the suitability of NUS for a real case study employing accelerated metabolite quantification, urinary specimens of apparently healthy volunteers of the GNC cohort were compared to those with chronic kidney disease of the GCKD study. Metabolites were analyzed which are relevant in the context of diabetic nephropathy[25,101,115-118] being the major cause of chronic kidney disease in the Western population.[92] For this, a set of metabolites expected to be relevant for the discrimination of GCKD and GNC specimens and the metabolites used for the spike-in experiments were considered. Urine metabolomics has been shown to relate specific metabolite changes to diabetic nephropathy.[92] One has to keep in mind that considerable binding of the internal standard TSP to protein in case of strong proteinuria may occur as present for some of the GCKD specimen (Table 1). Consequently, the signal of TSP may be reduced leading to an overquantfication of urinary metabolites.[58,119] As such, the concentration values obtained with both NUS and US have to be treated with care. The necessity of acquiring 2D NMR spectra of these cohort study urine specimens for reliable signal quantification is given since the metabolites under investigation here mutually overlap in 1D ^{1}H spectra. Although the lower limits of quantification (LLOQs) were higher for NUS than US, they were still sufficiently low to determine the urinary levels of metabolites of interest. Overall, there is a good agreement between the data obtained by US and 50% NUS, respectively, as evidenced by the Bland-Altman plots given that the mean difference between both methods lies at around zero, the standard deviation compared to the intensity range is small, and that there are no signal intensity dependency trends visible (Figure S14 and Figure S15 **a**). The only exception is the weak tryptophan signal for which larger differences were observed. The Bland-Altman plots comparing

the quantitative agreement between 1D ^{1}H and 50% NUS spectra (Figure S13), however, show signal intensity dependent differences predominantly for lactic acid and glutamine, both highly overlapped in 1D ^{1}H spectra and well resolved by 2D NMR. As shown in Figure S12 a, both US and 50% NUS ^{1}H,^{1}H COSY45 allow the reliable determination of fold changes for glutamine and lactic acid. Therefore, it is safe to assume that the observed variations are due to imperfect signal integration in 1D spectra, which is hampered despite signal deconvolution from extensive signal overlap present in biological matrices such as human urine. It has been shown that the quantification results obtained from 2D ^{1}H,^{13}C-HSQC spectra are superior to those obtained from 1D spectra.[58] Furthermore, the boxplots and *p*-values derived from the NUS and US data are comparable. The similarity of the US and 50% NUS data shows that NUS is suitable for quantifying compounds present at physiological concentrations in complex biological specimens in half the measurement time.

4.2. NUS for Enhanced Spectral Resolution

Applying NUS in metabolomics to aim at an enhanced spectral resolution in the indirect dimension has so far only been partly exploited for example for the analysis of carbon isotopomers.[57] Therefore as its second usage, NUS was utilized to increase the spectral resolution in acquired spectra of urine and cancer cell samples. In the case of urine, enhanced resolution NUS was applied to a highly concentrated urine specimen derived from the cohort study dataset while for cancer cell metabolomics, two different cell lines modified in their LDHA expression were utilized. To this end, first the gain in metabolite signals and spectral information in the NUS compared to both a time-equivalent and an enhanced resolution US spectrum was analyzed. Note that the enhanced resolution US spectrum possesses the same resolution as the NUS spectrum. It is demonstrated that NUS when applied for enhancing the resolution of two-dimensional homonuclear spectra compared to the time-equivalent US spectrum results in a higher total amount of peaks with more resolved peak shapes, newly emerged peaks, and separation of overlapping peaks. This shows that enhanced-resolution NUS compared to time-equivalent US leads to a gain in spectral information. Better-defined peak shapes of the same compound are

beneficial for compound analysis e.g. in terms of more reliable identification, more precise quantification like seen for glutamic acid in the cancer cell supernatants, and improved elucidation of coupling patterns. More peaks per compound due to enhanced resolution have been shown to allow improved isotopomere analysis of a given compound resulting from NUS to enhance the spectral resolution compared to the time-equivalent US spectrum.[57] An increase in spectral resolution in NUS spectra compared to time-equivalent US spectra given a complex mixture of cell lysates was previously shown for ^{1}H,^{13}C-HSQC spectra applying 25% NUS in a sine-weighted Poisson-gap sampling fashion and hmsIST (Harvard Medical School Iterative Soft Threshold) reconstruction resulting in well-resolved carbon isotopomere multiplet structures promoting proper coupling analysis.[57] The presence of newly emerged peaks in the NUS spectrum demonstrates that enhanced resolution can lower the detection limit of peaks that would otherwise get lost with lower spectral resolution. Resolving signal multiplets in the indirect dimension by an increase in resolution aids compound identification.[14] Corroborating to this contribution, Le Guennec *et al*. have shown on artificial metabolite mixtures that resolution-enhanced 2D ^{1}H,^{13}C-HSQC and ^{1}H,^{1}H-TOCSY spectra applying NUS choosing 3.125% and 12.5% of sparse sampling, respectively, were able to resolve peaks which were broadly overlapped in the time-equivalent US spectra.[14] The authors demonstrated a substantial increase in spectral resolution of signals derived from small molecules in a complex mixture by means of NUS without increase in measurement time and no introduction of false peaks.[14] Achieving separated compound signals aids in compound quantification and occurrence of less peak overlap in crowded regions allowing adjacent signals to be discriminated. The enhanced resolution NUS spectra show a decrease in sensitivity compared to the enhanced resolution US spectra of identical resolution. This is due to the fact that small imperfections in the reconstruction of the missing data points lead subsequently to a decrease in signal to noise ratio.[7] Hyberts *et al.* showed in 2007 that full separation of overlapped peaks in ^{1}H,^{13}C-HSQC spectra of a complex cell extraction mixture was only accomplished given high spectral resolution resulting in sharper peak shapes and increased peak heights, requiring, however, an undesirably long measurement time.[12] This explains why with enhanced-resolution NUS, the glutamic acid signal in the cancer cell supernatants could be consistently quantified while it was not quantifiable in all time-reduced NUS spectra because the resolution was not high enough to resolve this signal in all samples.

5. Conclusion

This is the first study to demonstrate that 50% NUS can be applied to the determination of metabolites in complex biological specimens for sufficiently concentrated compounds without a noteworthy drop in the number of reconstructed signals, accuracy, precision, and sensitivity using a combination of optimized NUS parameters. These are a sine-weighed Poisson-gap sampling applying a compressed sensing approach employing the iterative re-weighted least squares method for the reconstruction of 2D homonuclear $^{1}H,^{1}H$ spectra. Data clearly show that reliable metabolite quantification crucially depends on the NUS parameters chosen, emphasizing the importance of selecting the optimal set of NUS approaches.

NUS in 2D NMR spectroscopy promises to facilitate compound quantification and identification with the potential to complement or substitute 1D NMR measurements that are prone to signal overlap. As it was demonstrated in the context of chronic kidney disease and cancer, 2D NUS NMR measurements are well applicable to real case specimens with the potential to aid e.g. in earlier disease discovery or therapeutic treatment. Together with other advances in instrument design, such as state-of-the-art cryogenic probes, use of 2D NMR spectroscopy in large biomedical cohort studies seems feasible by means of NUS for accelerated acquisition with further reductions in measurement time to about one hour per specimen.

6. Appendix

6.1. Supplemental Figures

Accelerated Quantification Spike-In Plots

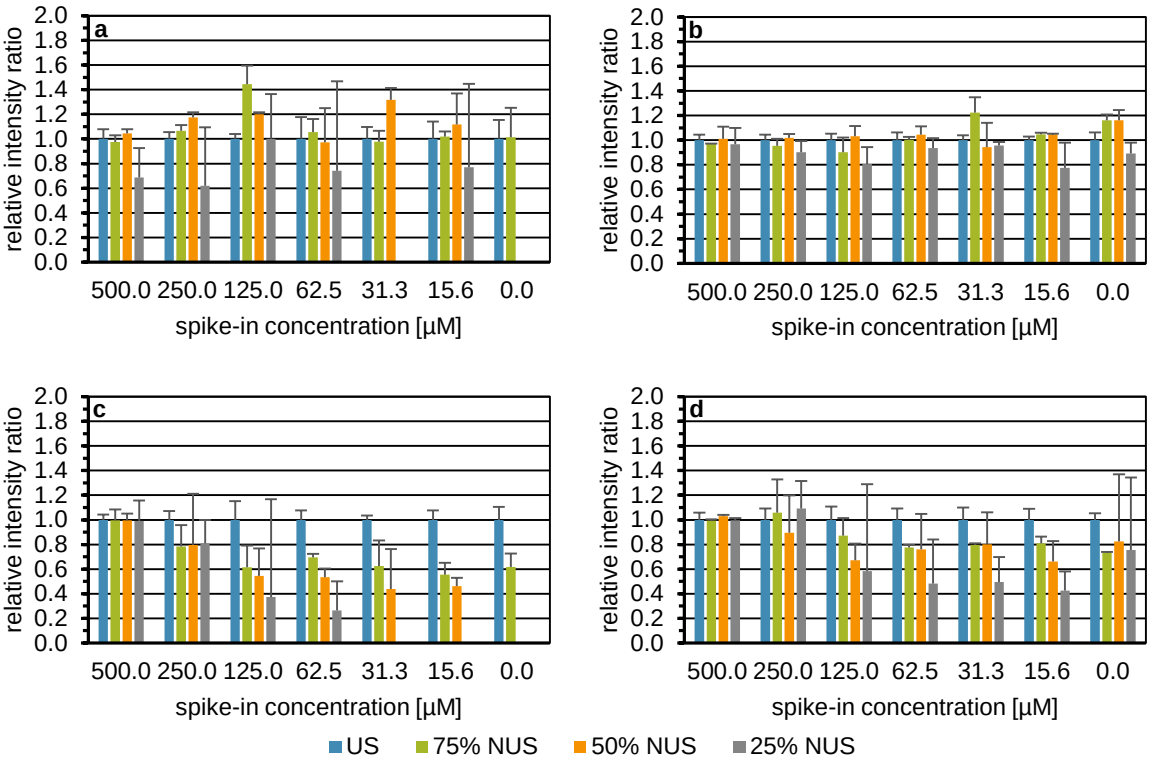

Figure S1. Signal reconstruction with R-MDD. Influence of the signal reconstruction with R-MDD on the recovery of the relative intensity of a selected cross signal in each spike-in sample and the blank control employing urine I, exemplarily shown for tryptophan (**a**), tyrosine (**b**), lactic acid (**c**), and threonine (**d**). US ^{1}H, ^{1}H TOCSY spectra (n = 5) indicated by blue bars. NUS ^{1}H, ^{1}H TOCSY spectra measured with 75%, 50%, and 25% of the linearly sampled data points depicted by green, orange, and gray bars, respectively. Each NUS spectrum was acquired with an exponentially weighted sampling scheme taking three seed values per NUS level. On the x-axis, the spike-in concentration given in micromolar is shown. The intensity ratio of the total cross peak integral scaled to the internal standard TSP of the metabolite signal (mean + SD) obtained with US or NUS to US is plotted on the y-axis. Published in von Schlippenbach *et al.* 2018.[69]

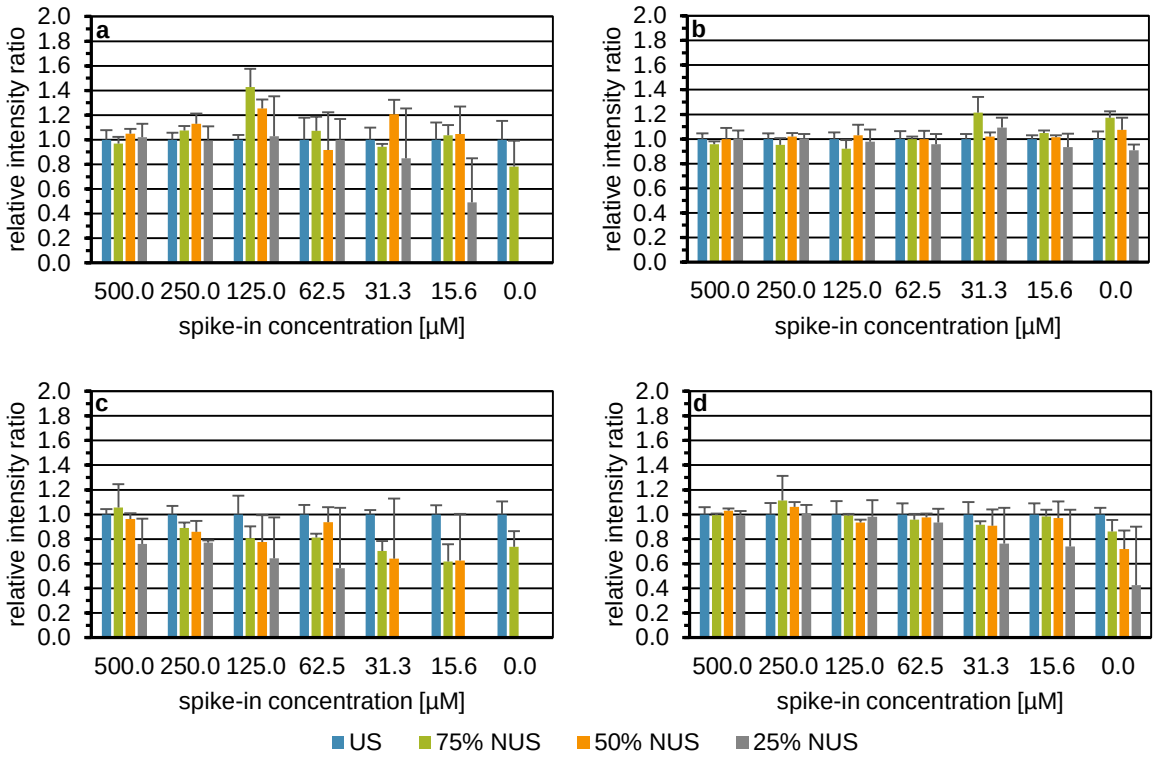

Figure S2. Signal reconstruction with CS-IRLS. Influence of the signal reconstruction with CS-IRLS on the recovery of the relative intensity of a selected cross signal in each spike-in sample and the blank control employing urine I, exemplarily shown for tryptophan (**a**), tyrosine (**b**), lactic acid (**c**), and threonine (**d**). US ^{1}H, ^{1}H TOCSY spectra (n = 5) indicated by blue bars. NUS ^{1}H, ^{1}H TOCSY spectra measured with 75%, 50%, and 25% of the linearly sampled data points depicted by green, orange, and gray bars, respectively. Each NUS spectrum was acquired with an exponentially weighted sampling scheme taking three seed values per NUS level. On the x-axis, the spike-in concentration given in micromolar is shown. The intensity ratio of the total cross peak integral scaled to the internal standard TSP of the metabolite signal (mean + SD) obtained with US or NUS to US is plotted on the y-axis. Published in von Schlippenbach *et al.* 2018.[69]

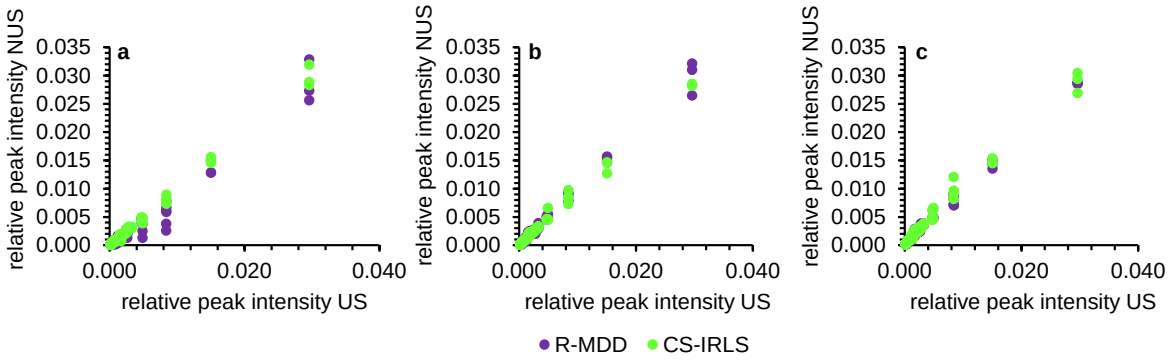

Figure S3. X/Y plots supplementing the corresponding bar charts on signal reconstruction influence. Scatter plots showing the correlation between US (x-axis) and NUS (y-axis) normalized peak volumes when implementing the reconstruction method recursive multidimensional decomposition (R-MDD) or the compressed sensing approach employing the iterative re-weighted least squares method (CS-IRLS) depicted by purple and green data points, respectively. The relative peak intensities, being the intensity ratio of the total cross peak integral of the corresponding metabolite signal scaled to the internal standard TSP, was obtained for US from the mean of five measurements while for NUS with 25% (**a**), 50% (**b**), or 75% (**c**) sampling density. Each data series corresponds to the relative peak intensity of a given metabolite over all spike-in concentrations for the number of observed recoveries (Table S1) having taken a defined seed value of three. Published in von Schlippenbach *et al.* 2018.[69]

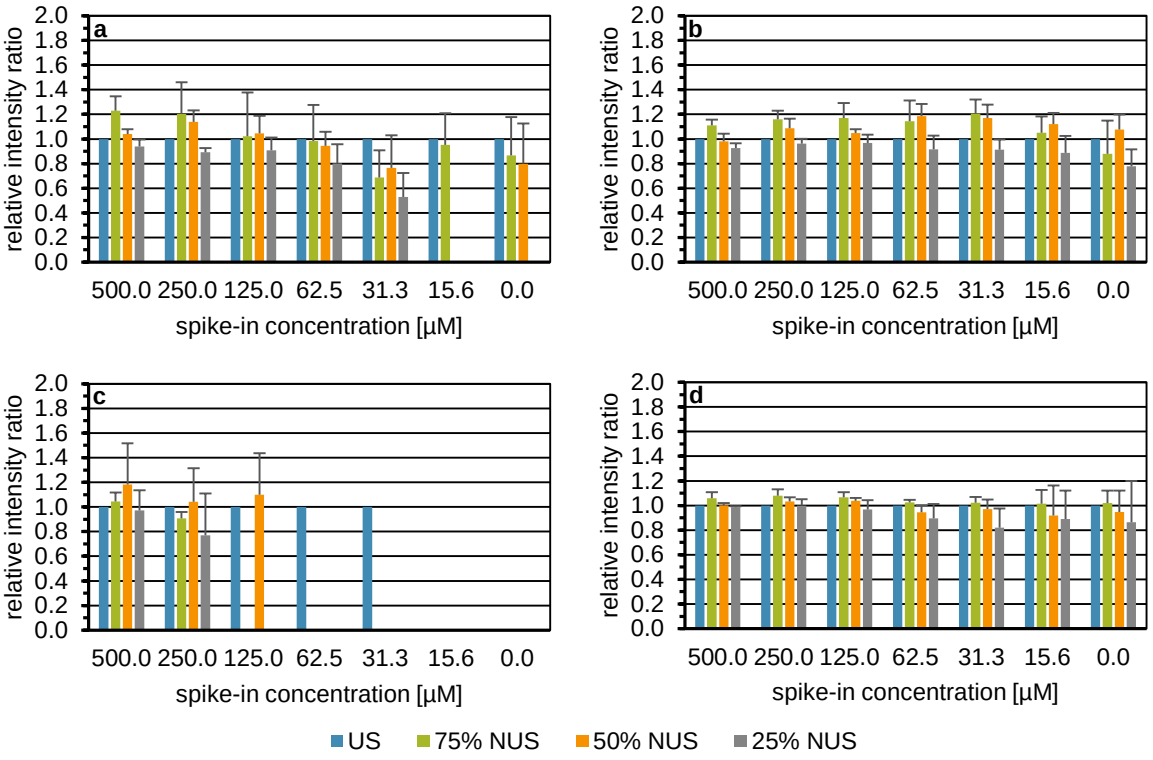

Figure S4. Use of unweighted sampling. Influence of the unweighted sampling scheme on the recovery of the relative intensity of a selected cross signal of tryptophan (**a**), glutamine (**b**), glutamic acid (**c**), and threonine (**d**) in each spike-in sample and the blank control employing urine I. US ^{1}H, ^{1}H TOCSY spectrum (n = 1) indicated by blue bars. NUS ^{1}H, ^{1}H TOCSY spectra simulated from the US spectrum displayed with 75%, 50%, and 25% of the linearly sampled data points depicted by green, orange, and gray bars, respectively. Each NUS spectrum was constructed with six seed values per NUS level and reconstructed with the compressed sensing approach employing the iterative re-weighted least squares method. On the x-axis, the spike-in concentration given in micromolar is shown. The intensity ratio of the total cross peak integral scaled to the internal standard TSP of the metabolite signal (mean + SD) obtained with US or NUS to US is plotted on the y-axis. Published in von Schlippenbach *et al.* 2018.[69]

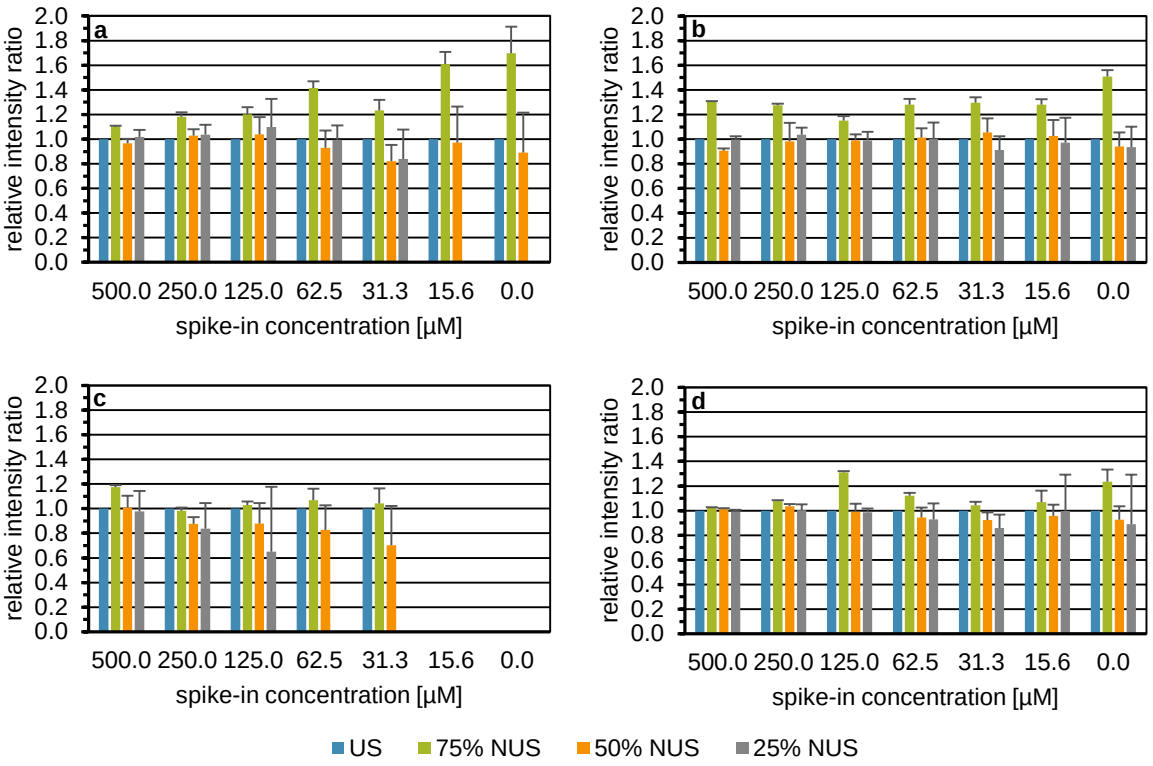

Figure S5. Use of exponentially weighted sampling. Influence of the exponentially weighted sampling scheme on the recovery of the relative intensity of a selected cross signal of tryptophan (**a**), glutamine (**b**), glutamic acid (**c**), and threonine (**d**) in each spike-in sample and the blank control employing urine I. US ^{1}H, ^{1}H TOCSY spectrum (n = 1) indicated by blue bars. NUS ^{1}H, ^{1}H TOCSY spectra simulated from the US spectrum displayed with 75%, 50%, and 25% of the linearly sampled data points depicted by green, orange, and gray bars, respectively. Each NUS spectrum was constructed with six seed values per NUS level and reconstructed with the compressed sensing approach employing the iterative re-weighted least squares method. On the x-axis, the spike-in concentration given in micromolar is shown. The intensity ratio of the total cross peak integral scaled to the internal standard TSP of the metabolite signal (mean + SD) obtained with US or NUS to US is plotted on the y-axis. Published in von Schlippenbach *et al.* 2018.[69]

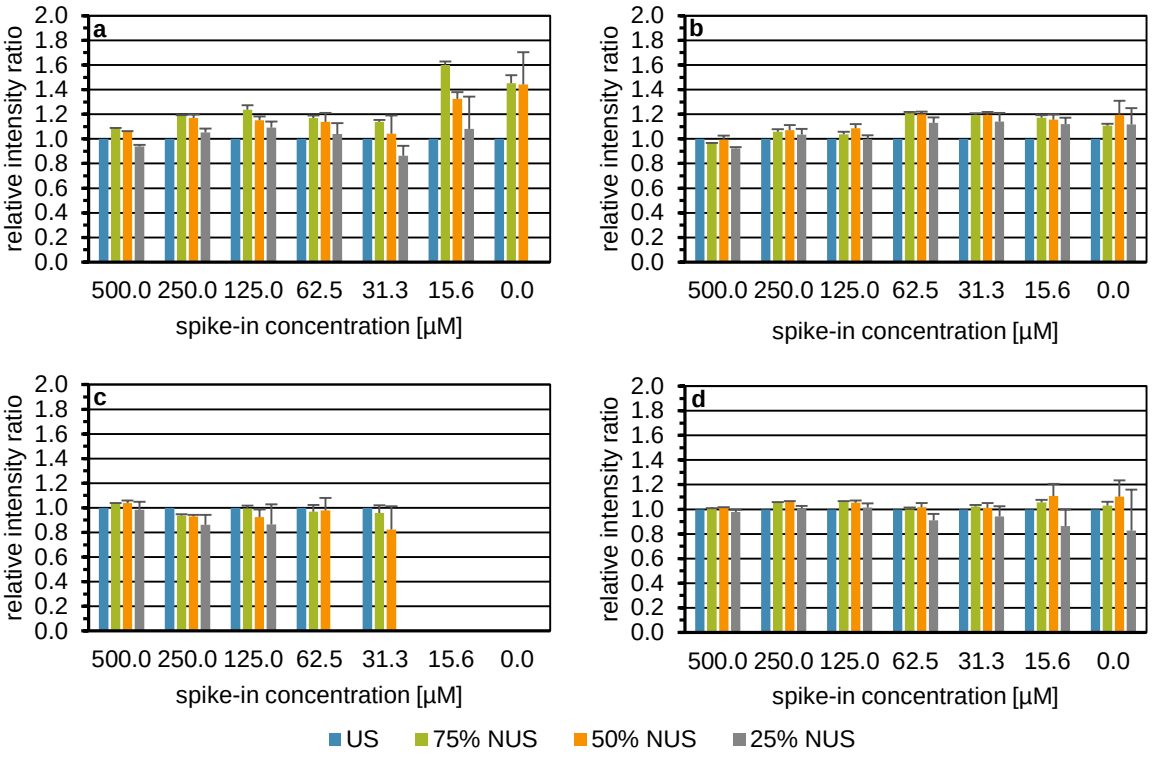

Figure S6. Use of sinusoidal Poisson-gap sampling. Influence of the sinusoidal Poisson-gap sampling scheme on the recovery of the relative intensity of a selected cross signal of tryptophan (**a**), glutamine (**b**), glutamic acid (**c**), and threonine (**d**) in each spike-in sample and the blank control employing urine I. US ^{1}H, ^{1}H TOCSY spectrum (n = 1) indicated by blue bars. NUS ^{1}H, ^{1}H TOCSY spectra simulated from the US spectrum displayed with 75%, 50%, and 25% of the linearly sampled data points depicted by green, orange, and gray bars, respectively. Each NUS spectrum was constructed with six seed values per NUS level and reconstructed with the compressed sensing approach employing the iterative re-weighted least squares method. On the x-axis, the spike-in concentration given in micromolar is shown. The intensity ratio of the total cross peak integral scaled to the internal standard TSP of the metabolite signal (mean + SD) obtained with US or NUS to US is plotted on the y-axis. Published in von Schlippenbach *et al.* 2018.[69]

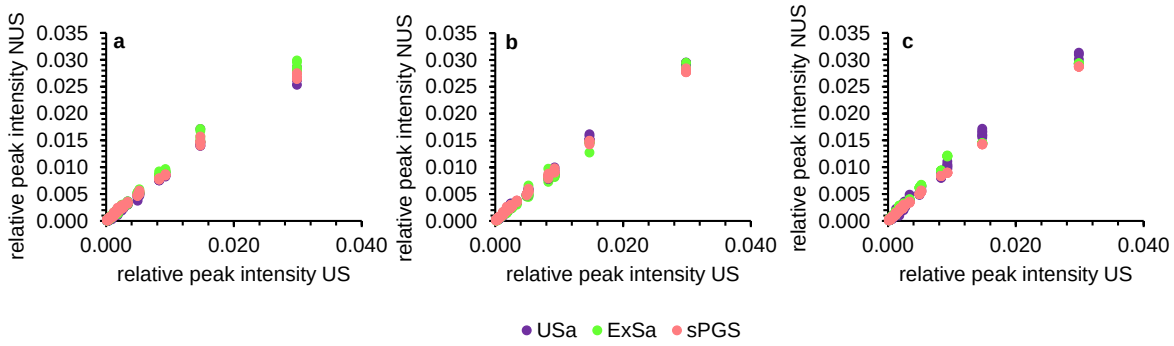

Figure S7. X/Y plots supplementing the corresponding bar charts on sampling scheme influence. Scatter plots showing the correlation between US (x-axis) and NUS (y-axis) normalized peak volumes when implementing the sampling schemes unweighted sampling (USa), exponentially weighted sampling (ExSa), or sine-weighted Poisson-gap sampling (sPGS) depicted by purple, green, and red data points, respectively. The relative peak intensities, being the intensity ratio of the total cross peak integral of the corresponding metabolite signal scaled to the internal standard TSP, was obtained for US from the measurement taken for generating simulated NUS spectra while for NUS with 25% (**a**), 50% (**b**), or 75% (**c**) sampling density. Each data series corresponds to the relative peak intensity of a given metabolite over all spike-in concentrations for the number of observed recoveries (Table S1) having taken a defined seed value of six. Published in von Schlippenbach *et al.* 2018.[69]

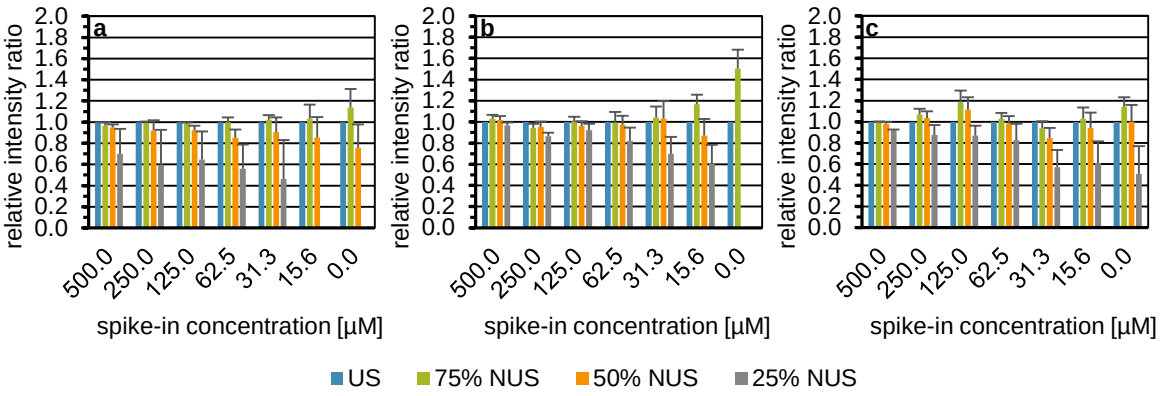

Figure S8. Comparison of spectra types. Influence of the spectral type on the recovery of the relative intensity of a selected cross signal of tryptophan (**a**), glutamic acid (**b**), and threonine (**c**) in each spike-in sample and the blank control employing urine I. US ^{1}H, ^{1}H COSY45 spectrum (*n* = 1) indicated by blue bars. NUS spectra simulated from the US spectrum displayed with 75%, 50%, and 25% of the linearly sampled data points depicted by green, orange, and gray bars, respectively. Each NUS spectrum was constructed with a sinusoidal Poisson-gap sampling scheme taking six seed values per NUS level and reconstructed with the compressed sensing approach employing the iterative re-weighted least squares method. On the x-axis, the spike-in concentration given in micromolar is shown. The intensity ratio of the total cross peak integral of the metabolite signal scaled to the internal standard TSP (mean + SD) obtained with US or NUS to US is plotted on the y-axis. Published in von Schlippenbach *et al.* 2018.[69]

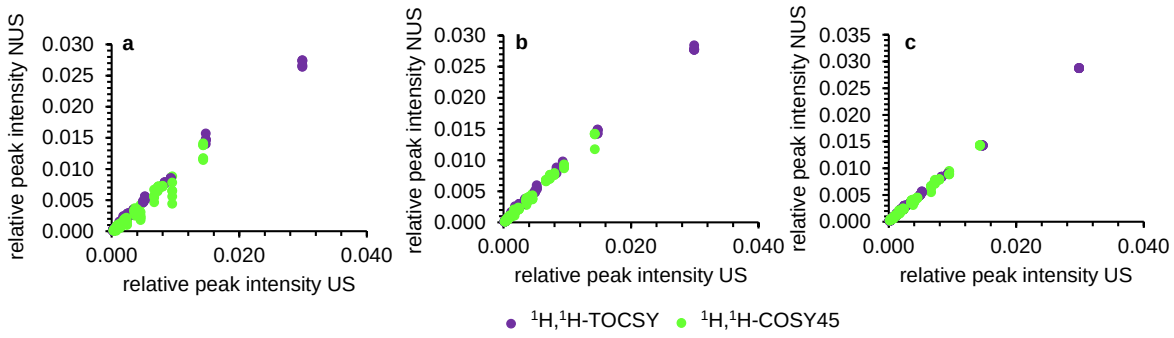

Figure S9. X/Y plots supplementing the corresponding bar charts on spectra type influence. Scatter plots showing the correlation between US (x-axis) and NUS (y-axis) normalized peak volumes when implementing ^{1}H,^{1}H TOCSY or ^{1}H,^{1}H-COSY45 depicted by purple and green data points, respectively. The relative peak intensities, being the intensity ratio of the total cross peak integral of the corresponding metabolite signal scaled to the internal standard TSP, was obtained for US from the measurement taken for generating simulated NUS spectra while for NUS with 25% (**a**), 50% (**b**), or 75% (**c**) sampling density. Each data series corresponds to the relative peak intensity of a given metabolite over all spike-in concentrations for the number of observed recoveries (Table S1) having taken a defined seed value of six. Published in von Schlippenbach *et al.* 2018.[69]

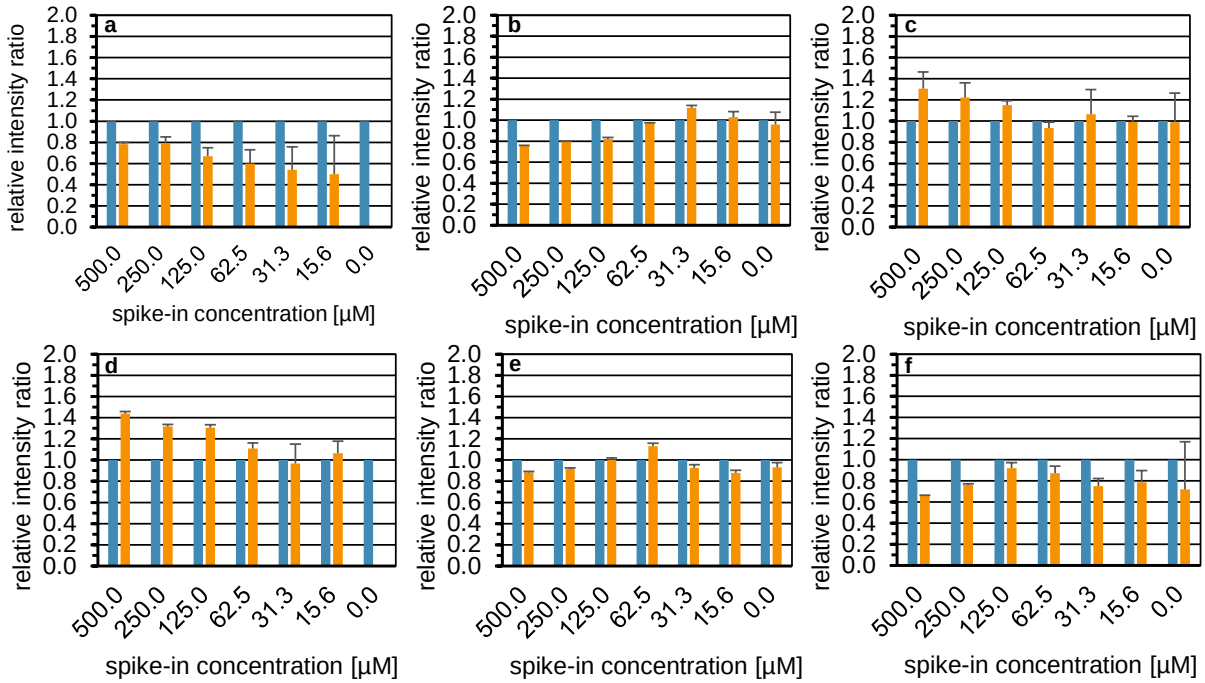

Figure S10. Signal reconstruction with CS-IST. Influence of the signal reconstruction with compressed sensing employing the iterative soft thresholding method on the recovery of the relative intensity of a selected cross signal of tryptophan (**a**), tyrosine (**b**), glutamine (**c**), glutamic acid (**d**), lactic acid (**e**), and threonine (**f**) in each spike-in sample and the blank control employing urine I. US ^{1}H,^{1}H-COSY45 spectrum (n = 1) indicated by blue bars. NUS spectra simulated from the US spectrum displayed with 50% of the linearly sampled data points depicted by orange bars. Each NUS spectrum was constructed with a sinusoidal Poisson-gap sampling scheme taking six seed values per NUS level. On the x-axis, the spike-in concentration given in micromolar is shown. The intensity ratio of the total cross peak integral of the metabolite signal scaled to the internal standard TSP (mean + SD) obtained with US or NUS to US is plotted on the y-axis. Published in von Schlippenbach *et al.* 2018.[69]

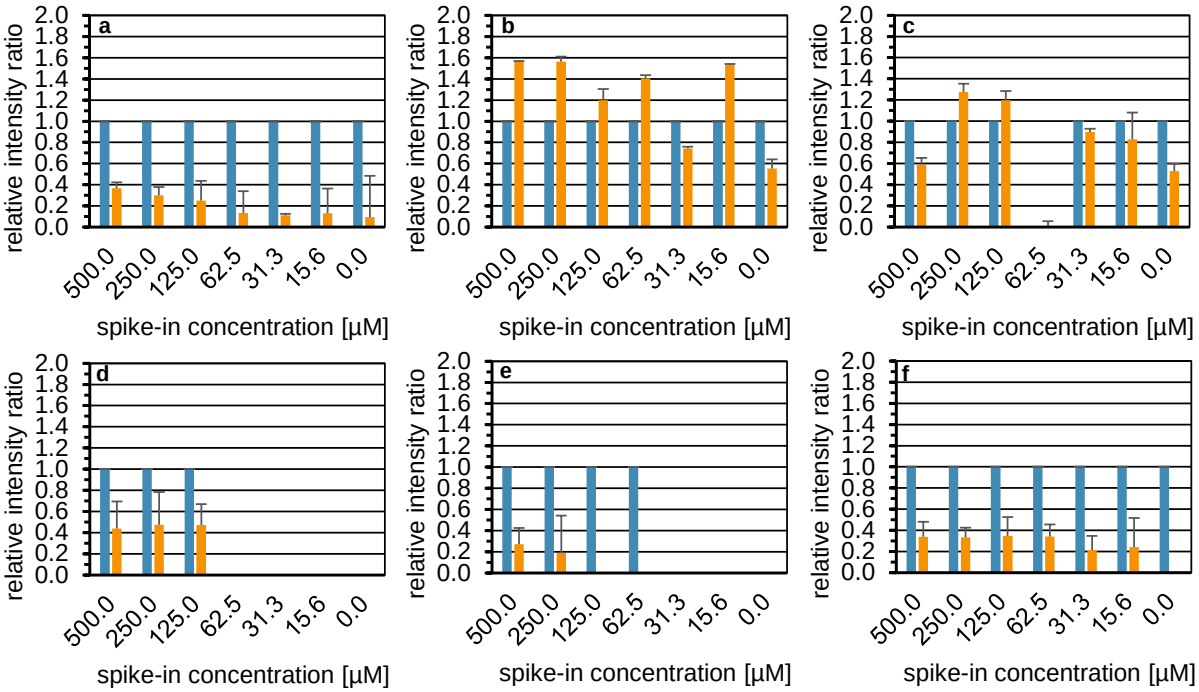

Figure S11. Signal reconstruction with MaxEnt. Influence of the signal reconstruction with maximum entropy on the recovery of the relative intensity of a selected cross signal of tryptophan (**a**), tyrosine (**b**), glutamine (**c**), glutamic acid (**d**), lactic acid (**e**), and threonine (**f**) in each spike-in sample and the blank control employing urine I. US ^{1}H,^{1}H-TOCSY spectrum (n = 1) indicated by blue bars. NUS spectra simulated from the US spectrum displayed with 50% of the linearly sampled data points depicted by orange bars. Each NUS spectrum was constructed with a sinusoidal Poisson-gap sampling scheme taking three seed values per NUS level. On the x-axis, the spike-in concentration given in micromolar is shown. The intensity ratio of the total cross peak integral of the metabolite signal scaled to the internal standard TSP (mean + SD) obtained with US or NUS to US is plotted on the y-axis. Published in von Schlippenbach *et al.* 2018.[69]

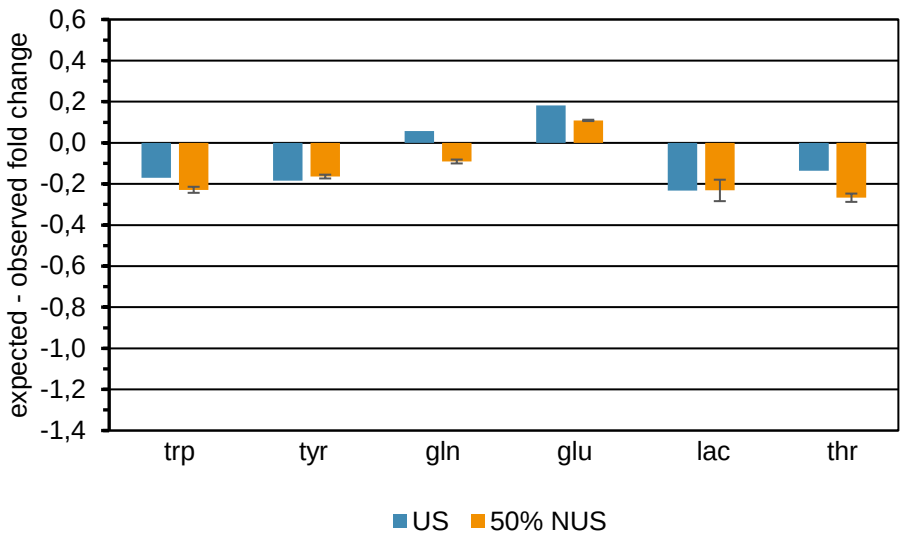

Figure S12a. Difference between expected and observed fold changes of each spike-in metabolite from the spike-in data employing urine I obtained with US or with 50% NUS. Here, fold changes of two were considered. For this, the relative signal intensity of a given metabolite in the blank control was subtracted from that in the spike-in samples. With six different spike-in concentration levels, this resulted in five fold changes of two per metabolite and spectrum. These five values were averaged to obtain one value per metabolite and spectrum. As each 50% NUS experiment was executed with six replicates (six seed values), this resulted in six values per metabolite. From this data, for all metabolites the mean ± SD were plotted. Data of the US ^{1}H,^{1}H-COSY45 spectrum (*n* = 1) are indicated by blue bars, 50% NUS by orange bars. Published in von Schlippenbach *et al.* 2018.[69]

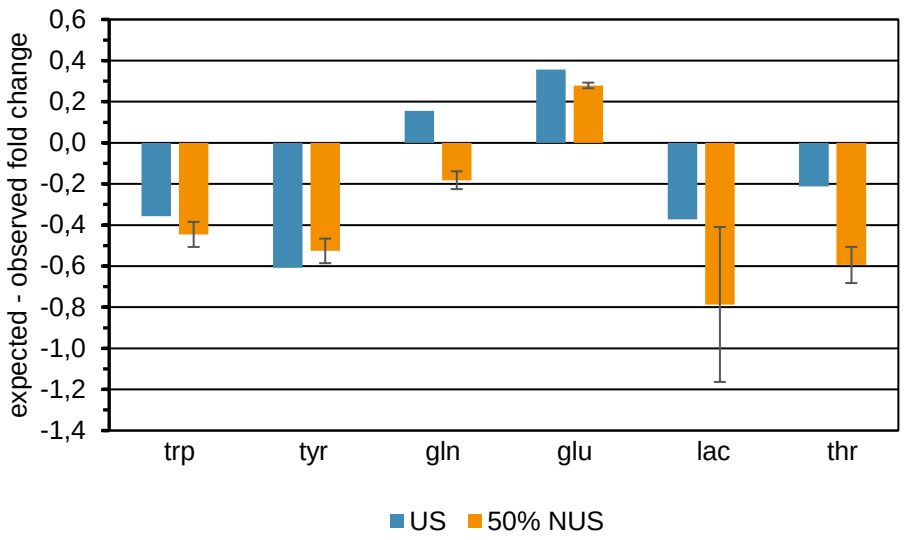

Figure S12b. Difference between expected and observed fold changes of each spike-in metabolite from the spike-in data employing urine I obtained with US or 50% NUS. Here, fold changes from all pairwise comparisons were considered. For this, the relative signal intensity of a given metabolite in the blank control was subtracted from that in the spike-in samples. With six different spike-in concentration levels, this resulted in fifteen fold changes per metabolite and spectrum. These fifteen values were averaged to obtain one value per metabolite and spectrum. As each 50% NUS experiment was executed with six replicates (six seed values), this resulted in six values per metabolite. From this data, for all metabolites the mean ± SD was plotted. Data of the US ^{1}H,^{1}H-COSY45 spectrum (*n* = 1) are indicated by blue bars, 50% NUS by orange bars. Published in von Schlippenbach *et al.* 2018.[69]

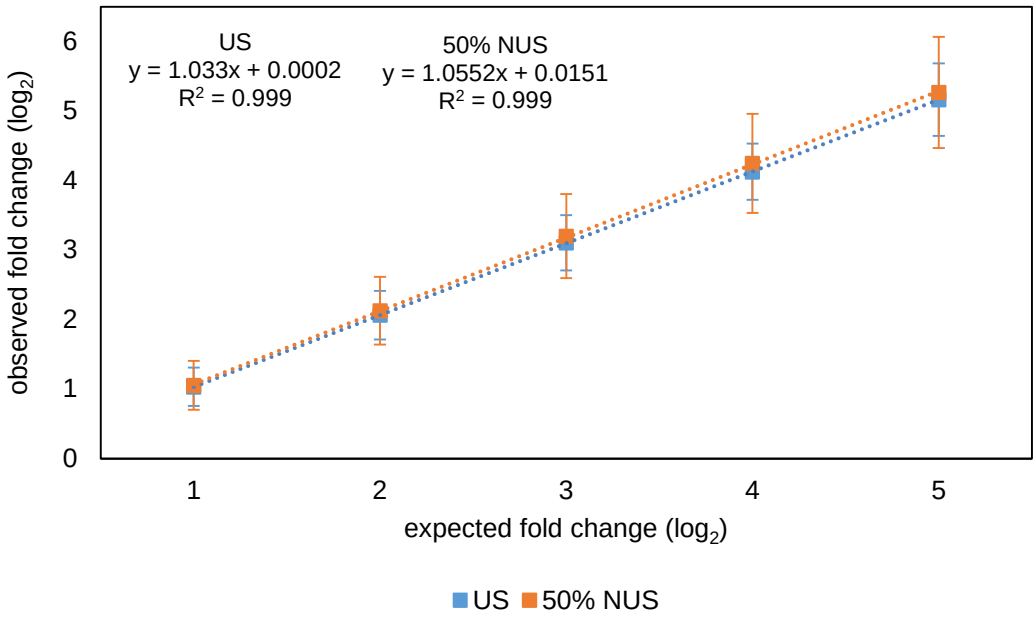

Figure S12c. Linear dependency between observed and expected fold changes over all metabolites including all fold changes from two to thirty-two from the spike-in data employing urine I. The data was log base 2 transformed and plotted as the mean ± SD. The dashed lines represent the regression lines for the US and 50% NUS data, the respective regression equations and coefficients of determination are given in the figure. Data of the US ^{1}H,^{1}H-COSY45 spectrum and the 50% NUS spectra are indicated by blue and orange squares. Published in von Schlippenbach *et al.* 2018.[69]

Application of Accelerated Quantification with NUS to Urinary Specimens of CKD Patients and Healthy Subjects

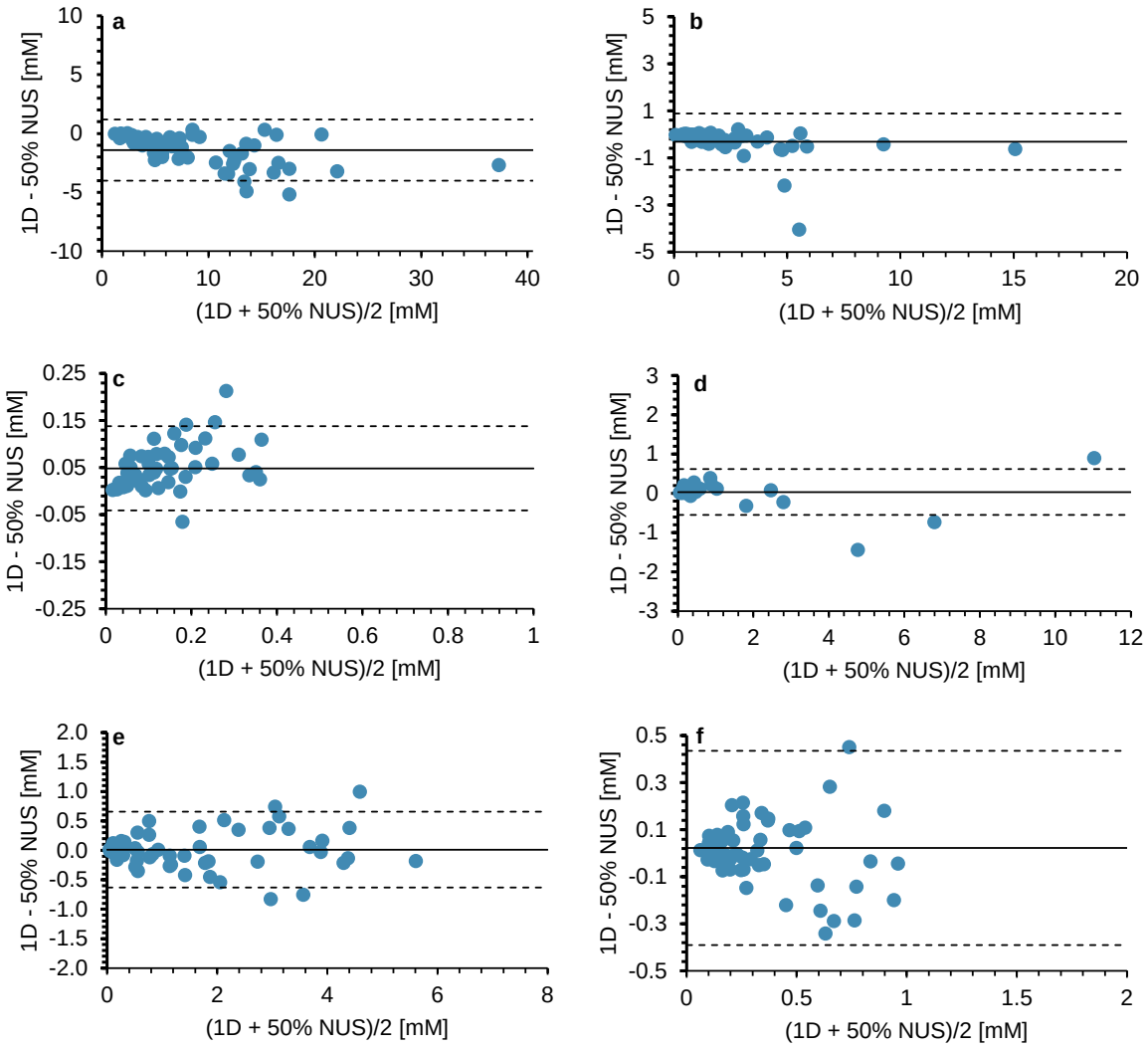

Figure S13. Agreement between 1D ^{1}H-NOESY and 2D ^{1}H,^{1}H-COSY45 50% NUS data of GCKD and GNC specimens. Bland-Altman plots showing the agreement between absolute metabolite quantification given in millimolar derived from 1D ^{1}H-NOESY or NUS ^{1}H,^{1}H-COSY45 spectra (*n* = 56 per metabolite and spectral type; for exceptions see legend Table S13) of selected metabolites, namely creatinine (**a**), hippuric acid (**b**), lactic acid (**c**), D-glucose (**d**), citric acid (**e**), and glutamine (**f**) in urine specimens from patients with CKD and healthy subjects (GNC). Pseudouridine was not considered because it was not present as a reference in the compound library of Chenomx NMR Suite 8.2. Note that the glucose level of one GCKD sample yielding a concentration of 26.23 mM (derived from 1D) or 26.58 mM (derived from 50% NUS) was not included in the Bland-Altman plot for reasons of depiction but considered for calculation of the mean ± 1.96*SD. The mean metabolite concentration of both methods is given on the x-axis, the difference between both on the y-axis. The solid line marks the mean difference between both methods, the dashed lines the 95% limits of agreement as mean ± 1.96*SD. Note that in case of strong proteinuria, as present for some of the GCKD specimens (Table 1), both the internal standard TSP as well as some of the metabolites may bind to proteins, potentially leading to inaccuracies in metabolite quantification for these specimens. Note that this effect is independent of the used spectra type and therefore, will not impact comparisons between spectra types. Published in von Schlippenbach *et al.* 2018.[69]

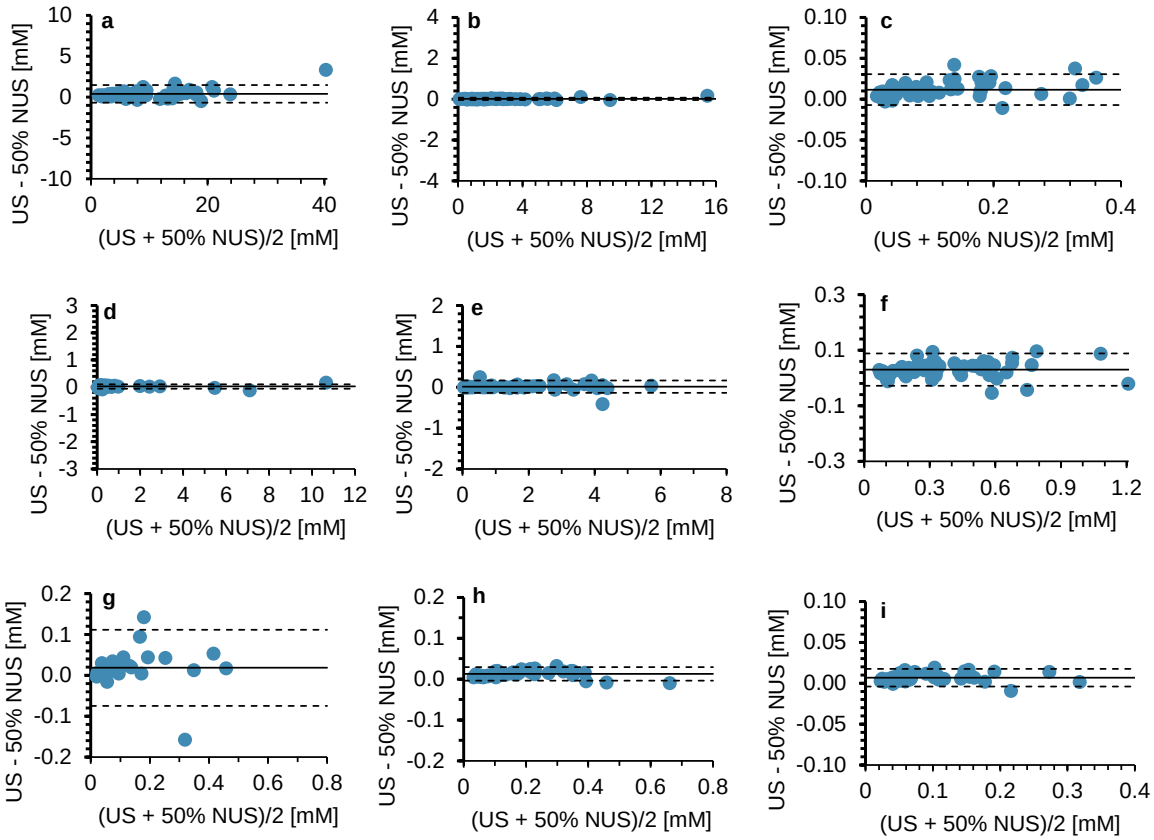

Figure S14. Agreement between 2D ^{1}H,^{1}H-COSY45 US and 50% NUS data of GCKD and GNC specimens. Bland-Altman plots showing the agreement between absolute metabolite quantification given in millimolar derived from US or NUS ^{1}H,^{1}H-COSY45 spectra (n = 56 per metabolite and sampling with the following exceptions due to missing values or quantified values below the lower limit of quantification (LLOQ): $n_{tryptophan}$ = 8, $n_{tyrosine}$ = 17, $n_{threonine}$ = 16; for further exceptions see legend Table S13) of selected metabolites, namely creatinine (**a**), hippuric acid (**b**), lactic acid (**c**), D-glucose (**d**), citric acid (**e**), pseudouridine (**f**), tryptophan (**g**), tyrosine (**h**), and threonine (**i**) in urine specimens from patients with CKD and healthy subjects (GNC). Note that the D-glucose level of one GCKD sample yielding a concentration of 26.62 mM (derived from US) or 26.58 mM (derived from 50% NUS) was not included in the Bland-Altman plot for reasons of depiction but considered for calculation of the mean ± 1.96*SD. The mean metabolite concentration of both methods is given on the x-axis, the difference between both on the y-axis. The solid line marks the mean difference between both methods, the dashed lines the 95% limits of agreement as mean ± 1.96*SD. Note that in case of strong proteinuria, as present for some of the GCKD specimens (Table 1), both the internal standard TSP as well as some of the metabolites may bind to proteins, potentially leading to inaccuracies in metabolite quantification for these specimens. Note that this effect is independent of the used spectra type and therefore, will not impact comparisons between spectra types. Published in von Schlippenbach *et al.* 2018.[69]

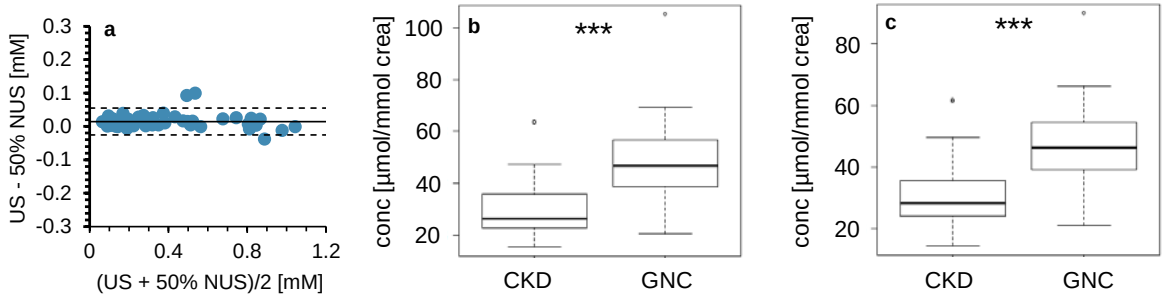

Figure S15. Absolute concentrations (**a**) of glutamine in urine specimens from CKD subjects and the GNC cohort respectively, in millimolar derived from 50% NUS (**b**) or US (**c**) ^{1}H,^{1}H-COSY45 spectra (*n* = 28 per group and sampling, for exceptions see Table S13). Note that in case of strong proteinuria, as present for some of the GCKD specimens (Table 1), both the internal standard TSP as well as some of the metabolites may bind to proteins, potentially leading to inaccuracies in metabolite quantification for these specimens. Note that this effect is independent of the used spectra type and therefore, will not impact comparisons between spectra types. Bland-Altman plots showing the agreement between absolute metabolite quantification given in millimolar derived from both 50% NUS and US spectra. The average metabolite concentration of both methods is given on the x-axis, the difference between the two sampling schemes on the y-axis. The solid line marks the mean difference, the dashed lines the 95% limits of agreement as mean ± 1.96*SD. For the boxplots, glutamine concentrations were normalized against the creatinine concentrations in millimolar. A Mann-Whitney *U*-test was applied to test for significant differences in normalized concentrations between the two groups. Abbreviations: conc, concentration; crea, creatinine. *** $p \leq 0.001$; for exact *p*-values see Table S13. Published in von Schlippenbach *et al.* 2018.[69]

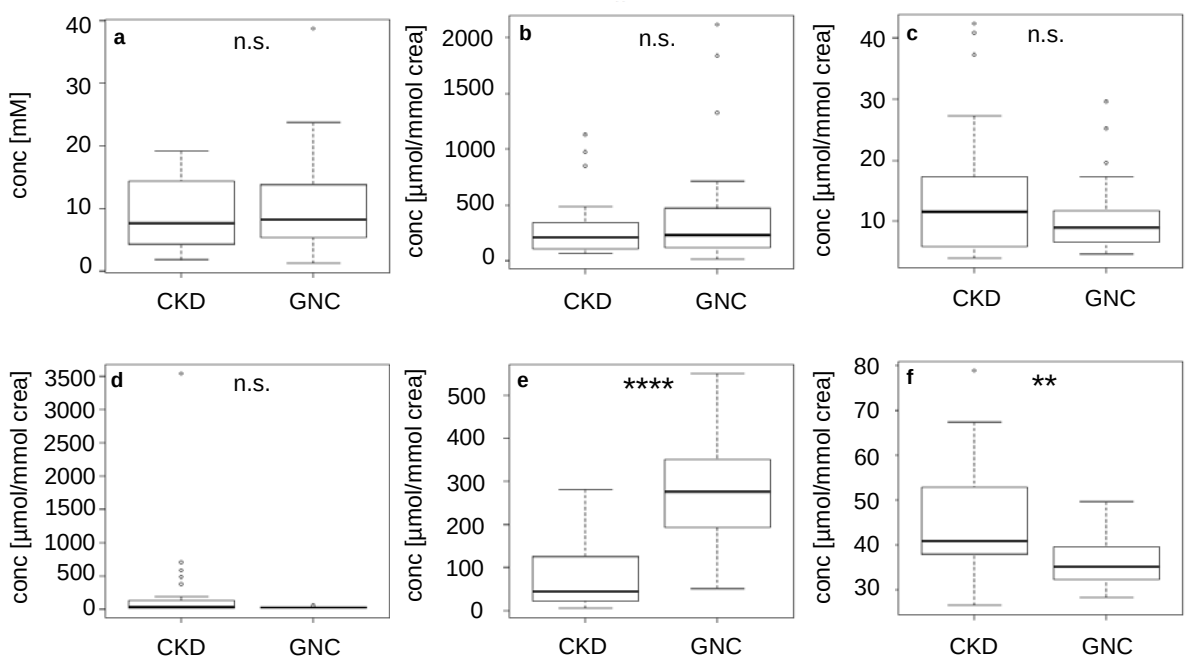

Figure S16. Quantification of cohort study metabolites with 50% NUS. Absolute quantification of selected metabolites, namely creatinine (**a**), hippuric acid (**b**), lactic acid (**c**), D-glucose (**d**), citric acid (**e**), and pseudouridine (**f**) in urine specimens from patients with CKD and healthy subjects (GNC), given on the x-axis, depicted as boxplots. The metabolite concentrations given in micromolar derived from 50% NUS ^{1}H,^{1}H-COSY45 spectra (n = 28 per group, for exceptions see Table S13; note: n = 7 CKD and n = 5 spectra from healthy specimens contained increased F_1 ridges, predominantly between 3.20 and 4.10 ppm) were normalized to the corresponding creatinine concentration in millimolar except for creatinine itself in each sample shown on the y-axis. A Mann-Whitney *U*-test was applied to test for significant differences in normalized concentrations between both groups. Abbreviations: conc, concentration; crea, creatinine. Indications: n.s., not significant; ** $p \leq 0.01$, *** $p \leq 0.001$, **** $p \leq 0.0001$; for exact p-values see Table S13. Published in von Schlippenbach *et al.* 2018.[69]

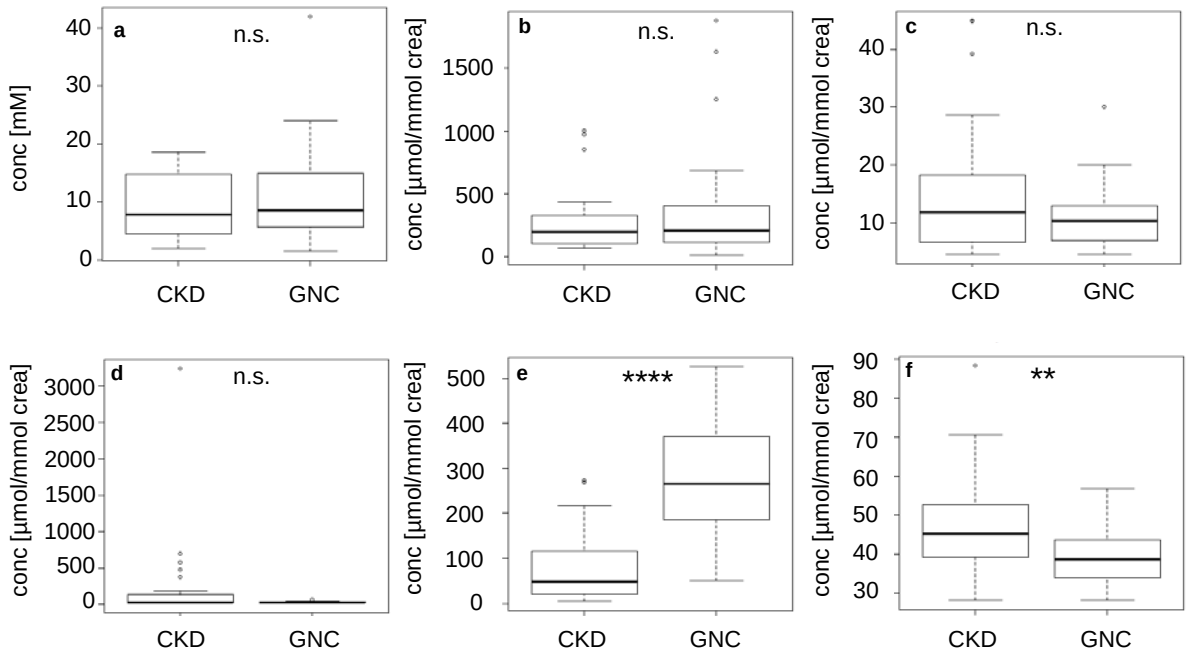

Figure S17. Quantification of cohort study metabolites with US. Absolute quantification of selected metabolites, namely creatinine (**a**), hippuric acid (**b**), lactic acid (**c**), D-glucose (**d**), citric acid (**e**), and pseudouridine (**f**) in urine specimens from patients with CKD and healthy subjects (GNC), given on the x-axis, depicted as boxplots. The metabolite concentrations given in micromolar derived from US ^{1}H,^{1}H-COSY45 spectra (n = 28 per group, for exceptions see Table S13; note: n = 7 CKD and n = 5 spectra from healthy specimens contained increased F_1 ridges, predominantly between 3.20 and 4.10 ppm) were normalized to the corresponding creatinine concentration in millimolar except for creatinine itself in each sample shown on the y-axis. A Mann-Whitney U-test was applied to test for significant differences in normalized concentrations between both groups. Abbreviations: conc, concentration; crea, creatinine. Indications: n.s., not significant; ** $p \leq 0.01$, *** $p \leq 0.001$, **** $p \leq 0.0001$; for exact p-values see Table S13. Published in von Schlippenbach *et al.* 2018.[69]

6.2. Supplemental Tables

Accelerated Quantification Spike-Ins Tables

Table S1. Number of observed recoveries observed per parameter for the spike-in data employing urine I. The analysis of initially employed reconstruction algorithms and sampling schemes is based on ^{1}H,^{1}H-TOCSY spectra. To determine the optimal spectra type, the last column contains data from NUS ^{1}H,^{1}H-COSY45 spectra reconstructed with CS-IRLS and generated with sPGS. Note that for glutamic acid, only five signals were considered as its signal intensities in the blank sample and lowest spike-in concentration were not present or too low for reliable integration even in the US ^{1}H-^{1}H-TOCSY spectra leading to 40 instead of 42 expected recoveries per NUS level and to 120 expected recoveries over all NUS levels. Abbreviations: R-MDD, recursive multidimensional decomposition; CS-IRLS, compressed sensing approach employing the iterative re-weighted least squares method; UwSa, unweighted sampling; ExSa, exponentially weighted sampling; sPGS, sine-weighted Poisson-gap sampling. Published in von Schlippenbach *et al.* 2018.[69]

NUS level	**Reconstruction algorithms**		**Sampling schemes**			**Spectra type**
	R-MDD	CS-IRLS	UwSa	ExSa	sPGS	^{1}H,^{1}H-COSY45
all	103	112	98	112	113	118
75%	39	40	33	40	40	40
50%	37	38	34	39	40	40
25%	27	34	31	33	33	38

Table S2. Comparison of initially employed reconstruction algorithms, sampling schemes, and spectra types for the spike-in data of urine I. *P*-values derived from the comparison of the quantitative performance of NUS utilizing different reconstruction algorithms, sampling schemes or spectra types using the Wilcoxon signed-rank test[a] or the Friedman test[b] on ratios (accuracy) and CVs (precision) derived from recoveries over all spike-in metabolites and concentrations either over all NUS levels or per NUS level. Data concerning the reconstruction algorithms and sampling schemes are based on ^{1}H,^{1}H-TOCSY spectra. Abbreviations: R-MDD, recursive multidimensional decomposition; CS-IRLS, compressed sensing approach employing the iterative re-weighted least squares method; UwSa, unweighted sampling; ExSa, exponentially weighted sampling; sPGS, sine-weighted Poisson-gap sampling; CV, coefficient of variation. Published in von Schlippenbach *et al.* 2018.[69]

NUS level	**Reconstruction algorithms[a]**		**Sampling schemes[b]**		**Spectra types[a]**	
	R-MDD vs. CS-IRLS		UwSa vs. ExSa vs. sPGS		^{1}H,^{1}H-TOCSY vs. ^{1}H,^{1}H-COSY45	
	ratio	CV	ratio	CV	ratio	CV
all	4.109e-6	0.037	2.536e-8	< 2.2e-16	1.075e-4	4.585e-8
75%	0.032	0.100	4.027e-7	3.851e-9	0.150	1.162e-6
50%	0.164	0. 695	2.384e-10	1.801e-5	0.002	0.179
25%	7.838e-5	0.091	8.164e-8	2.427e-7	0.080	1.790e-4

Table S3. Quantitative performance of initially employed reconstruction algorithms and sampling schemes for the spike-in data of urine I. Means of the ratios (accuracy) and CVs (precision) derived from recoveries over all spike-in metabolites and concentrations either over all NUS levels or per NUS level for comparing the quantitative performance of NUS utilizing different reconstruction algorithms or sampling schemes employing ^{1}H,^{1}H-TOCSY spectra. Abbreviations: R-MDD, recursive multidimensional decomposition; CS-IRLS, compressed sensing approach employing the iterative re-weighted least squares method; UwSa, unweighted sampling; ExSa, exponentially weighted sampling; sPGS, sine-weighted Poisson-gap sampling; CV, coefficient of variation. Published in von Schlippenbach *et al.* 2018.[69]

NUS level	**Reconstruction algorithms**				**Sampling schemes**					
	R-MDD		CS-IRLS		UwSa		ExSa		sPGS	
	ratio	CV	ratio	CV	ratio	CV	ratio	CV	ratio	CV
all	0.89	17.16	0.96	12.30	0.97	12.06	1.02	9.59	1.03	5.39
75%	0.95	8.89	0.98	7.23	1.03	12.49	1.17	4.36	1.06	2.56
50%	0.94	15.13	0.99	12.98	1.00	11.63	0.92	10.87	1.05	6.49
25%	0.74	31.88	0.89	17.50	0.88	12.06	0.96	14.40	0.98	7.49

Table S4. Comparison of sampling schemes for the spike-in data of urine I. *P*-values derived from comparing the quantitative performance of NUS utilizing different sampling schemes with each other were obtained having applied the Nemenyi post hoc test on ratios (accuracy) and CVs (precision) derived from recovery plots over all spike-in metabolites and concentrations either over all NUS levels or per NUS level. Data are based on $^{1}H,^{1}H$-TOCSY spectra. Abbreviations: UwSa, unweighted sampling; ExSa, exponentially weighted sampling; sPGS, sine-weighted Poisson-gap sampling. Published in von Schlippenbach *et al.* 2018.[69]

NUS level	**Sampling schemes**					
	ratio			CV		
	UwSa vs. ExSa	UwSa vs. sPGS	ExSa vs. sPGS	UwSa vs. ExSa	UwSa vs. sPGS	ExSa vs. sPGS
all	3.9e-5	1.8e-7	0.54	0.88	4.8e-14	2.9e-13
75%	4.6e-6	0.97	1.4e-5	0.06526	2.3e-9	0.00027
50%	0.17	1.0e-5	3.9e-10	0.93987	0.00034	8.2e-5
25%	1.8e-5	1.8e-5	1	0.53767	0.00053	4.6e-6

Table S5. Quantitative performance of spectra types for the spike-in data of urine I. Means of the ratios (accuracy) and CVs (precision) over all spike-in metabolites and concentrations either derived from the depicted recoveries over all NUS levels or per NUS level. Note that 40 out of 42 expected recoveries per NUS level and 120 out of 126 expected recoveries over all NUS levels were considered. Abbreviation: CV, coefficient of variation. Published in von Schlippenbach *et al.* 2018.[69]

NUS level	**Spectra type**	
	^{1}H,^{1}H-COSY45	
	ratio	CV
all	0.93	8.89
75%	1.02	5.66
50%	0.96	7.82
25%	0.80	13.43

Table S6. Comparison of NUS levels for the spike-in data of urine I. *P*-values derived from comparing the quantitative performance of NUS mutually were obtained having applied the Friedman test[a] and consecutive Nemenyi post hoc test[b] on ratios (accuracy) or on CVs (precision) over all spike-in metabolites and concentrations derived from the given recovery plot. Abbreviation: CV, coefficient of variation. Published in von Schlippenbach *et al.* 2018.[69]

NUS level							
Ratio				CV			
all NUS levels[a]	75% vs. 50% NUS[b]	75% vs. 25% NUS[b]	50% vs. 25% NUS[b]	all NUS levels[a]	75% vs. 50% NUS[b]	75% vs. 25% NUS[b]	50% vs. 25% NUS[b]
<2.2e-16	4.9e-4	2.5e-14	2.7e-06	4.0e-6	0.065	2.1e-6	0.018

Table S7. Number of observed recoveries observed per applied additional reconstruction algorithm for the spike-in data employing urine I. Data are based on 50% NUS ^{1}H,^{1}H-COSY45[a] and ^{1}H,^{1}H-TOCSY[b] spectra generated with sine-weighted Poisson-gap sampling. Note that all 42 expected recoveries were considered. Abbreviations: CS-IRLS, compressed sensing approach employing the iterative re-weighted least squares method; CS-IST, compressed sensing approach employing the iterative soft thresholding method; MaxEnt, maximum entropy. Published in von Schlippenbach *et al.* 2018.[69]

NUS level	**Reconstruction algorithms**		
	CS-IRLS[a]	CS-IST[a]	MaxEnt[b]
50%	41	40	31

Table S8. Quantitative performance of additional reconstruction algorithms for the spike-in data of urine I. Means of the ratios (accuracy) and CVs (precision) derived from recoveries over all spike-in metabolites and concentrations for comparing the quantitative performance of 50% NUS utilizing different supplementary reconstruction algorithms employing ^{1}H,^{1}H-COSY45[a] and ^{1}H,^{1}H-TOCSY[b] spectra. Abbreviations: CS-IRLS, compressed sensing approach employing the iterative re-weighted least squares method; CS-IST, compressed sensing approach employing the iterative soft thresholding method; MaxEnt, maximum entropy; CV, coefficient of variation. Published in von Schlippenbach *et al.* 2018.[69]

NUS level	**Reconstruction algorithms**					
	CS-IRLS[a]		CS-IST[a]		MaxEnt[b]	
	ratio	CV	ratio	CV	ratio	CV
50%	0.96	8.01	0.93	8.47	0.61	13.70

Table S9. Comparison of additional reconstruction algorithms for the spike-in data of urine I. *P*-values derived from the comparison of the quantitative performance of NUS utilizing the different supplementary reconstruction algorithms using the Friedman test on ratios (accuracy) and CVs (precision) derived from recoveries over all spike-in metabolites and concentrations. Data are based on 50% NUS ^{1}H,^{1}H-COSY45[a] and ^{1}H,^{1}H-TOCSY[b] spectra generated with sine-weighted Poisson-gap sampling. Abbreviations: CS-IRLS, compressed sensing approach employing the iterative re-weighted least squares method; CS-IST, compressed sensing approach employing the iterative soft thresholding method; MaxEnt, maximum entropy; CV, coefficient of variation. Published in von Schlippenbach *et al.* 2018.[69]

NUS level	**Reconstruction algorithms**	
	CS-IRLS[a] vs. CS-IST[a] vs. MaxEnt[b]	
	ratio	CV
50%	2.3e-6	0.51

Table S10. Comparison of additional reconstruction algorithms for the spike-in data of urine I. *P*-values derived from comparing the quantitative performance of NUS utilizing different supplementary reconstruction algorithms with each other were obtained having applied the Nemenyi post hoc test on ratios (accuracy) derived from recovery plots over all spike-in metabolites and concentrations. Data are based on 50% NUS ^{1}H,^{1}H-COSY45[a] and ^{1}H,^{1}H-TOCSY[b] spectra generated with sine-weighted Poisson-gap sampling. Abbreviations: CS-IRLS, compressed sensing approach employing the iterative re-weighted least squares method; CS-IST, compressed sensing approach employing the iterative soft thresholding method; MaxEnt, maximum entropy. Published in von Schlippenbach *et al.* 2018.[69]

NUS level	**Reconstruction algorithms**		
	ratio		
	CS-IRLS[a] vs. CS-IST[a]	CS-IRLS[a] vs. MaxEnt[b]	CS-IST[a] vs. MaxEnt[b]
all	0.52	4.7e-6	6.1e-4

Table S11. Concentration-dependent quantitative performance for spike-in metabolites for the spike-in data of urine I. Ratios (accuracy) and coefficients of variation (precision) derived from recovery plots of 50% NUS ^{1}H,^{1}H-COSY45 spectra for all added concentrations given in micromolar and the mean or median of all spike-in metabolites, namely tryptophan (Trp), tyrosine (Tyr), glutamine (Gln), glutamic acid (Glu), lactic acid (Lac), and threonine (Thr). Abbreviations: conc., concentration; CV, coefficient of variation. Published in von Schlippenbach *et al.* 2018.[69]

Spike-in conc. [µM]	**Trp**		**Tyr**		**Gln**		**Glu**		**Lac**		**Thr**	
	ratio	CV	ratio	CV	ratio	CV	ratio	CV	ratio	CV	ratio	CV
0.0	0.76	22.29	1.02	9.34	0.98	7.85	-	-	0.92	13.00	1.00	15.68
15.6	0.85	19.42	1.08	4.67	0.95	1.71	0.87	15.81	0.88	10.91	0.94	14.23
31.3	0.91	13.82	1.05	10.48	0.96	4.65	1.03	16.62	0.87	9.35	0.84	9.72
62.5	0.85	7.83	0.88	14.90	0.98	3.40	0.97	8.34	1.03	3.73	0.98	7.14
125.0	0.92	4.21	0.93	10.21	1.04	3.27	0.96	4.44	1.00	2.21	1.11	11.69
250.0	0.92	9.90	1.01	2.05	0.98	4.45	0.95	5.13	1.00	1.35	1.04	6.36
500.0	0.95	2.61	0.97	7.29	1.01	1.40	1.02	3.48	0.99	1.69	0.98	1.82
median	0.91	-	1.01	-	0.98	-	0.97	-	0.99	-	0.98	-
mean	-	11.44	-	8.42	-	3.82	-	8.97	-	6.03	-	9.52

Table S12. Concentration-dependent quantitative performance for spike-in metabolites for the spike-in data of urine II. Ratios (accuracy) and coefficients of variation (precision) derived from recovery plots of 50% NUS ^{1}H,^{1}H-COSY45 spectra for all added concentrations given in micromolar and the mean or median of all spike-in metabolites, namely tryptophan (Trp), tyrosine (Tyr), glutamine (Gln), glutamic acid (Glu), lactic acid (Lac), and threonine (Thr). Abbreviations: conc., concentration; CV, coefficient of variation. Published in von Schlippenbach *et al.* 2018.[69]

Spike-in conc. [µM]	**Trp**		**Tyr**		**Gln**		**Glu**		**Lac**		**Thr**	
	ratio	CV	ratio	CV	ratio	CV	ratio	CV	ratio	CV	ratio	CV
0.0	-	-	-	-	0.94	3.82	-	-	0.91	10.61	0.82	6.62
15.6	0.76	59.96	0.89	3.68	0.91	6.51	0.94	9.65	0.86	10.56	0.88	8.05
31.3	1.21	33.86	0.93	4.95	0.98	10.54	1.04	6.74	0.90	8.12	0.88	12.53
62.5	0.78	21.39	0.89	3.55	0.92	8.25	1.03	8.31	1.07	8.72	0.90	6.58
125.0	0.87	16.54	1.02	1.34	0.89	6.40	1.05	6.58	1.05	8.59	0.89	6.72
250.0	0.88	10.38	1.00	0.90	0.83	5.49	1.01	1.86	1.01	3.55	0.90	8.00
500.0	0.94	4.51	1.00	2.00	1.05	4.96	0.96	3.33	1.00	2.78	0.98	5.34
median	0.88	-	0.96	-	0.92	-	1.02	-	1.00	-	0.89	-
mean	-	24.44	-	2.73	-	6.57	-	6.08	-	7.56	-	7.71

Application of Accelerated Quantification with NUS to Urinary Specimens of CKD Patients and Healthy Subjects

Table S13. Comparison of US and accelerated quantification with NUS. *P*-values derived from comparing metabolite levels in the cohort study urine specimens from patients with CKD and healthy subjects were obtained having applied the Mann-Whitney *U*-test on relative intensities per metabolite or over all metabolites in specimens from patients with CKD or healthy subjects, normalized to the corresponding creatinine value in each sample derived from measured US or 50% NUS ^{1}H,^{1}H-COSY45 spectra (*n* = 28 per group and sampling; exceptions due to missing values: [a]n_{GCKD} = 27). Published in von Schlippenbach *et al.* 2018.[69]

Metabolite	^{1}H,^{1}H COSY45 US	^{1}H,^{1}H COSY45 50% NUS
Creatinine	0.7145	0.7024
Hippuric acid	0.4297	0.3925
Lactic acid	0.4773[a]	0.4568[a]
D-Glucose	0.3836	0.4203
Citric acid	1.616e-8	8.173e-9
Glutamine	1.24e-4	1.24e-4
Pseudouridine	2.338e-3	1.448e-3
Over all	0.9236	0.9456

LLOQs Cohort Study Metabolites

Table S14. LLOQs. LLOQs of the quantified metabolite signals in the cohort study urine specimens given in micromolar derived from US or 50% NUS ^{1}H,^{1}H-COSY45 spectra of the calibration samples. Published in von Schlippenbach *et al.* 2018.[69]

Metabolite	^{1}H,^{1}H COSY45 US [µM]	^{1}H,^{1}H COSY45 50% NUS [µM]
Creatinine	78.13	312.50
Hippuric acid	4.88	9.77
Lactic acid	9.77	9.77
D-Glucose	39.06	39.06
Citric acid	4.88	9.77
Glutamine	9.77	9.77
Pseudouridine	19.53	39.06

6.3. Simulation of NUS Spectra

For generating simulated NUS spectra, the TopSpin 3.1 AU programs “splitser” and “fidtoser” were modified accordingly with the help of Thorsten Rehberg. The “splitser” command was adapted to extract from an acquired US spectrum individual FIDs according to the sampling density, sampling scheme, and seed value intended. The adapted “fidtoser” command writes the extracted FIDs to a new ser file matching the NUSLIST point schedule to give the simulated NUS spectrum. The NUSLIST comprises one column per indirect dimension containing the data point to be considered, being complex for ^{1}H,^{1}H-TOCSY spectra meaning that the complex time domain signal is composed of magnetization along the x- and y-direction,[54] starting with the indices 0 adjusted to the sampled NUS points of the simulated NUS spectrum.

The codes for the adapted “splitser” and “fidtoser” command are exemplarily shown below, comprising the 128 indirect data points corresponding to a 25% NUS dataset with sine-weighted Poisson-gap sampling given the default seed value of TopSpin 3.1.

modified “splitser” schedule:

```
int td;

GETCURDATA
FETCHPAR1S("TD",&td)
int
a[128]={1,2,3,4,5,6,7,8,9,10,11,12,13,14,15,16,19,20,23,24,25,
26,27,28,29,30,35,36,41,42,47,48,49,50,55,56,61,62,65,66,69,70
,71,72,75,76,79,80,87,88,91,92,93,94,99,100,101,102,107,108,11
1,112,117,118,125,126,131,132,141,142,151,152,165,166,171,172,
177,178,179,180,191,192,195,196,205,206,225,226,237,238,243,24
4,255,256,263,264,279,280,301,302,317,318,329,330,343,344,357,
358,365,366,379,380,397,398,405,406,417,418,433,434,459,460,47
3,474,487,488,509,510};
i1=0;
TIMES(128)
  RSER(a[i1],a[i1],1);
  i1 ++;
END
QUITMSG("--- splitser finished ---")
```

modified “fidtoser” schedule

```
int
a[128]={1,2,3,4,5,6,7,8,9,10,11,12,13,14,15,16,19,20,23,24,25,
26,27,28,29,30,35,36,41,42,47,48,49,50,55,56,61,62,65,66,69,70
,71,72,75,76,79,80,87,88,91,92,93,94,99,100,101,102,107,108,11
1,112,117,118,125,126,131,132,141,142,151,152,165,166,171,172,
177,178,179,180,191,192,195,196,205,206,225,226,237,238,243,24
4,255,256,263,264,279,280,301,302,317,318,329,330,343,344,357,
358,365,366,379,380,397,398,405,406,417,418,433,434,459,460,47
3,474,487,488,509,510};

char nm1[PATH_MAX];
int ne = 128;
int proc1 = 1;

strcpy(nm1, name);
GETSTRING("Enter name of 1D series:", nm1)

USECURPARS
int i=0;
TIMES(ne)
  WSER(loopcount1+1, nm1, a[i], proc1, disk, user)
  i += 1;
END
QUIT
```

References

1. Holmes, E. *et al.* 750 MHz ^{1}H NMR spectroscopy characterisation of the complex metabolic pattern of urine from patients with inborn errors of metabolism: 2-hydroxyglutaric aciduria and maple syrup urine disease. *J. Pharm. Biomed. Anal.* **15**, 1647-1659 (1997).
2. Palmer, M. R. *et al.* Sensitivity of Nonuniform Sampling NMR. *J. Phys. Chem. B* **119**, 6502-6515 (2015).
3. Dass, R. *et al.* Fast 2D NMR Spectroscopy for In vivo Monitoring of Bacterial Metabolism in Complex Mixtures. *Front. Microbiol.* **8**, 1-12 (2017).
4. Kazimierczuk, K. & Orekhov, V. Non-uniform sampling: post-Fourier era of NMR data collection and processing. *Magn. Reson. Chem.* **53**, 921-926 (2015).
5. Mobli, M., Hoch, J. C. & King, G. F. Fast Acquisition Methods in Multidimensional NMR in *Biomolecular NMR Spectroscopy* (eds. Dingley, A. J. & Pascal, S. M.) 305 - 337 (IOS Press, 2011).
6. Maciejewski, M. W., Mobli, M., Schuyler, A. D., Stern, A. S. & Hoch, J. C. Data Sampling in Multidimensional NMR: Fundamentals and Strategies in *Novel Sampling Approaches in Higher Dimensional NMR* (eds. Billeter, M. & Orekhov, V. Y.) 49-77 (Springer, 2011).
7. Claridge, T. D. W. *High-Resolution NMR Techniques in Organic Chemistry* 185-186 (Elsevier, 2016).
8. Rouger, L., Gouilleux, B. & Giraudeau, P. Fast n-Dimensional Data Acquisition Methods in *Encyclopedia of Spectroscopy and Spectrometry* (eds. Lindon, J., Tranter, G. E. & Koppenaal, D.) 1-10 (Elsevier, 2016).
9. Le Guennec, A., Giraudeau, P. & Caldarelli, S. Evaluation of Fast 2D NMR for Metabolomics. *Anal. Chem.* **86**, 5946-5954 (2014).
10. Reardon, P. N., Marean-Reardon, C. L., Bukovec, M. A., Coggins, B. E. & Isern, N. G. 3D TOCSY-HSQC NMR for metabolic flux analysis using non-uniform sampling. *Anal. Chem.* **88**, 2825-2831 (2016).
11. Sidebottom, P. J. A new approach to the optimisation of non-uniform sampling schedules for use in the rapid acquisition of 2D NMR spectra of small molecules. *Magn. Reson. Chem.* **54**, 689-694 (2016).
12. Hyberts, S. G. *et al.* Ultrahigh-Resolution ^{1}H-^{13}C HSQC Spectra of Metabolite Mixtures Using Nonlinear Sampling and Forward Maximum Entropy Reconstruction. *J. Am. Chem. Soc.* **129**, 5108-5116 (2007).
13. Rai, R. K. & Sinha, N. Fast and Accurate Quantitative Metabolic Profiling of Body Fluids by Nonlinear Sampling of ^{1}H–^{13}C Two-Dimensional Nuclear Magnetic Resonance Spectroscopy. *Anal. Chem.* **84**, 10005-10011 (2012).
14. Le Guennec, A., Dumez, J. N., Giraudeau, P. & Caldarelli, S. Resolution-enhanced 2D NMR of complex mixtures by non-uniform sampling. *Magn. Reson. Chem.* **53**, 913-920 (2015).
15. Giraudeau, P. Quantitative 2D liquid-state NMR. *Magn. Reson. Chem.* **52**, 259-272 (2014).
16. Hyberts, S. G., Arthanari, H. & Wagner, G. Applications of non-uniform sampling and processing. *Top. Curr. Chem.* **316**, 125-148 (2012).
17. Kidney Disease: Improving Global Outcomes (KDIGO) CKD Work Group. KDIGO 2012 Clinical Practice Guideline for the Evaluation and Management of Chronic Kidney Disease. *Kidney Int. Supplements* **3**, 1-150 (2013).
18. Zhang, A., Sun, H., Qiu, S. & Wang, X. Metabolomics insights into pathophysiological mechanisms of nephrology. *Int. Urol. Nephrol.* **46**, 1025-1030 (2014).
19. Eckardt, K.-U. *et al.* Evolving importance of kidney disease: from subspecialty to global health burden. *The Lancet* **382**, 158-169 (2013).
20. Jha, V. *et al.* Chronic kidney disease: global dimension and perspectives. *The Lancet* **382**, 260-272 (2013).

21. Inker, L. A. *et al.* Estimating Glomerular Filtration Rate from Serum Creatinine and Cystatin C. *N. Engl. J. Med.* **367**, 20-29 (2012).

22. Kalim, S. & Rhee, E. P. An overview of renal metabolomics. *Kidney Int.*, 1-9 (2016).

23. Arora, S. Renal function in diabetic nephropathy. *World J. Diabetes* **1**, 48-56 (2010).

24. Eckardt, K.-U. *et al.* The German Chronic Kidney Disease (GCKD) study: design and methods. *Nephrol. Dial. Transplant* **27**, 1454-1460 (2012).

25. Stec, D. F. *et al.* Alterations of Urinary Metabolite Profile in Model Diabetic Nephropathy. *Biochem. Biophys. Res. Commun.* **456**, 610-614 (2015).

26. Weinberg, R. A. *The Biology of Cancer* 44, 46f., 400f., 588 (Garland Science, 2007).

27. Hanahan, D. & Weinberg, R. A. The Hallmarks of Cancer. *Cell* **100**, 57-70 (2000).

28. Alberts, B., Johnson, A., Lewis, J., Raff, M., Roberts, K., Walter, P. *Molecular Biology of the Cell* 1206 (Garland Science, 2008).

29. Hanahan, D., Weinberg, R.A. Hallmarks of Cancer: The Next Generation. *Cell* **144**, 646-674 (2011).

30. Vander Heiden, M. G., Cantley, L.C., Thompson, C.B. Understanding the Warburg Effect: The Metabolic Requirements of Cell Proliferation. *Science* **324**, 1029-1033 (2009).

31. Brand, A. *et al.* LDHA-Associated Lactic Acid Production Blunts Tumor Immunosurveillance by T and NK Cells. *Cell Metab.* **24**, 657-671 (2016).

32. Pavlova, N. N. & Thompson, C. B. The Emerging Hallmarks of Cancer Metabolism. *Cell Metabolism* **23**, 27-47 (2016).

33. Coller, H. A. Is Cancer a Metabolic Disease? *Am. J. Pathol.* **184**, 4-17 (2014).

34. Gottfried, E., Kreutz, M., Mackensen, A. Tumor metabolism as modulator of immune response and tumor progression. *Semin. Cancer Biol.* **22**, 335-341 (2012).

35. Dettmer, K. *et al.* Distinct metabolic differences between various human cancer and primary cells. *Electrophoresis* **34**, 2836-2847 (2013).

36. Kroemer, G. & Pouyssegur, J. Tumor Cell Metabolism: Cancer's Achilles' Heel. *Cancer Cell* **13**, 472-482 (2008).

37. Fischer, K. *et al.* Inhibitory effect of tumor cell derived lactic acid on human T cells. *Blood* **109**, 3812-3819 (2007).

38. Baumann, F. *et al.* Lactate promotes glioma migration by TGF-β2–dependent regulation of matrix metalloproteinase-2. *Neuro Oncol.* **11**, 368-380 (2009).

39. Xie, H. *et al.* Targeting Lactate Dehydrogenase-A Inhibits Tumorigenesis and Tumor Progression in Mouse Models of Lung Cancer and Impacts Tumor-Initiating Cells. *Cell Metabolism* **19**, 795-809 (2014).

40. Fantin, V. R., St-Pierre, J. & Leder, P. Attenuation of LDH-A expression uncovers a link between glycolysis, mitochondrial physiology, and tumor maintenance. *Cancer Cell* **9**, 425-434 (2006).

41. Lindon, J. C. & Nicholson, J. K. Spectroscopic and Statistical Techniques for Information Recovery in Metabonomics and Metabolomics. *Annu. Rev. Anal. Chem.* **1**, 45-69 (2008).

42. Newgard, C. B. Metabolomics and Metabolic Diseases: Where Do We Stand? *Cell Metab.* **25**, 43-56 (2017).

43. Nicholson, J. K., Lindon, J.C., Holmes, E. 'Metabonomics': understanding the metabolic responses of living systems to pathophysiological stimuli via multivariate statistical analysis of biological NMR spectroscopic data. *Xenobiotica* **29**, 1181- 1189 (1999).

44. Fiehn, O. Metabolomics – the link between genotypes and phenotypes. *Plant Mol. Biol.* **48**, 155-171 (2002).

45. Larive, C. K., Barding Jr., G. A. & Dinges, M. M. NMR Spectroscopy for Metabolomics and Metabolic Profiling. *Anal. Chem.* **87**, 133-146 (2014).

46. Bingol, K. & Brüschweiler, R. Multidimensional Approaches to NMR-Based Metabolomics. *Anal. Chem.* **86**, 47-57 (2013).

47. Wishart, D. S. *et al.* HMDB: a knowledgebase for the human metabolome. *Nucleic Acids Res.* **37**, D603-D610 (2009).

48. Dunn, W. B. & Ellis, D. I. Metabolomics: Current analytical platforms and methodologies. *Trends Anal. Chem.* **24**, 285-294 (2005).

49. Kohler, I., Verhoeven, A., Derks, R. J. E. & Giera, M. Analytical pitfalls and challenges in clinical metabolomics. *Bioanalysis* **8**, 1509–1532 (2016).

50. Everett, J. R. A New Paradigm for Known Metabolite Identification in Metabonomics/Metabolomics: Metabolite Identification Efficiency. *Comput. Struct. Biotechnol. J.* **13**, 131-144 (2015).

51. Wishart, D. S. Quantitative metabolomics using NMR. *Trends Anal. Chem.* **27**, 228-237 (2008).

52. Dieterle, F. *et al.* NMR and MS Methods for Metabonomics in *Drug Safety Evaluation: Methods and Protocols* (ed. Gautier, J.-C.) 385-415 (Humana Press, % Springer Science+Business Media, LLC, 2011).

53. Bothwell, J. H. F. & Griffin, J. L. An introduction to biological nuclear magnetic resonance spectroscopy. *Biol. Rev.* **86**, 493-510 (2011).

54. Ross, A., Schlotterbeck, G., Dieterle, F. & Senn, H. NMR Spectroscopy Techniques for Application to Metabonomics in *The Handbook of Metabonomics and Metabolomics* (eds. Lindon, J., Nicholson, J. & Holmes, E.) 55-112 (Elsevier, 2007).

55. Cavanagh, J., Fairbrother, W. J., Palmer III, A. G., Rance, M. & Skelton, N. J. *Protein NMR Spectroscopy: Principles and Practice* (Elsevier Academic Press, 1995).

56. Schuyler, A. D., Maciejewski, M. W., Arthanari, H. & Hoch, J. C. Knowledge-based nonuniform sampling in multidimensional NMR. *J. Biomol. NMR* **50**, 247-262 (2011).

57. Lee, S. *et al.* Carbon Isotopomer Analysis with Non-Unifom Sampling HSQC NMR for Cell Extract and Live Cell Metabolomics Studies. *Anal. Chem.* **89**, 1078-1085 (2016).

58. Gronwald, W. *et al.* Urinary Metabolite Quantification Employing 2D NMR Spectroscopy. *Anal. Chem.* **80**, 9288-9297 (2008).

59. Beckonert, O. *et al.* Metabolic profiling, metabolomic and metabonomic procedures for NMR spectroscopy of urine, plasma, serum and tissue extracts. *Nat. Protoc.* **2**, 2692-2703 (2007).

60. Hoch, J. C., Maciejewski, M. W., Mobli, M., Schuyler, A. D. & Stern, A. S. Nonuniform Sampling and Maximum Entropy Reconstruction in Multidimensional NMR. *Acc. Chem. Res.* **47**, 708-717 (2014).

61. Orekhov, V. Y. & Jaravine, V. A. Analysis of non-uniformly sampled spectra with multi-dimensional decomposition. *Prog. Nucl. Magn. Reson. Spectrosc.* **59**, 271-292 (2011).

62. Gryk, M. R., Vyas, J. & Maciejewski, M. W. Biomolecular NMR Data analysis. *Prog. Nucl. Magn. Reson. Spectrosc.* **56**, 329-345 (2010).

63. Mobli, M. Reducing seed dependent variability of non-uniformly sampled multidimensional NMR data. *J. Magn. Reson.* **256**, 60-69 (2015).

64. Rovnyak, D. *et al.* Accelerated acquisition of high resolution triple-resonance spectra using non-uniform sampling and maximum entropy reconstruction. *J. Magn. Reson.* **170**, 15-21 (2004).

65. Lemak, A. *et al.* A novel strategy for NMR resonance assignment and protein structure determination. *J. Biomol. NMR* **49**, 27-38 (2011).

66. Nagana Gowda, G. A. & Raftery, D. Recent Advances in NMR-Based Metabolomics. *Anal. Chem.* **89**, 490-510 (2016).

67. Bouatra, S. *et al.* The Human Urine Metabolome. *PLoS ONE* **8**, 1-28 (2013).

68. German National Cohort (GNC) Consortium. The German National Cohort: aims, study design and organization. *Eur. J. Epidemiol.* **29**, 371-382 (2014).

69. Schlippenbach, T. v., Oefner, P. J. & Gronwald, W. Systematic Evaluation of Non-Uniform Sampling Parameters in the Targeted Analysis of Urine Metabolites by ^{1}H,^{1}H 2D NMR Spectroscopy. *Sci. Rep.* **8**, 4249; 10.1038/s41598-018-22541-0 (2018).

70. Levey, A. S. *et al.* A New Equation to Estimate Glomerular Filtration Rate. *Ann. Intern. Med.* **150**, 604-613 (2009).

71. Giavazzi, R. & Garofalo, A. Syngeneic Murine Metastasis Models: B16 Melanoma in *Methods in Molecular Biology: Metastasis Research Protocols, Volume 2* (eds. Dwek, M., Schumacher, U. & Brooks, S. A.) 223-229 (Humana Press, 2014).

72. Wang, B. *et al.* A Novel, Clinically Relevant Animal Model of Metastatic Pancreatic Adenocarcinoma Biology and Therapy. *Int. J. Pancreatol.* **29**, 37-46 (2001).

73. Wishart Research Group. HMDB Version 3.0. *The Human Metabolome Database* http://www.hmdb.ca (2012).

74. Zacharias, H. U. *et al.* Current Experimental, Bioinformatic and Statistical Methods used in NMR Based Metabolomics. *Curr. Metabolomics* **1**, 253-268 (2013).

75. Aoto, P. C., Fenwick, R. B., Kroon, G. J. A. & Wright, P. E. Accurate scoring of non-uniform sampling schemes for quantitative NMR. *J. Magn. Reson.* **246**, 31-35 (2014).

76. Hoch, J. C., Maciejewski, M. W. & Filipovic, B. Randomization improves sparse sampling in multidimensional NMR. *J. Magn. Reson.* **193**, 317-320 (2008).

77. Rai, R. K., Tripathi, P. & Sinha, N. Quantification of Metabolites from Two-Dimensional Nuclear Magnetic Resonance Spectroscopy: Application to Human Urine Samples. *Anal. Chem.* **81**, 10232-10238 (2009).

78. Hyberts, S. G., Takeuchi, K. & Wagner, G. Poisson-Gap Sampling and Forward Maximum Entropy Reconstruction for Enhancing the Resolution and Sensitivity of Protein NMR Data. *J. Am. Chem. Soc.* **132**, 2145-2147 (2010).

79. Gerhard Wagner Lab. Schedule Generator Version 3.0. *Harvard Medical School* http://gwagner.med.harvard.edu/intranet/hmsIST/gensched_new.html (2013-14).

80. Hyberts, S. G., Milbradt, A. G., Wagner, A. B., Arthanari, H. & Wagner, G. Application of iterative soft thresholding for fast reconstruction of NMR data non-uniformly sampled with multidimensional Poisson Gap scheduling. *J. Biomol. NMR* **52**, 315-327 (2012).

81. Random Number Generator. *Stat Trek* http://stattrek.com/statistics/random-number-generator.aspx (2017).

82. Jaravine, V., Ibraghimov, I. & Orekhov, V. Y. Removal of a time barrier for high-resolution multidimensional NMR spectroscopy. *Nat. Methods* **3**, 605-607 (2006).

83. Kazimierczuk, K. & Orekhov, V. Y. Accelerated NMR Spectroscopy by Using Compressed Sensing. *Angew. Chem. Int. Ed.* **50**, 5556-5559 (2011).

84. Mobli, M. & Hoch, J. C. Maximum Entropy Spectral Reconstruction of Nonuniformly Sampled Data. *Concepts Magn. Reson. Part A* **32**, 436-448 (2008).

85. Willcott, M. R. MestRe Nova. *JACS* **131**, 13180-13180 (2009).

86. Hoch, J. C. & Stern, A. S. *NMR Data Processing* (Wiley, 1996).

87. Maciejewski, M. W. *et al.* NMRbox: A Resource for Biomolecular NMR Computation. *Biophys. J.* **112**, 1529-1534 (2017).

88. Delaglio, F. *et al.* NMRPipe: A multidimensional spectral processing system based on UNIX pipes. *J. Biomol. NMR* **6**, 277-293 (1995).

89. Sanders, J. N. *et al.* Compressed Sensing for Multidimensional Spectroscopy Experiments. *J. Phys. Chem. Lett.* **3**, 2697-2702 (2012).

90. Shchukina, A., Kasprzak, P., Dass, R., Nowakowski, M. & Kazimierczuk, K. Pitfalls in compressed sensing reconstruction and how to avoid them. *J. Biomol. NMR* **68**, 79-98 (2017).

91. Klein, M. S., Oefner, P. J. & Gronwald, W. MetaboQuant: a tool combining individual peak calibration and outlier detection for accurate metabolite quantification in 1D ^{1}H and ^{1}H-^{13}C HSQC NMR spectra. *BioTechniques* **54**, 251-256 (2013).

92. Barrios, C., Spector, T. D. & Menni, C. Blood, urine and faecal metabolite profiles in the study of adult renal disease. *Arch. Biochem. Biophys.* **589**, 81-92 (2016).

93. U. S. Department of Health and Human Services. Guidance for Industry: Bioanalytical Method Validation. *Center for Drug Evaluation and Research (CDER), Center for Veterinary Medicine (CVM)* https://www.fda.gov/downloads/Drugs/Guidance/ucm070107.pdf (2001).

94. Ott, R. L. & Longnecker, M. *An Introduction to Statistical Methods and Data Analysis* 96ff., 209, 229, 231, 302, 308, 355, 384ff., 410, 438 f. (DuxburyPress/Thomson Learning, 2001).

95. Shapiro, S. S. & Wilk, M. B. An Analysis of Variance Test for Normality (Complete Samples). *Biometrika* **52**, 591-611 (1965).

96. McCrum-Gardner, E. Which is the correct statistical test to use? *Br. J. Oral Maxillofac. Surg.* **46**, 38-41 (2008).

97. Pohlert, T. The Pairwise Multiple Comparison of Mean Ranks Package (PMCMR). *R package*, 1-27 (2014).

98. McGuinness, K. A. Of rowing boats, ocean liners and tests of the ANOVA homogeneity of variance assumption. *Austral. Ecology* **27**, 681-688 (2002).

99. Faul, F., Erdfelder, E., Lang, A.-G. & Buchner, A. G*Power 3: A flexible statistical power analysis program for the social, behavioral, and biomedical sciences. *Behav. Res. Methods* **39**, 175-191 (2007).

100. Faul, F., Erdfelder, E., Buchner, A. & Lang, A.-G. Statistical power analyses using G*Power 3.1: Tests for correlation and regression analyses. *Behav. Res. Methods* **41**, 1149-1160 (2009).

101. Wei, T. *et al.* Metabonomic analysis of potential biomarkers and drug targets involved in diabetic nephropathy mice. *Sci. Rep.* **5**, 1-14 (2015).

102. Mobli, M., Maciejewski, M. W., Schuyler, A. D., Stern, A. S. & Hoch, J. C. Sparse sampling methods in multidimensional NMR. *PCCP* **14**, 10835-10843 (2012).

103. Emwas, A.-H. *et al.* Standardizing the experimental conditions for using urine in NMR-based metabolomic studies with a particular focus on diagnostic studies: a review. *Metabolomics* **11**, 872-894 (2015).

104. Maciejewski, M. W., Schuyler, A. D. & Hoch, J. C. Practical Nonuniform Sampling and Non-Fourier Spectral Reconstruction for Multidimensional NMR in *Protein NMR: Methods and Protocols* (ed. Ghose, R.) 341-352 (Humana Press, % Springer Science+Business Media, LLC, 2018).

105. Matsuki, Y., Eddy, M. T. & Herzfeld, J. Spectroscopy by Integration of Frequency and Time Domain Information for Fast Acquisition of High-Resolution Dark Spectra. *J. Am. Chem. Soc.* **131**, 4648-4656 (2009).

106. Coggins, B. E., Werner-Allen, J. W., Yan, A. & Zhou, P. Rapid Protein Global Fold Determination Using Ultrasparse Sampling, High-Dynamic Range Artifact Suppression, and Time-Shared NOESY. *J. Am. Chem. Soc.* **134**, 18619-18630 (2012).

107. Ying, J., Delaglio, F., Torchia, D. A. & Bax, A. Sparse multidimensional iterative lineshape-enhanced (SMILE) reconstruction of both non-uniformly sampled and conventional NMR data. *J. Biomol. NMR* **68**, 101-118 (2017).

108. Shrot, Y. & Frydman, L. Compressed sensing and the reconstruction of ultrafast 2D NMR data: Principles and biomolecular applications. *J. Magn. Reson.* **209**, 352-358 (2011).

109. Holland, D. J., Bostock, M. J., Gladden, L. F. & Nietlispach, D. Fast Multidimensional NMR Spectroscopy Using Compressed Sensing. *Angew. Chem.* **123**, 6678-6681 (2011).

110. Hyberts, S. G., Robson, S. A. & Wagner, G. Exploring Signal-to-noise Ratio and Sensitivity in Non-Uniformly Sampled Multi-Dimensional NMR Spectra. *J. Biomol. NMR* **55**, 167-178 (2013).

111. Kazimierczuk, K., Misiak, M., Stanek, J., Zawadzka-Kazimierczuk, A. & Koźmiński, W. Generalized Fourier Transform for Non-Uniform Sampled Data in *Novel Sampling Approaches in Higher Dimensional NMR* (eds. Billeter, M. & Orekhov, V. Y.) 79-124 (Springer, 2011).

112. Mayzel, M., Rosenlöw, J., Isaksson, L. & Orekhov, V. Y. Time-resolved multidimensional NMR with non-uniform sampling. *J. Biomol. NMR* **58**, 129-139 (2014).

113. Hyberts, S. G., Arthanari, H., Robson, S. A. & Wagner, G. Perspectives in Magnetic Resonance: NMR in the Post-FFT Era. *J. Magn. Reson.* **241**, 60-73 (2014).

114. Wist, J. Complex mixtures by NMR and complex NMR for mixtures: experimental and publication challenges. *Magn. Reson. Chem.* **55**, 22-28 (2017).

115. van der Kloet, F. M. *et al.* Discovery of early-stage biomarkers for diabetic kidney disease using ms-based metabolomics (FinnDiane study). *Metabolomics* **8**, 109-119 (2012).

116. Sharma, K. *et al.* Metabolomics Reveals Signature of Mitochondrial Dysfunction in Diabetic Kidney Disease. *J. Am. Soc. Nephrol.* **24**, 1901-1912 (2013).

117. Pena, M. J. *et al.* Urine and plasma metabolites predict the development of diabetic nephropathy in individuals with Type 2 diabetes mellitus. *Diabetic Med.* **31**, 1138-1147 (2014).

118. Messana, I. *et al.* Proton nuclear magnetic resonance spectral profiles of urine in type II diabetic patients. *Clin. Chem.* **44**, 1529-1534 (1998).

119. Wallmeier, J. *et al.* Quantification of Metabolites by NMR Spectroscopy in the Presence of Protein. *J. Proteome Res.* **16**, 1784-1796 (2017).

Danksagung

An dieser Stelle möchte ich mich bei all denen bedanken, die mich während meiner Doktorarbeit begleitet und unterstützt haben. Mein besonderer Dank geht an:

Prof. Dr. Peter J. Oefner für die Möglichkeit, meine Doktorarbeit an seinem Institut durchzuführen, das stetige Interesse an meiner Arbeit und die konstruktive Anleitung

Prof. Dr. Wolfram Gronwald für das interessante und spannende Thema, die Weitergabe fachlicher Expertise sowie seine freundliche Betreuung und kostbare Zeit für wertvolles feedback

Claudi Samol für die zuverlässige, große Unterstützung bei den Laborarbeiten und Messungen sowie ihre ausgesprochen hilfsbereite und ansteckend fröhliche Art

Thorsten Rehberg für die unentbehrlichen Beiträge zur Ermöglichung der Simulation von NUS Spektren mit TopSpin 3.1

Prof. Dr. Michael Leitzmann und **Dr. Inga Schlecht** für die Bereitstellung der GNC Urinproben sowie Weitergabe der zugehörigen Studienteilnehmer-Charakteristiken

AG Prof. Dr. Marina Kreutz für die Durchführung der Zellkulturexperimente und Bereitstellung der Zellproben

Prof. Dr. Dieter Kube und **Prof. Dr. Rainer Merkl** für ihr Engagement als Mentoren begleitet von fruchtbaren Diskussionen und Ratschlägen

Fritz Kastner und **Dr. Ilya Shenderovich** für die Beratung und technische Hilfe am Spektrometer

alle weiteren (ehemaligen) Mitglieder des Instituts für Funktionelle Genomik für die gute Zusammenarbeit und Hilfsbereitschaft, den regen Austausch, die gesellige Atmosphäre und den tollen Zusammenhalt, insbesondere **Michael Altenbuchinger**, **Raffaela Berger**, **Katja Dettmer-Wilde**, **Lisa Ellmann**, **Julia Engelmann**, **Eva Engl**, **Franziska Görtler**, **Paul Heinrich**, **Bianca Höfelschweiger**, **Michael Huttner**, **Christian Kohler**, **Chen Li**, **Kathi Limm**, **Claudio Lottaz**, **Nadine Nürnberger**, **Paula Perez-Rubio**, **Elke Perthen**, **Sharon Peterson**, **Jörg Reinders**, **Tobias Schmid**, **Philipp Schwarzfischer**, **Farhad Shakeri**, **Hans Simbürger**, **Prof. Dr.**

Rainer Spang, **Frank Stämmler**, **Nicholas Strieder**, **Xueni Sun**, **Franziska Taruttis**, **Franzi Vogl**, **Chris Wachsmuth**, **Magda Waldhier**, **Jens Wallmeier** und **Helena Zacharias**

die Mitarbeiter des KFB **Christoph Möhle, Susanne Schwab**, **Jutta Schipka**, und **Thomas Stempfl** für die kollegiale Atmosphäre

und nicht zuletzt meine ehemaligen WG-Mitbewohner, Freunde, Eltern und meinen Freund für die liebevolle Unterstützung, offenen Ohren und vielen aufbauenden Worte.